

2000

Airborne remote sensing of forest leaf area index in mountainous terrain

Johnson, Ryan L.

Lethbridge, Alta. : University of Lethbridge, Faculty of Arts and Science, 2000

<http://hdl.handle.net/10133/90>

Downloaded from University of Lethbridge Research Repository, OPUS

Airborne Remote Sensing of Forest Leaf Area Index in Mountainous Terrain

Ryan L. Johnson
B.Sc., University of Lethbridge, 1997

A Thesis
Submitted to the Council on Graduate Studies
of The University of Lethbridge
in Partial Fulfillment of the
Requirements for the Degree

Master of Science

Lethbridge, Alberta, Canada,
January, 2000

© Ryan Johnson 2000

Dedication

For my Family,

My parents, Bob and Linda and my sister Amber without whose love and support I could never have finished this. Thank you very much, I love you.

Abstract

Leaf area index (LAI) provides forestry information that is important for regional scale ecological models and in studies of global change. This research examines the effects of mountainous terrain on the radiometric properties of multispectral CASI imagery in estimating ground-based optical measurements of LAI, obtained using the TRAC and LAI-2000 systems. Field and image data were acquired summer 1998 in Kananaskis, Alberta, Canada. To account for the influence of terrain a new modified approach using the Li and Strahler Geometric Optical Mutual Shadowing (GOMS) model in 'multiple forward mode' (MFM) was developed. This new methodology was evaluated against four traditional radiometric corrections used in combination with spectral mixture analysis (SMA) and NDVI. The MFM approach provided the best overall predictions of LAI measured with ground-based optical instruments, followed by terrain normalized SMA, SMA without terrain normalization and NDVI.

Acknowledgements

There are many people that supported this research. First, I would like to thank Dr. Derek Peddle, my thesis supervisor. Derek provided the opportunity, environment and support to make my research project possible, as well as endless enthusiasm and encouragement throughout the entire project. Dr. Ron Hall provided a great deal to my thesis. Ron's insight and explanations of forest ecosystems has provided a greater depth of understanding to my work. Ron also provided invaluable support in terms of his time and research equipment. I would like to extend a special thanks to Dr. James Byrne. Jim allowed me to follow my own research interests, and supported my decisions, which was a turning point in my life. Dr. Bob Rogerson provided help with my writing as well as always reminding me to step back and look at the problem as a whole. I thank Dr. Arthur Roberts, Simon Fraser University, for his insights and suggestions, which improved the final version of this thesis. Dennis Sheppard provided a tremendous amount of computer, software and technical support without which my thesis would have still been a work in progress. I would also like to acknowledge Dr. Ralph Cartar for his efforts in chairing my thesis defense as well as his written comments and suggests.

Financial support for this research was provided by the following grants awarded to Dr. Derek Peddle: NSERC Research and Equipment Grants, Alberta Research Excellence and IIPP Grants, the University of Lethbridge Research Fund, University of Lethbridge Faculty Research Grants, Natural Resources Canada and an Alberta STEP Grant.

I gratefully acknowledge Dr. Steven Franklin, Dr. Ron Hall and Dr. Bradley Wilson as well as collaborating staff and students at the University of Lethbridge, University of Calgary, Canadian Forest Service-Edmonton, and the University of Regina who provided support to the field and image data acquisition. Grace Lebel and staff at the Kananaskis Field Stations are thanked for providing logistical support in the field. Airborne CASI image acquisition and pre-processing was performed by Itres Research Limited of Calgary. The digital elevation model was kindly provided by Mr. Craig Stewart of the Miistakis Institute for the Rockies. I also acknowledge Dr. Alan Strahler and Dr. X. Li of Boston University for provision of the GOMS model software to Dr. Peddle through Dr. Forrest Hall of NASA GSFC, which was instrumental to the success of this thesis research.

Table of Contents

Dedication	iii
Abstract	iv
Acknowledgements	v
Table of Contents	vi
List of Figures	ix
List of Equations	xii
List of Tables.....	xiii
CHAPTER ONE	1
1 INTRODUCTION.....	1
1.1 Introduction.....	1
1.2 Research Objectives.....	3
1.3 Organization of the Thesis.....	4
CHAPTER TWO	6
2 LITERATURE REVIEW	6
2.1 Introduction.....	6
2.2 Global Climate Change, Forests and Remote Sensing	7
2.2.1 Global Climate Change	7
2.2.2 Forests and The Global Carbon Cycle	10
2.2.3 The Role of Remote Sensing.....	11
2.3 Estimation of Biophysical Parameter.....	12
2.3.1 Remote Sensing and Forestry Information.....	12
2.3.2 Factors Affecting the Spectral Response of Forests.....	13
2.3.2.1 Spectral Reflectance.....	13
2.3.2.2 Factors Internal to the Forest Stand	15
2.3.2.3 Factors External to the Forest Stand	17
2.3.3 Biophysical Parameters	18
2.4 Remote Sensing Methods for Biophysical Information Extraction.....	20
2.4.1 Multispectral Classification.....	20
2.4.2 Band Ratios and Vegetation Indices	21
2.4.3 Texture	23
2.5 Spectral Mixture Analysis.....	24
2.5.1 Theory	24
2.5.2 Methods.....	26
2.5.3 Forestry Applications	28
2.6 Spectral Endmembers	30
2.6.1 Reference Endmembers.....	32
2.6.2 Image Endmembers.....	33
2.6.3 Modeled Endmembers.....	34
2.7 Geometric Optical Reflectance Models	35
2.7.1 Theory	35
2.7.2 Forestry Applications	39

2.8	Terrain Normalization of Spectral Data.....	40
2.8.1	Theory	40
2.8.1.1	Radiometric Normalization of Spectral Data.....	41
2.8.1.2	Cosine Correction	43
2.8.1.3	Statistical-Empirical Method	44
2.8.1.4	C-Correction	45
2.8.1.5	Minnaert Correction.....	46
2.8.2	Sun-Canopy-Sensor Geometric Approach.....	47
2.9	Chapter Summary	49
CHAPTER THREE.....		50
3	METHODS.....	50
3.1	Introduction.....	50
3.2	Study Area and Data Set.....	51
3.2.1	Kananaskis Study Area	51
3.2.2	Field Data Collection and Processing	53
3.2.2.1	Ground Spectral Measurement	53
3.2.2.2	Spectroradiometer Instrumentation.....	54
3.2.2.3	Reflectance Calibration.....	56
3.2.2.4	Reflectance Data and Post-processing.....	56
3.2.2.5	Airborne Image Calibration	57
3.2.2.6	Endmember Spectra Collection	58
3.2.2.7	Forest Structural Data	63
3.2.2.8	Plot Location.....	64
3.2.2.9	Field and Image Position	65
3.2.3	Ground Based LAI Estimation.....	67
3.2.3.1	LAI-2000 Instrument	67
3.2.3.2	TRAC Instrument.....	69
3.2.4	Remote Sensing Imagery and Digital Elevation Data.....	70
3.2.4.1	Airborne Imagery.....	70
3.2.4.2	Image Preprocessing	75
3.2.4.3	Digital Elevation Model.....	76
3.3	Spectral Mixture Analysis.....	76
3.4	Component Endmember Specification	78
3.4.1	Reference Endmember Set	78
3.4.2	Image Endmember Set	80
3.4.3	Integrated Endmember Set	81
3.5	Spectral Mixture Analysis Post Processing, Evaluation and LAI Prediction	83
3.5.1	Spatial Aggregation of Fractions to the Plot Scale	83
3.5.2	Scene Fraction Validation	84
3.5.3	Leaf Area Index Prediction	85
3.6	Geometric Optical Reflectance Modeling	86
3.6.1	Multiple Forward Mode (MFM) Approach	87
3.6.2	Multiple Forward Mode User Interface	91
3.6.3	Multiple Forward Mode Parameterization	93
3.6.4	Terrain Normalization	94

3.7 Chapter Summary	99
CHAPTER FOUR.....	100
4 RESULTS AND DISCUSSION.....	100
4.1 Introduction.....	100
4.2 Spectral Mixture Analysis.....	101
4.2.1 Scene Fraction Validation	101
4.2.2 LAI Prediction using Spectral Mixture Analysis	107
4.2.3 Multivariate Regression using NDVI and SMA Fractions	110
4.3 Multiple Forward Mode Results	112
4.3.1 SMA and MFM Fraction Matching	115
4.3.1.1 MFM prediction of Leaf Area Index	115
4.3.2 Discussion	119
4.4 Chapter Summary	123
CHAPTER FIVE.....	125
5 CONCLUSIONS	125
5.1 Summary of Results.....	125
5.2 Conclusions.....	126
5.3 Contribution to Research	129
5.4 Future Research	129
References Cited	131
Appendix 1 Model Inputs and Multiple Forward Mode Software.....	141

List of Figures

- Figure 2-1 Trend in atmospheric CO₂ concentration. Top graph: Since 1751 over 265 billion tons of carbon have been released to the atmosphere from the consumption of fossil fuels. Bottom graph: Per capita CO₂ emissions from Canada peaked in 1979 at 4.7 metric tons of carbon per person and the 1996 estimate of 3.8 metric tons of carbon per person is among the highest of the major fossil-fuel CO₂-emitting nations. (CDIAC, 1999) 9
- Figure 2-2. Typical Spectral Response Characteristics of Green Vegetation (Guyot et al, 1989). Noticeable features are the green peak near 0.5 μm between the two chlorophyll absorption bands and the red edge near 0.7 μm marking the transition between the visible and near infrared bands, and strong water absorption bands in the short-wave infrared. 14
- Figure 2-3 Differences in the spectral signal due to phenological changes (Blackburn and Milton, 1995). As the phenologic stage of the tree progresses several changes are visible in the spectral curve: the elevation of the green peak and infrared plateau as well as the slope of the red edge. Each of these characteristics helps in the information extraction. 16
- Figure 2-4 The left image is a fraction image at 1m resolution. The right image is the same image draped over the RMS error. Non-forested areas such as the parking lot or areas of high relief exposed rock have the highest errors since these are not characterized by the forest endmember set..... 25
- Figure 2-5 A conceptualized view of a forest canopy as seen by a remote sensing instrument, showing the three main scene components: sunlit canopy, sunlit background and shadow. 31
- Figure 2-6 Left image: CASI band 1 versus band 2 – axis have been rotated to provide the best view of the relative spectral properties of various ground materials. Endmember values for each scene component are located at the vertices of a simplex in spectral space, shown as the white triangle. Right image: Shows the spatial positions in the image of those pixels shown in spectral space (colours match in both images). 32
- Figure 2-7 The GOMS model characterizes forest vegetation (individual tree crowns) as discrete three-dimensional spheroids, note the input parameters: h = tree height, r = crown radius and b = crown depth. The right image shows a simulated assemblage of trees, shadow and background in a pixel. 38
- Figure 2-8 Diagram showing the zenith angle, Z , incident angle Z' , surface slope = angle of exitance, E , solar azimuth, A_o , aspect of the surface, A_p , and aspect of the surface, A_z (After Holben and Justice, 1980)..... 42
- Figure 3-1 Study Area. The Barrier Lake study site is located in Kananaskis Provincial Park, Alberta, Canada, on the eastern slopes of the Canadian Rockies. Barrier Lake is centered at $115^{\circ}4'20''\text{W}$, $51^{\circ}1'13''\text{N}$. Photo A was taken looking south toward the end of Barrier Lake. Photo B was taken looking across Barrier Lake towards the southern knoll, to show the variability in terrain in the study area. The locations of the images are shown on a Landsat TM image (red arrows). 52
- Figure 3-2 ASD spectroradiometer setup for radiance measurements in the southern parking lot during image acquisition. 55
- Figure 3-3 Calibration targets placed in the southern parking lot during image acquisition. Each target was 3 X 3 m to ensure that a pure pixel of each target could be located in the 60cm, 1m and 2m data sets. The collection site was established in an open area away from adjacent vegetation to avoid any illumination variations. 58

Figure 3-4 The collections of apparent reflectance spectra to represent the shadow endmember in the reference endmember set.	60
Figure 3-5 Reference endmembers reflectance spectra for a Lodgepole pine stand, measured with the spectroradiometer. The reference measurement for sunlit pine canopy is shown in green; sunlit background is shown in blue and the apparent reflectance value for the shadow pine endmember is shown in red.	61
Figure 3-6 Spectroradiometer measurements of calibration targets collected during image acquisition. These measurements were subsequently resampled to the CASI band set and used in the atmospheric correction.	62
Figure 3-7 Plot Layout. Each plot was aligned with Magnetic North and a consistent labeling scheme (plot corners and center) was used to allow easy comparison between plots.	65
Figure 3-8 Ground Control Points (GCPs) were established throughout the study area and accurate locations were established for each using a DGPS systems, these targets were then used to test the positional accuracy of the image data set.	66
Figure 3-9 Sub-area of multi-scale CASI imagery collected over Kananaskis Provincial Park. The southern parking lot used for radiometric data collection is shown near the center of each image.	71
Figure 3-10 The ASD measurements collected in the field were resampled to the 8 CASI bands using a linear spectral response function. The reference measurement for sunlit pine is shown in green; sunlit background is shown in blue and the apparent reflectance value for the shadowed pine endmember is shown in red.	73
Figure 3-11 Influence of terrain on stand structure. Terrain influences the relative amount of shadow and background visible to the sensor, which influences the overall pixel brightness. Pixel brightness decreases from sun-facing to facing away from the sun. NOTE: Sun-Canopy-Sensor geometry does not vary with terrain, therefore BRDF effects are minimal.	88
Figure 3-12 Graphical representation of the look-up tables produced using the MFM approach. A) variation in modeled reflectance; B) variation in shadow fraction. Each diagram is in the principal plane of the sun with a SZA of 45° and an azimuth of 180° . Negative slope values represent slopes facing the sun while positive slopes are facing away from the sun. Three stand densities are shown for a pine stand with 30%, 50% and 80% crown closure (CC). Note the increased effect terrain has on both reflectance and shadow fraction in lower density stands.	90
Figure 3-13 MFM graphical user interface provides the user with an easy way of parameterizing the model.	93
Figure 3-14 Forest reflectance as a function of terrain. Shaded surface represents the relative change in reflectance as a function of terrain variables (slope and aspect). The wire mesh surface represents a generic terrain surface. Forest structure is constant with a 50% crown closure, terrain was modeled at 45° aspect intervals and slope was modeled with 10° intervals. The sun position would be behind the shaded surface casting light towards the front.	96

Figure 3-15 Forest shadow fraction as a function of terrain. Shaded surface represents the relative change in shadow as a function of terrain variables (slope and aspect). The wire mesh surface represents a generic terrain surface. Forest structure is constant with a 50% crown closure, terrain was modeled at 45° aspect intervals and slope was modeled with 10° intervals. The sun position would be behind the shaded surface casting light towards the front.....	97
Figure 4-1 The over correction produced by the cosine correction adjusted the raw DN's to such an extent that the different endmember sets were no longer able to characterize the scene components. As a result, the cosine correction was removed from subsequent analyses.....	102
Figure 4-2 Difference between the scene fractions produced using the reference endmember set and ML supervised classification under different terrain normalization conditions. The minimum and maximum difference is shown for each scene component, C (sunlit canopy), S (shadow) and B (sunlit background). The best overall results were without terrain normalization.....	104
Figure 4-3 Difference between the scene fractions produced using the image endmember set and ML supervised classification using different terrain normalizations. The minimum and maximum difference is shown for each scene component, C (sunlit canopy), S (shadow) and B (sunlit background). The best overall results were found without terrain normalization.....	105
Figure 4-4 Difference between the scene fractions produced using the integrated endmember set and ML supervised classification using different terrain normalizations. The minimum and maximum difference is shown for each scene component, C (sunlit canopy), S (shadow) and B (sunlit background). The best overall results were without terrain normalization.....	106
Figure 4-5 Difference between the scene fractions produced using the MFM model and ML supervised classification using each endmember set. The minimum and maximum difference is shown for each scene component, C (sunlit canopy), S (shadow) and B (sunlit background).....	114
Figure 4-6 The magnitude of the coefficient of determination for each method tested is shown for predicting TRAC LAI.....	120
Figure 4-7 The magnitude of the coefficient of determination for each method tested is shown for predicting LAI-2000 eLAI	121

List of Equations

Equation 2-1 Normalized Difference Vegetation Index	22
Equation 2-2 The equations that govern linear spectral mixture analysis	27
Equation 2-3 Root Mean Square Error.....	28
Equation 2-4 The Cosine Correction.....	43
Equation 2-5 The Statistical-Empirical Correction.....	44
Equation 2-6 The C-Correction.....	45
Equation 2-7 The Minnaert Correction	46
Equation 3-1 Surface Reflectance Equation.....	57

List of Tables

Table 2-1 Factors Internal and External to the Forest Canopy which affect reflectance (after Guyot et al. 1989).	16
Table 2-2 Selected Forest Biophysical Parameters (after Wulder, 1998)	19
Table 2-3 Required inputs into the GOMS Optical Reflectance Model.	38
Table 3-1 CASI Image Band Set collected at all spatial resolutions.	72
Table 3-2 Description of reference endmembers and reflectance curves of Sunlit Background, Sunlit Canopy and Shadow.....	79
Table 3-3 Description of image endmembers and reflectance curves of Sunlit Background, Sunlit Canopy and Shadow.....	81
Table 3-4 Description of integrated endmembers and reflectance curves of Sunlit Background, Sunlit Canopy and Shadow	82
Table 3-5 The number of regression trials is a function of different combinations of various options and data sets available in the study.	85
Table 3-6 The number of regression trials is a function of different combinations of various options and data sets available in the study.	99
Table 4-1 Magnitude of the regression coefficient of determination (r^2) using SMA applied to images corrected with different terrain normalization methods to predict TRAC LAI at 1m image pixel resolutions. The best scene fraction for each SMA trial is shown in brackets for sunlit canopy (c), sunlit background (b) and shadow (s).....	108
Table 4-2 Magnitude of the regression coefficient of determination (r^2) using SMA applied to images corrected with different terrain normalization methods to predict TRAC LAI at 2m image pixel resolutions. The best scene fraction: for each SMA trial is shown in brackets for sunlit canopy (c), sunlit background (b) and shadow (s).....	108
Table 4-3 Magnitude of the regression coefficient of determination (r^2) using SMA applied to images corrected with different terrain normalization methods to predict LAI-2000 eLAI at 1m image pixel resolutions. The best scene fraction: for each SMA trial is shown in brackets for sunlit canopy (c), sunlit background (b) and shadow (s).....	109
Table 4-4 Magnitude of the regression coefficient of determination (r^2) using SMA applied to images corrected with different terrain normalization methods to predict LAI-2000 eLAI at 2m image pixel resolutions. The best scene fraction: for each SMA trial is shown in brackets for sunlit canopy (c), sunlit background (b) and shadow (s).....	109
Table 4-5 Improvements provided by incorporating NDVI into the prediction of TRAC LAI and LAI-2000 eLAI using the uncorrected SMA fractions at 1m image pixel resolution.	111
Table 4-6 Improvements Provided by Incorporating NDVI into the Prediction of TRAC LAI and LAI-2000 eLAI using the Uncorrected SMA Fractions at 2m image pixel resolution.	111
Table 4-7 Magnitude of the regression coefficient of determination (r^2) using the MFM approach to predict TRAC LAI at the 1m and 2m image resolutions. The best result is shown in bold for each image resolution.....	117

Table 4-8 Magnitude of the regression coefficient of determination (r^2) using the MFM approach to predict LAI-2000 eLAI at the 1m and 2m image resolutions. The best result is shown in bold for each image resolution.	117
Table 4-9 Improvements provided by the Multiple Forward Mode Approach to Predict TRAC LAI.....	118
Table 4-10 Improvements provided by the Multiple Forward Mode Approach to Predict LAI-2000 eLAI.....	118

CHAPTER ONE

INTRODUCTION

1.1 Introduction

Remote sensing of forest leaf area in mountainous terrain is important to a wide range of forest management and research fields (NRC, 1995, 1998). Accurate estimates of leaf area index (LAI) are required in studies of ecophysiology, atmosphere-ecosystem interactions and global change. LAI is defined as one half the total leaf area per unit ground area (Chen et al, 1996). LAI is one of the primary forest structural measures used in remote sensing and processed-based models to characterize forest canopies because of the importance of green leaves in many biological and physical processes in forest canopies (Sellers et al, 1986; Sellers, 1987; Running and Coughlan, 1988; Bonan, 1993). LAI was identified by Running et al, (1986) as the single most important variable that can be derived from remote sensing that is of most importance to ecologists. In this thesis, remote sensing image processing techniques are developed and applied to improve the estimation of LAI in mountainous terrain. This is important, since significant portions of the Earth's forests are located in mountainous regions, and also, the topic has particular relevance to forest management in western Canada.

This research builds on earlier successes using spectral mixture analysis (SMA) in making accurate estimates of forest biophysical parameters in low relief environments (Hall et al, 1995, 1996; Peddle et al, 1995, 1999b). Spectral mixture analysis separates individual pixels into the main scene components that contribute to the radiance recorded by the sensor.

In highly structured conifer canopies, the main components that contribute to pixel level brightness include sunlit canopy, sunlit background and shadow. The fundamental concept of spectral mixture analysis is that the spectral properties of each of these components combine and contribute to the overall pixel radiance value based on their spatial abundance on the ground visible to the sensor. The spectral properties of each scene component are isolated and measured (termed a spectral endmember) to determine the spatial abundance of scene components at the sub-pixel scale. The abundance of each component is highly related to forest structure, which is the basis for the strong predictive capability of spectral mixture analysis. As forest structure changes so does the relative amount of each scene component visible to the sensor. This methodology has been shown to provide better predictions over traditional methods such as vegetation indices. For example, the Normalized Difference Vegetation Index (NDVI) does not account explicitly for the influence of background vegetation and shadow on pixel level reflectance (Hall et al, 1995), thereby reducing the ability to make accurate estimations of forest biophysical parameters.

In a high relief, forested environment, terrain variations further influence the abundance of these scene components visible to the sensor. Terrain affects the position of trees within the canopy relative to the sensor, thus changing the contribution of sunlit canopy, sunlit background, and shadow to the overall pixel radiance recorded by the sensor. Therefore, the thrust of this research is the development of new image processing techniques that are able to account for variations in the sub-pixel scale scene fractions induced by terrain. The concepts presented here include the use of traditional terrain normalization methods based on pixel level illumination values, as well as the use of forest reflectance models which provide the ability to account for both forest structure and terrain on pixel level reflectance.

The main hypothesis of this research is that a terrain normalization method that explicitly accounts for forest structure will provide better estimation of LAI in mountainous terrain compared to illumination based corrections. In testing this hypothesis, a new way of using geometric optical reflectance models in a *multiple forward mode* (MFM) is introduced for mountainous terrain applications. A controlled experiment was designed to test the ability of spectral mixture analysis and the multiple forward mode reflectance modeling for predicting ground based optical measurements of leaf area index. Unique aspects of this research include a co-registered multi-scale Compact Airborne Spectrographic Imager (CASI) image data set, detailed forest structural measurements collected for input to forest reflectance models and for validation purposes, and the use of a variety of ground-based optical instruments to estimate leaf area index in the field.

1.2 Research Objectives

The main objective of this thesis is to:

- Devise and test an improved method for estimating leaf area index in mountainous terrain from airborne remote sensing imagery.

Secondary objectives are:

- Evaluate the utility of different methods of obtaining spectral endmembers for use with the spectral mixture analysis algorithm and the forest reflectance model.

- Compare terrain normalization methods for their relative suitability to improve scene fraction extraction using spectral mixture analysis.
- Test the ability of spectral mixture analysis to predict leaf area index in mountainous environments with and without traditional illumination based terrain normalization algorithms.
- Develop a new approach to using geometric optical reflectance models in mountainous terrain that can account for variation in both forest structure and terrain. Develop an understanding of the relationship between terrain and scene component fractions at the sub-pixel scale.
- Compare results obtained using spectral mixture analysis and the forest reflectance model to more traditional vegetation index approach.
- Investigate the possibility of using vegetation indices in combination with the other methods to test the information content each provides to the prediction of LAI.

1.3 Organization of the Thesis

This thesis is organized into five chapters. In this chapter, the thesis has been introduced and the research objectives stated.

In Chapter Two, a review of the pertinent background literature and a broad overview of the research context are presented. The context of this research as well as the role of remote

sensing are established. Factors affecting forest reflectance and methods used to extract biophysical information in mountainous terrain are also described, including a review of spectral mixture analysis, canopy reflectance modeling, and terrain normalization.

In Chapter Three, research methodologies are presented. The study area, field data collection and image data set are first described to provide a setting for the analysis. Techniques for LAI prediction using spectral mixture analysis and forest reflectance models in mountainous terrain are then outlined. Three types of endmember sets are described for these analyses: reference, image and integrated. Two analyses are described in this chapter. The first analysis is designed to test spectral mixture analysis for predicting ground based optical measurements of forest leaf area. Four radiometric corrections were applied to airborne imagery prior to separate spectral mixture analyses. These were the Cosine, C-correction, Statistical-Empirical and Minneart Corrections. The second analysis tested the ability of forest reflectance models to account for terrain in the prediction of forest leaf area. The development of a new multiple forward-mode approach to reflectance modeling in mountainous terrain is described for this purpose.

In Chapter Four, the results of the analysis are presented. First, a validation of scene fractions from SMA is performed. Following this, the results of SMA trials with and without terrain normalization and those from the forest reflectance model are compared in terms of their ability to predict LAI using scene fraction values. SMA and MFM results are also compared to baseline results using a vegetation index (NDVI). The utility of each method is discussed in the context of acquiring estimates of LAI over mountainous terrain.

In Chapter Five, a summary of the thesis is presented and conclusions are drawn. The contributions this study has made to research and areas for future research are also discussed.

CHAPTER TWO

LITERATURE REVIEW

2.1 Introduction

In this chapter, a review of the literature dealing with remote sensing of forest biophysical parameters is presented. The review begins with a brief discussion of the much broader research context of global climate change, the carbon cycle, the importance of mountain forests and the role of remote sensing. Next, the forest biophysical parameters of interest are identified and described. Following this is a description of the factors affecting remotely sensed forest data, including spectral reflectance patterns of vegetation, and factors both internal and external to the canopy. Finally, a review of the major remote sensing image analysis approaches used to estimate these parameters is presented. This includes vegetation indices, multispectral classification, texture analysis, spectral mixture analysis, reflectance models, and terrain correction methods. In this review, emphasis is placed on spectral mixture analysis, geometric optical reflectance models and terrain normalization methods, as these topics are more pertinent to this research.

2.2 Global Climate Change, Forests and Remote Sensing

2.2.1 Global Climate Change

Until recently, there has been debate over the causes of the warming trends in global temperature. Scientists were uncertain whether the warming trends in temperature reflected natural variations in the earth's climate, or whether in fact the trend could be attributed to anthropogenic activities. However, the recent conference on the Intergovernmental Panel on Climate Change (an international body of scientists charged with studying global warming) reported a conclusion, based on the findings of over 2,500 peer-reviewed articles that "*the balance of evidence suggests that there is a discernible human influence on global climate*" (UCS, 1999).

Global change can be defined as changes in the global environment (including alterations in climate, land productivity, atmospheric chemistry, ecological systems, and oceans or other water resources) that may alter the capacity of the Earth to sustain life (CDIAC, 1999). Global Circulation Models (GCMs) predict a warmer overall climate worldwide with increased atmospheric greenhouse gases: notably CO₂, CH₄, N₂O, CFCs, CCL₄ and other compounds (Gates, 1990a, 1990b).

At the start of the industrial revolution the concentrations of CO₂ in the atmosphere were thought to be about 290 PPM (Kimmins, 1997). Scientists are predicting that these levels could increase to 600 PPM doubling the concentration of CO₂ in the atmosphere by the year 2050 (UCS, 1999). The increases in CO₂ emissions in Canada since the industrial revolution are shown in Figure 2-1. The amount of warming that will occur and the likely outcomes of such increases in CO₂ concentrations are still in dispute. These questions about

the future state of the environment at both regional and global scales can be answered only through theoretical model simulations and predictions due to the complexity and scales of these systems.

One area of focus in global change studies is forest productivity as forests contribute significantly to sequestering CO₂ from the atmosphere. Processed-based ecological models, such as FOREST-BGC (Running and Gower, 1991), BIOME-BGC (Running and Hunt, 1994) and BEPS (Chen et al, 1998) have been developed to explore forest productivity. These models allow simulations of forest processes under different climate conditions, atmospheric properties and stand structures, as well as providing estimates of variables which are hard to measure directly, such as gas exchange within the canopy (Running and Hunt, 1994). As we shall see later in this chapter, forest information such as leaf area index is important for parameterizing these models, and is a variable which can be obtained from remote sensing imagery.

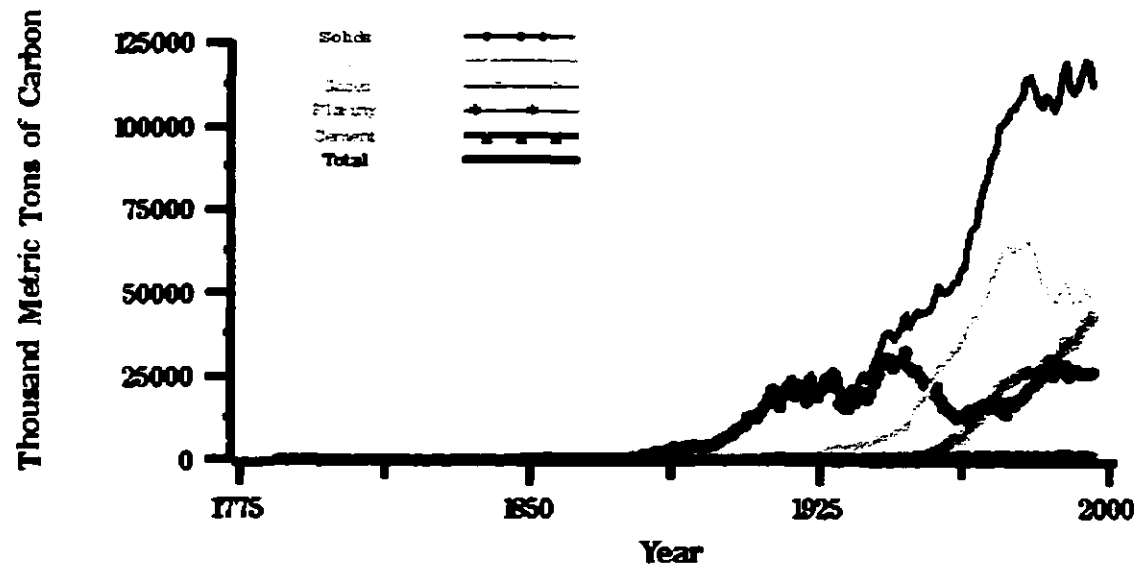
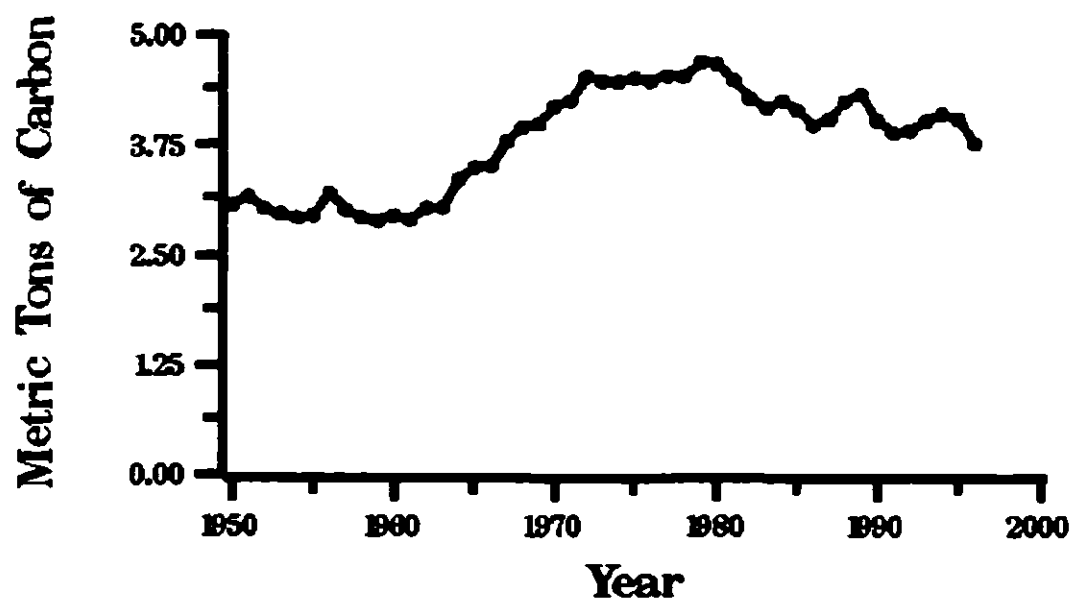
Total CO₂ emissions for Canada 1775 to 1998Per capita CO₂ emission estimates for Canada.

Figure 2-1 Trend in atmospheric CO₂ concentration. Top graph: Since 1751 over 265 billion tons of carbon have been released to the atmosphere from the consumption of fossil fuels. Bottom graph: Per capita CO₂ emissions from Canada peaked in 1979 at 4.7 metric tons of carbon per person and the 1996 estimate of 3.8 metric tons of carbon per person is among the highest of the major fossil-fuel CO₂-emitting nations. (CDIAC, 1999)

2.2.2 Forests and The Global Carbon Cycle

The forest ecosystem plays a significant role in the levels of CO₂ in the atmosphere, accounting for 90% of the terrestrial carbon storage (Gates, 1990a). Carbon is one of the main constituents of tree growth. Trees sequester CO₂ from the atmosphere through the processes of photosynthesis. Photosynthesis is the process by which plants are able to absorb specific wavelengths of light (photosynthetically active radiation, PAR) and convert them into chemical bond energy of glucose using carbon dioxide and water (Kimmins, 1997). Respiration refers to the energy of photosynthesis used up during plant growth, maintenance and CO₂ release (Kimmins, 1997). Photosynthesis and respiration work together in controlling the amount of CO₂ that can be absorbed from the atmosphere and stored as biomass (Jarvis, 1989, Jarvis and Dewar, 1993). The rates of photosynthesis and respiration are influenced by many site factors, including CO₂ concentration in the atmosphere, surface temperature, nutrient, and water availability and plant physiology. There is still debate over what effects an increased CO₂ or doubled CO₂ concentration will have on the growth rates of trees, the variability of forests in boundary zones (e.g. southern limit of the boreal forest), and natural landscape integrity (Graham et al, 1990). Comprehensive spatial data are needed, to build global scale models of forest productivity. Many of the earth's forests are in mountainous terrain. From both a modeling and remote sensing perspective, high relief environments add another layer of complexity to the understanding of forests. Terrain variations affect light and water regimes, soil types, forest structure and ultimately forest productivity. These variations must be accounted for explicitly in both ecological models and image processing techniques used to extract quantitative forest information.

2.2.3 The Role of Remote Sensing

Remote sensing has developed beyond being a tool used by ecologists to obtain general information about spatially explicit problems into a normative method and a basis on which much ecological investigation begins (Franklin, 1999¹; Running and Gower, 1991; Pitt et al, 1997). Several processed-based ecological models such as FOREST-BGC (Running and Gower, 1994) and, BIOME-BGC (Running and Hunt 1994) have been developed from their conception to use input variables derived from remote sensing data. Remote sensing serves two critical roles in ecological studies. First, remote sensing provides the only source of digital, spatially comprehensive, consistent information needed to generate initial conditions as inputs to ecological models which require estimations of forest cover and LAI (Peddle, 1997; Franklin, 1999¹). Remote sensing also enables problems to be studied at different scales as it is the only means of acquiring quantitative, spatially continuous, timely information over a broad range of spatial scales. Remote sensing provides the ability to analyze problems at the local, regional and global scale. This range of information enables researchers to explore issues involved with scaling our ecological knowledge from large to small scales. Second, remote sensing can be used to validate model output and to help refine model parameters (Roughgraden et al, 1991). There are different variables, which are of interest to ecologists, as well as many factors that influence the ability and quality of data that can be extracted from remotely sensed data. These topics will be covered in the next section.

2.3 Estimation of Biophysical Parameter

2.3.1 Remote Sensing and Forestry Information

To take advantage of the timely, synoptic information that remote sensing can provide, variations in site characteristics must be linked to observable forest features. Fundamentally, remote sensing does not measure any forest characteristic directly; rather, data collected by the sensor (e.g. reflected solar energy) are used to infer biophysical information about the ecosystem by using algorithms that estimate physical units (APAR, evaporation, LAI, soil moisture) from sensor units (radiance) (Ustin et al., 1991). Many of the processes of interest to the ecologists are not directly observable using remote sensing, such as gas exchanges between the canopy and the atmosphere, or processes of nutrient cycling. For example, a tree's requirement for light (PAR radiation) is closely linked to its use of CO₂, and associated rates of water vapor loss, and photosynthesis, are directly related to chlorophyll density which can be derived from remote sensing (Seller, 1987). Therefore, relationships between observable forest characteristics and these processes of interest have been developed. What is observable by remote sensing are differences in the spectral reflectance patterns of canopy and understory vegetation influenced by factors such as the health or spatial arrangement of the stand. Characteristics of the plant canopies (composition, height, and density) are collectively strong indicators of the state of the ecosystem as a whole, and represent the physical interface between optical remote sensing and forest ecology (Treitz and Howarth, 1996). Radar and other remote sensing methods are also related to characteristics of forest structure. However, these do not have the same links to the physical processes of the forest canopy such as photosynthesis as optical remote

sensing techniques. The properties outlining the spectral response of individual leaves and vegetation canopies are discussed below, and followed by a review of the major forest biophysical parameters estimated using remote sensing.

2.3.2 Factors Affecting the Spectral Response of Forests

2.3.2.1 Spectral Reflectance

Numerous studies have explored the relationship between remotely sensed visible and infrared reflectance and forest biophysical parameters (e.g. Running et al. 1986; Franklin 1986; Guyot et al, 1989; Carter, 1989). Generally, three spectral ranges or domains can be identified in the electromagnetic spectrum for which different factors affect the optical properties of leaves, as shown in Figure 2-2. The visible domain (400-700 nm) represents the main range of light absorption by plants (Guyot et al, 1989). The main sources of light absorption are chlorophyll *a* and *b* and carotenoids (xanthophyll and anthocyanines) in the chloroplast cells. Two distinct spectral absorption bands are visible at 450 nm and 670 nm and represent the absorption due to chlorophyll *a* and *b*, respectively which are the dominant pigments during the growth phase of plants. These chlorophyll absorption bands are located in the blue and red portions of the visible spectrum, producing a peak in the green spectrum at 550nm, giving leaves their green colour.

The near infrared region (700-1300 nm) is dominated by the influence of leaf structure. Pigments and cellulose are generally transparent to near infrared wavelengths consequently; there is very little absorption in this region. A plateau in spectral reflectance whose intensity depends on the internal structure of leaves, as well as the amount of

mesophyll (internal leaf structural material) characterizes this region. Leaf reflectance increases with more heterogeneous cell shapes and with more cell layers, and intercellular spaces and with increased cell size. The near infrared spectral region can be separated into two sections: (1) between 700 - 1100 nm, where the reflectance is high, except for several water absorption bands (960 and 1100 nm) and (2) between 1100 and 1300 nm, which corresponds to the transition between the higher near infrared reflectance and water-related absorption bands of the short-wave infrared. The last optical domain is the short-wave infrared (1300-2500 nm) which is characterized by leaf water content. Water strongly absorbs radiation at 1450, 1950 and 2500nm because of this, these spectral regions are not used for reflectance measurements. In the rest of the short-wave infrared, reflectance is inversely related to leaf moisture content.

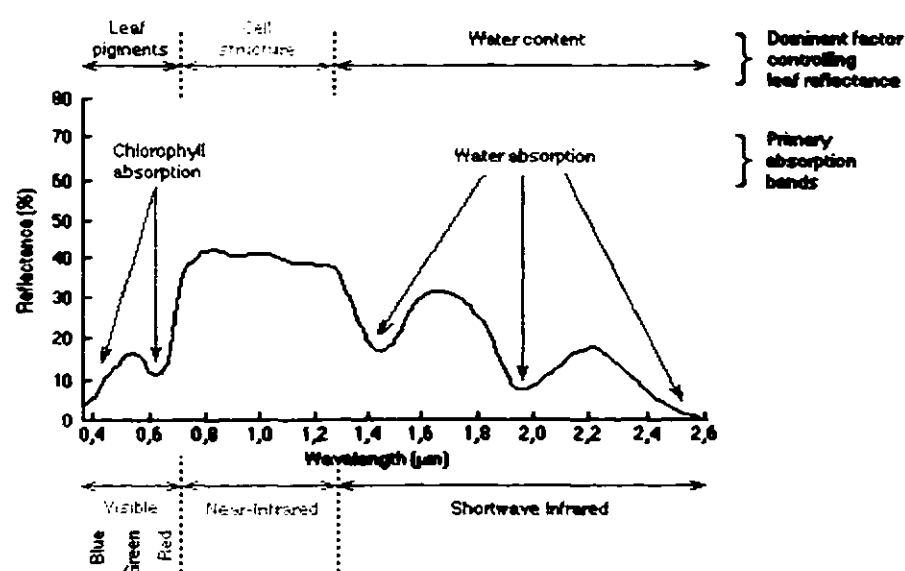


Figure 2-2. Typical Spectral Response Characteristics of Green Vegetation (Guyot et al, 1989). Noticeable features are the green peak near 0.5 μm between the two chlorophyll absorption bands and the red edge near 0.7 μm marking the transition between the visible and near infrared bands, and strong water absorption bands in the short-wave infrared.

As explained above there is an inverse relationship between the amount of green vegetation and red reflectance which can be accounted for by the increased absorption by chlorophyll. In contrast, the reflectance in the near infrared spectrum is generally high and increases weakly with increased biomass. These relationships are the foundation of biophysical information extraction using remote sensing (Running et al. 1986; Peterson et al, 1987; Curran et al, 1992). A more detailed study by Curran (1989) showed there were approximately 42 spectral absorption bands which could be attributed to different elements in leaves. Beyond the basic spectral characteristics of leaves, there are also a number of internal and external stand characteristics, which influence the spectral signal recorded by remote sensors (Table 2-1).

2.3.2.2 Factors Internal to the Forest Stand

Internal influences on the forest stand include the effects of canopy geometry, optical properties of the understory, and stand vigor (Treitz and Howarth, 1996) (Table 2-1). Canopy geometry or structure (density and crown closure) influences the relative contribution of the overstory and understory to the overall spectral response pattern. Variations in canopy geometry results in different amounts of sunlit canopy, sunlit background and shadow visible to the sensor thus changing the radiance recorded by the sensor. Optical properties of the soil and background can have a large effect on the total signal received by a sensor, particularly in low density stands where the ground cover is highly visible. Finally, stand vigor and health will influence the light absorption by chlorophyll and other photoactive pigments.

Table 2-1 Factors Internal and External to the Forest Canopy which affect reflectance (after Guyot et al, 1989).

Internal Factors	External Factors
Background Influence	Sensor Resolution
Canopy Structure/Geometry	Solar Zenith Angle
Canopy Reflectance	Solar Azimuth
	View Zenith
	View Azimuth
	Terrain

The forest is a living entity and is influenced by diurnal, seasonal and annual cycles in site characteristics such as temperature and light regimes. As a function of these cycles, the structure and productivity of the stand change. As a result so do the spectral patterns of the forest stand (Bonan, 1991). Blackburn and Milton (1995) have shown that the seasonal differences in spectral response can be attributed to differences in canopy structure and the phenological stage of trees (Figure 2-3).

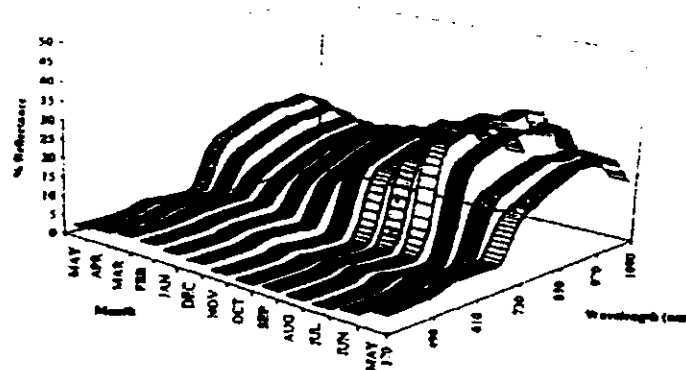


Figure 2-3 Differences in the spectral signal due to phenological changes (Blackburn and Milton, 1995). As the phenologic stage of the tree progresses several changes are visible in the spectral curve: the elevation of the green peak and infrared plateau as well as the slope of the red edge. Each of these characteristics helps in the information extraction.

2.3.2.3 Factors External to the Forest Stand

Factors external to the stand include elements such as size of the view area, atmospheric conditions, and sun and sensor geometry (Table 2-1). The size of the view area, or Instantaneous Field of View (IFOV) of the sensor, will influence the variability of the data in the image. Larger pixels tend to reduce the variability in the image whereas higher spatial resolution images maintain much of the variability of the landscape.

Terrain influences the sun/surface/sensor geometry and accounts for a significant difference in the spectral response pattern of forest stands over differing terrain. The sun/surface/sensor geometry affects the spectral response pattern in two significant ways. First, at different times of the day, light will penetrate to different depths of the canopy, which will change the relative proportions of the canopy and background presented to the sensor. Second, the reflectance of a vegetation canopy is dependent on sensor view angle, as canopies do not reflect as Lambertian surfaces. The atmosphere is another significant influence on the signal received at the sensor.

Different atmospheric conditions will influence the amount of direct and diffuse irradiance reaching the surface, thereby influencing the intensity of the reflected signal. The atmosphere can also influence the amount of reflected radiance reaching the sensor through scattering and absorption.

2.3.3 Biophysical Parameters

Important forest biophysical parameters that characterize forest structure include leaf area index, biomass, and net primary production (Table 2-2). Forest structure is defined as the above ground spatial arrangement of trees both, horizontally and vertically. Some definitions also include reference to the change in their organization over time (Spurr and Barnes, 1973, 1980). The horizontal dimension is associated with stand density and distribution whereas the vertical dimension is associated with tree height and the height distribution of the canopy (Wulder, 1998b). Forest structure is a result of competition for resources (light, nutrients, and water), disturbance, and the successional phase of the site (Kimmins, 1997a, 1997b). Examples of important structural parameters include leaf area index, biomass, and above ground net primary productivity (ANPP). The ability to measure or estimate these components permits estimation of environmental factors such as hydrologic regime, canopy albedo, forest productivity and soil nutrient availability (Wulder, 1998). These structural variables are defined next.

The definition of leaf area index used here is a measure of the one sided unit area of foliage per unit ground area, rather than the one sided projected area, which does not account for all the interactions of light within the canopy (Chen et al, 1996). Biomass is the total amount of vegetation present at a particular site at a specific time. Two ways forest production can be described are gross and net production. Gross production refers to the total increases in organic matter plus losses to respiration per unit area and time (Kimmins, 1997a). Net Production refers to the total increase in organic matter per unit area and time less respiration losses (Kimmins, 1997a). Respiration losses refers to the energy of photosynthesis which is used up during plant growth and maintenance (Kimmins, 1997a).

Table 2-2 Selected Forest Biophysical Parameters (after Wulder, 1998)

Parameter	Details	Reference
Leaf Area Index (LAI)	-a measure of the amount of foliage per unit ground area	Cheng et al. 1996
Biomass	-total amount of vegetation measured for a given time and location	Kimmins, 1997a
Above Ground Net Primary Production (ANPP)	-the rate of increase in above ground organic matter after losses to respiration	Kimmins, 1997a Spurr and Barnes, 1973

Currently, ecologists face the challenge of integrating their understanding of plant atmosphere interactions at the leaf scale into models at regional and global scales (Schuepp, 1993). This may be facilitated by process-based models capable of integrating basic processes of plant atmosphere exchange over a broad range of scales. These models require timely, synoptic observations of the ecosystem. In quantifying energy and mass exchange by plant canopies, LAI has been identified as the single most important ecological variable which can be derived from remote sensing of coniferous forests (Running et al, 1986). LAI is the focus of much research in remote sensing of vegetation. The following section outlines several methods and concerns involved with the extraction of biophysical data from remotely sensed data.

2.4 Remote Sensing Methods for Biophysical Information Extraction

2.4.1 Multispectral Classification

The intent of multispectral classification is to categorize all the pixels in an image into land cover classes or themes (Franklin, 1984; Franklin et al, 1986). Multispectral classification analyzes the spectral characteristics of each pixel within an image and assigns individual pixels to categories based on similar spectral properties. Classification is often used in remote sensing applications and provides important landcover information to a biophysical analysis. The scale of the data collected, the spectral bands recorded, and the complexity of the environment under investigation influence classification accuracy. The spatial resolution of the data affects the detail of the information classes that can be derived from the image (Wulder, 1998), whereas spectral and radiometric resolution affects the separability of the classes. Spectral response patterns are often used as a definition of a uniquely occurring combination of elements which will be identifiable on the surface (Jensen, 1996). The composition of the canopy (density, crown closure), however may result in different forest species producing spectrally similar response patterns (Hall and Crown, 1987). This point adds significant uncertainty to the classification procedure and may lead to spectral classes representing several ground cover classes (information classes).

When used properly, multispectral classification is an accurate method of assigning pixel values to information classes. Consideration of image properties, classification algorithm and the definition of classes are important in this process. There are two general methods of classification, supervised and unsupervised. Supervised classification requires *a priori* knowledge of the area to establish the class structure and select training sites on the

image to classify the remaining pixels. A training site is a collection of pixels, which represents a class and captures its spectral variability. Unsupervised classification requires no *a priori* knowledge of the area. It separates the image into statistically similar spectral groups. These spectral groups do not necessarily correspond directly to information classes and are manually assigned to an information class after the classification.

Advanced classification algorithms have been developed to process more complex data sets, such as higher dimensional or hyperspectral imagery, and spatial, terrain or multi-source spatial information. Examples of these advanced methods include contextual neural networks and evidential reasoning classifiers (Peddle, 1995). The evidential reasoning approach (Peddle, 1995) allows incorporation of many types and scales of data into the classification and has been shown to improve the classification accuracy in complex environments compared to maximum likelihood and neural network approaches (Duguay and Peddle, 1995; Peddle and Duguay, 1998).

2.4.2 Band Ratios and Vegetation Indices

Vegetation indices take advantage of the differential reflectance characteristics of green vegetation in the visible and near infrared bands. Typically healthy vegetation absorbs strongly in the visible bands due to the influence of photo-active pigments such as chlorophyll and reflects strongly due to the internal structure of the vegetation in the infrared spectrum as discussed earlier. By comparing ratios of the relative brightness values of the visible bands to the infrared bands, estimates of vegetative biomass can be made (Tucker, 1979). These ratios are related to the health and amount of green vegetation on the surface

(Curran and Williamson, 1987). As either the health or amount of vegetation changes so does leaf structure and the amount of chlorophyll in the canopy and therefore the ratio values will also change which provides the correlation between these indices and forest biophysical parameters.

Probably the most commonly used vegetation index is the Normalized Difference Vegetation Index or NDVI (Rouse, 1972) which takes the ratio of red to near infrared radiation (Equation 2-1).

Equation 2-1 Normalized Difference Vegetation Index

$$\text{NDVI} = (\text{NIR} - \text{R}) / (\text{NIR} + \text{R})$$

Where:

NIR = digital number recorded for the Near Infrared band

R = digital number recorded for the Red band

The effect of normalizing this ratio is that the values will range from -1 (no or very low vegetation) to 1 (dense vegetation cover). NDVI has been related to several biophysical parameters such as LAI and biomass (Running et al, 1986; Franklin, 1986). However, it is limited at LAI values over approximately 3 (Running et al, 1986; Wulder et al., 1998; Baret and Guyot, 1991, Chen and Guilbeault, 1996) because the ratio of red to near infrared reaches an asymptote. Vegetation indices are also influenced by the effects of understory vegetation (ground cover reflective properties) which can lead to problems in making accurate estimates of forest parameters (Hall et al, 1995; Sellers, 1987; Peddle, 1997). Sellers (1987) suggested that reflectance data derived from vegetation indices are more related to instantaneous rates associated with the canopy such as Gross Primary Production

or evapotranspiration rather than estimates of the state of the canopy such as LAI or biomass. However, **Wulder et al, (1998)** have shown improvements in the estimates of LAI using NDVI by incorporating texture values as a surrogate for forest structure. NDVI can also be useful in change detection studies, as many years of satellite data are available and this approach can be easily implemented between imaging dates, provided the data sets have been atmospherically corrected or normalized to one another.

2.4.3 Texture

Spatial information often plays an important role in the interpretation of remotely sensed data in forested areas (**Bruniquel-Pinel and Gastellu-Etchegorry, 1998; Wulder, 1998; Peddle et al, 1999b**). Texture is the analysis of pattern variability represented in adjacent pixel values (**Townshend and Justice, 1981; Curran, 1988**). These include the extraction of textural features from the image's Fourier power spectrum, local statistical properties of neighborhoods and gray-level spatial dependence or co-occurrence matrices (**Franklin and Peddle, 1987**). There are many procedures used in deriving texture from imagery which are dependent on image spatial resolution (**Wulder et al, 1996**)

Texture derivatives provide new layers of image data and can provide additional information (**Franklin and Peddle, 1989; 1990**). Texture has been used in a number of applications, however, in forested scenes texture is most related to forest structure. **Wulder et al, (1998)** have shown that texture acts as a surrogate for forest structure and can be related to LAI. The variation in texture is related to changes in the spatial arrangement of vegetation. Image spatial resolution is important when considering texture. Coarse spatial

image resolutions tend to have lower variability between pixels than high spatial resolution images, as most of the variance has been incorporated into the pixel (Wulder et al., 1998). When processing imagery to assess textural information, several of the factors that need to be addressed include: i) the operating window size that can be related to the size of the feature being observed (Peddle and Franklin, 1991); ii) the data variance within the image channel (Wulder et al., 1998a); iii) and the algorithm to be used. The inclusion of texture measures into the estimation of LAI using NDVI have increased the accuracy of LAI by approximately 20% over that obtained using NDVI alone based on an airborne CASI image dataset (Wulder et al, 1998).

2.5 Spectral Mixture Analysis

2.5.1 Theory

Spectral Mixture Analysis (SMA) is used to quantify the subpixel abundance of scene components (Adams et al, 1993; Tompkins et al, 1997). SMA is based on the concept that the Instantaneous Field of View (IFOV) of a sensor contains a number of spectrally different surface components which combine to create the overall reflectance recorded by the sensor (Adams et al., 1993). The concept of mixed pixels was first identified by Horwitz et al (1971), who saw the influence of these mixtures in an agricultural setting.

Spectral Mixture Analysis works by identifying the individual components expected to contribute to the overall pixel level reflectance. Once the scene components have been identified and their spectral properties obtained as spectral endmembers, the SMA algorithm then evaluates each pixel and estimates the spatial abundance of each material needed to sum

to the overall pixel brightness value. The algorithm expresses the amount of each material as a fraction of total pixel area (one fraction per each component). The fraction varies between 0 to 1, with 0 indicating that this material is not present and did not contribute to the overall pixel brightness, and 1 indicating that the pixel is composed entirely of that material. The fraction values must sum to 1 since each is expressed as a fraction of the total pixel area. If the fractions do not sum to 1, or if individual fractions are less than 0 (underflow) or greater than 1 (overflow) the endmembers used did not accurately characterize the materials in the pixel. A root mean square (RMS) error is also given for each pixel, which is also useful for assessing the accuracy of the endmembers (Figure 2-4). It is important to note that SMA depends on the accurate characterization of the endmembers (Adams et al, 1993, Tompkins et al, 1997). If the endmembers of their spectral values are incorrect in a physical sense the fractional abundances produced using SMA will be in error.

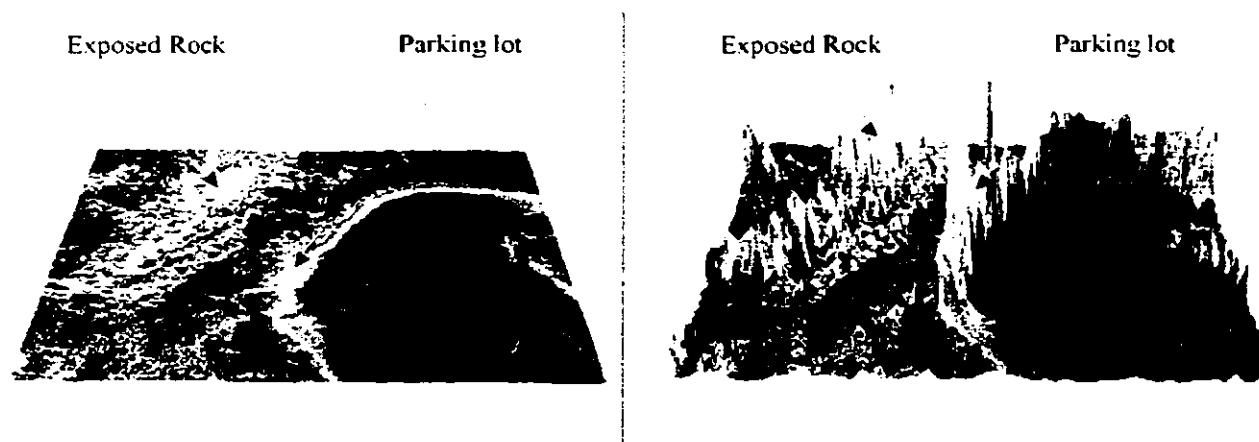


Figure 2-4 The left image is a fraction image at 1m resolution. The right image is the same image draped over the RMS error. Non-forested areas such as the parking lot or areas of high relief exposed rock have the highest errors since these are not characterized by the forest endmember set.

The number of endmembers that can be accurately separated within a pixel is a function of the dimensionality of the image data. The number of uncorrelated wave bands determines the dimensionality of the image data. As was discussed earlier in section 2.3.2.1, the interaction of light and vegetation can be divided into three main segments, the visible, the near infrared and the short wave infrared. Each of these segments behaves similarly, providing little new information. Thus, it is the number of uncorrelated bands that determines the number of scene components which can be successfully unmixed; for example no more than three or four scene components for a Landsat band set (Hall et al, 1995).

2.5.2 Methods

Most spectral mixture analysis applications have used a linear mixing assumption. The linear model assumes that the radiative transfer among individual vegetation components (twigs, leaves, bark, etc.) can be greatly simplified and expressed as a single scattering albedo (Mustard and Pieters, 1989). This assumption simplifies the mixture problem and allows the spectral variability of a scene to be modeled as a linear combination of endmembers. Linear mixture analysis is based on the assumption that each pixel is composed of a combination of scene components weighted by their surface abundances, and that the pixel spectrum is a linear combination of the endmember reflectance spectra (Tompkins et al, 1997). This assumption does not hold exactly but is a reasonable approximation that allows the simplification of an enormous problem (Hall et al, 1995). The general equations that govern linear spectral mixture analysis are shown in Equation 2-2 and 2-3. A linear combination of

spectral endmembers is used to decompose or unmix the reflectance spectrum of each pixel R_c , into fractional abundance f_i of its endmembers, $R_{e,ij}$. When using this method, the constraints of fraction overflow and underflow and summation to unity are generally applied.

Equation 2-2 The equations that govern linear spectral mixture analysis (Van der Meer, 1996).

$$R_c = \sum_{j=1}^n f_j R_{e,ij} + \epsilon_i \quad \text{and} \quad \sum_{j=1}^n f_j \leq 1 \text{ and } > 0$$

Where:

- R_c = the reflectance of the mixed spectrum in image band i for each pixel
- f_i = the fraction of each endmember j
- $R_{e,ij}$ = the reflectance of the endmember spectrum j in band i
- n = is the total number of endmembers
- ϵ_i = the residual error

A best-fit solution to this equation can be found by means of a linear least-squares approximation which minimizes the residual error, ϵ_i . The residual error is defined as the difference between the measured and modeled DN in each band (Equation 2.3). The residual errors from each band are summed and averaged to produce a root mean square (RMS) error.

Equation 2-3 Root Mean Square Error

$$\text{RMS} = \sum_{k=1}^m \left\{ \sum_{j=1}^n (R_{jk} - R'_{jk})^2 / n \right\}^{1/2} / m$$

Where:

RMS = error calculated from the difference of the modeled (R_{jk}) and measured (R'_{jk}) pixel spectrum.

n = the number of spectral bands

m = the number of pixels with in the image.

R_{jk} = modeled pixel spectrum

R'_{jk} = measured pixel spectrum

Finally the sum of the abundances are calculated on a pixel-by-pixel basis to produce the RMS error. Each of these fractions and the estimate of RMS error are calculated pixel-by-pixel across the entire image. As a result each endmember fraction and the RMS error can be displayed in image format to illustrate the spatial variability of scene fractions and SMA errors (e.g. Figure 2-4).

2.5.3 Forestry Applications

Spectral mixture analysis has proven a robust method for the extraction of biophysical data from remotely sensed imagery in low relief environments. Significant improvements over more traditional methods, such as vegetation indices, have been shown (Hall et al., 1995; Peddle, 1997; Mustard and Pieters, 1989). Once SMA has produced component fractions they can be related to the biophysical parameters of interest through regression analysis. This method accounts for some of the factors which have limited the success of

other approaches based on overall pixel level reflectance (Peddle, 1997), such as the influence of background reflectance on vegetation indices. The relative abundance of each component within the IFOV will change with differences in forest structure and biophysical parameters, which is the basis for using SMA fractions to predict biophysical data. Hall et al. (1995) have shown empirically and theoretically that the areal proportions of these radiometric elements are related to a number of stand biophysical parameters. Specifically, they showed that the shadow fraction increased with increased LAI; this relationship will be important to this thesis research. This method represents a shift away from direct inference of biophysical data from pixels to use of sub-pixel scale information.

Little work has been reported in the literature that deals explicitly with spectral mixture analysis in high relief environments. It has been shown that the relative proportions of scene component fractions are a function of stand structure; however, they will also be influenced by terrain and illumination geometry. In low relief situations, illumination is a function of the sun and sensor location. In high relief environments, this geometry is also influenced by local terrain. Therefore, for a given image date and time in high relief environments, there will be variation in surface illumination geometry across the scene. This will influence the scene component fractions visible to the sensor, in turn influencing the fractions determined using SMA. For example, a forest stand with the same structure and density under different illumination conditions will have different scene component abundances visible to the sensor. These changes have not been documented, so their influence on the prediction of forest biophysical parameters is not known.

2.6 Spectral Endmembers

The identification and spectral properties of the individual scene components that are expected to contribute to the overall pixel level reflectance are important concepts in spectral mixture analysis as well as with forest reflectance models (discussed later).

Endmember selection is based on identifying the individual components expected to contribute to the overall pixel level reflectance recorded by the sensor. In a forestry setting, it is known that stand-level reflectance of canopies with distinct geometric features, such as conifers, are related to sunlit canopy, sunlit background, and shadow (Li and Strahler, 1985; Jasinski, 1991). Figure 2-5 shows conceptually the main scene components that contribute to the pixel radiance, these are called endmembers. Once the endmembers have been identified, their spectral properties are obtained. For both spectral mixture analysis and forest reflectance models, the purest (without the presence of other surface materials) spectral response patterns of these scene components are required.

Endmember spectra values for each scene component are located at the vertices of a simplex in spectral space, occurring at the *end* of a spectral continuum associated with each material (hence the term 'endmember'), as shown in (Figure 2-6). Endmember values represent the purest spectral measurement for each of the scene components. All the pixels which lie within the simplex will be composed of different compositions of scene components. In a physical sense, different mixtures of forest scene components represent different forest structures. Pixels outside the simplex would be comprised of materials not accounted for with this endmember set. For example, in a forestry setting, a road passing through the image would not be characterized using the sunlit canopy, sunlit background and

shadow endmembers, and therefore would be outside the simplex. These endmember values can be estimated, measured or modeled in a number of ways. Generally there are two approaches: reference endmembers and image endmembers, as discussed next.

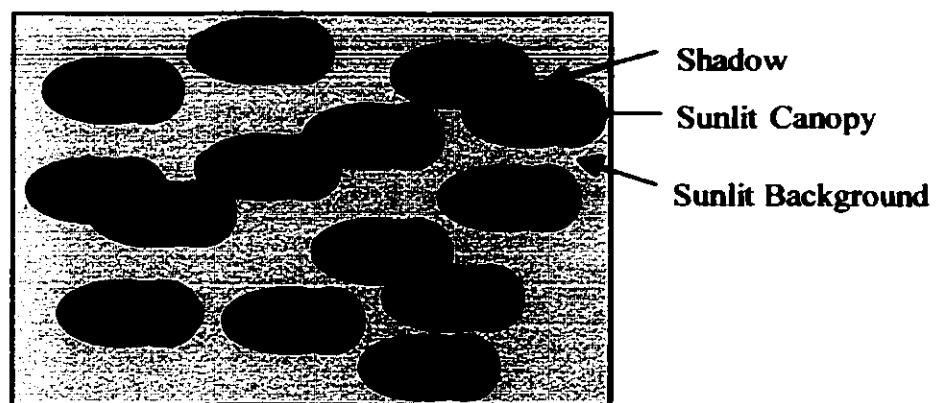


Figure 2-5 A conceptualized view of a forest canopy as seen by a remote sensing instrument, showing the three main scene components; sunlit canopy, sunlit background and shadow.

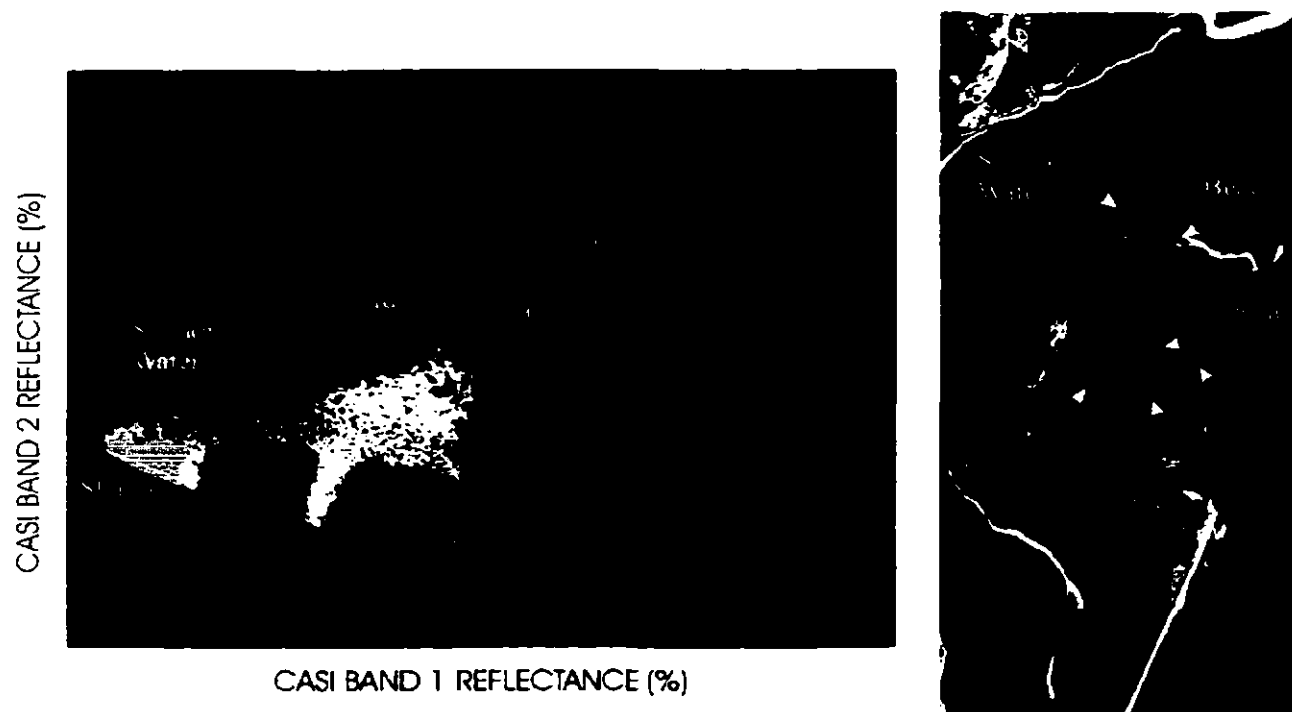


Figure 2-6 Left image: CASI band 1 versus band 2 – axis have been rotated to provide the best view of the relative spectral properties of various ground materials. Endmember values for each scene component are located at the vertices of a simplex in spectral space, shown as the white triangle. Right image: Shows the spatial positions in the image of those pixels shown in spectral space (colours match in both images).

2.6.1 Reference Endmembers

The spectral properties of reference endmembers are obtained using a spectroradiometer either in the field or in a laboratory setting. A reference endmember represents the purest measurement of an endmember value. However, the use of reference endmembers depends on having a well-calibrated image. If the reference endmember spectra collected on the ground are to be related to an image, both the image and endmember measurement need to be calibrated to reflectance, which is the fundamental unit of measurement in remote sensing. Reflectance is a measure of the spectral properties of a

material once the influence of the atmosphere, illumination and view angle have been removed. The concept of reflectance will be expanded on later. The use of reference endmembers is also dependent on the assumption that the sample material adequately represents the spectra of the endmember in the scene (Tompkins et al, 1997). For example, a field or laboratory spectrum of the sunlit canopy maybe difficult to capture in a single spectral measurement, since the combination of needles and branches which most appropriately characterizes the sunlit proportion of the canopy may be difficult to reproduce and measure. However, carefully collected reference endmembers can provide an accurate measure of the spectral properties of the main scene components.

2.6.2 Image Endmembers

Image endmembers are selected directly from the imagery and there is no need for field or laboratory measurements or detailed image calibration. However, depending on the image spatial resolution and the size of the scene component features, individual pixels within an image may not always represent a pure sample of a scene component. Pixels may be deemed to contain homogeneous samples of the components of interest and can serve as spectral endmembers. Image endmembers are usually selected through an iterative process, similar to the process of selecting training sites in supervised classification. The difference between the two being that endmember selection is focused on selecting the purest sample of a surface material in an image rather than a training area which is a set of pixels that characterize the full variability of a class. Within the image, pixels are chosen from those areas that are thought to contain homogeneous samples of the endmember material. These

initial endmembers are used to produce fraction values and an estimate of RMS error for each pixel in the image. These initial selections are improved through a process of iterative fraction validation. The fraction values produced using the SMA algorithm are compared to fraction values assessed either manually or through a classification approach (discussed later). The error between the two methods is used to iteratively improve the initial endmember selection.

2.6.3 Modeled Endmembers

Another approach to the trial and error method would be a statistical approach such as principle component analysis (PCA) or convex hull geometry (Tomkpins et al, 1997, Peddle, 1997). These methods attempt to locate endmembers in spectral space. PCA is used to determine the dimensionality of the image data, which defines the number of endmembers. Then an n-dimensional polyhedron is fit to the data using convex hull geometry, essentially fitting all the data within the smallest possible simplex. Unfortunately, these calculated endmembers must be used with caution, as they may not be realistic in a physical sense. Peddle (1997) suggested that the uncertainty associated with the physical representation of modeled endmembers makes their use inappropriate in complex environments from which quantitative information extraction is the goal. Canopy reflectance models have also been used to model endmember values, as in Hall et al, (1995, 1996) and Peddle et al, (1999b).

2.7 Geometric Optical Reflectance Models

Physical models of forest stands provide a powerful image-processing tool for the extraction of forest structural information from remote sensing imagery. Physically based algorithms have not been as widely used as empirically based spectral or textural methods, although there are several researchers who have focused on these methods (Strahler and Jupp, 1990; Franklin et al., 1991; Woodcock et al., 1994; Wu and Strahler, 1994; Li and Strahler, 1985).

Goel (1998) provided a good review of the different types of canopy reflectance models. He categorized them into four groups: (1) geometric optical (2) turbid medium (3) hybrid models of 1 and 2 and (4) computer simulations. The type of model used will depend on the focus of the study; to derive forest related parameters from airborne or satellite images, geometric optical models have been recommended (Li and Strahler, 1986, Gemmell, 1998). Previous studies have shown that geometric optical models have been able to provide useful biophysical information (Hall et al, 1995; Peddle, 1997; Woodcock et al, 1997). The development of geometric optical models and use of the Geometric Optical Mutual Shadowing (GOMS) model used in this study are described in the following sections.

2.7.1 Theory

In the geometric optical approach to forest reflectance modeling, the bi-directional reflectance is modeled as a purely geometric phenomenon (Li and Strahler, 1985). These models treat vegetation canopies as collections of individual, discrete three-dimensional objects, which cast shadows onto a contrasting background. The driving variables are the

shape of the objects, their count density and their spatial arrangement which control the amount of sunlit canopy, sunlit background and shadow visible to the sensor at a given view and illumination angle (Li and Strahler, 1992). Geometric optical models have progressed from simple cylinder model representations which characterized the tree crown as cylinders defined by the height and width of tree crowns as observed in the field (Jasinski and Eagleson, 1989, 1990). The advantage of these models is that only a small number of inputs are required, however the cylinder shape does not always accurately characterize the canopy which can lead to difficulties in representing canopy shadow. Li and Strahler (1985) introduced the next advancement in geometric optical models. This new model represented individual trees as cones, that provided a better characterization of the bi-directional reflectance of the canopy. The model could also be run in both forward and inverse mode. In forward mode the model predicts pixel brightness values based on size, shape, density and illumination angles. In inverse mode it estimates the mean height, shape and density of the canopy based on pixel brightness values in the image.

The next evolution in geometric optical models (Li and Strahler, 1982) still incorporates the two modeling modes but introduces a spheroid shape to characterize tree canopies and the ability to account for terrain variations and off-nadir view angles. This model (Li and Strahler, 1992) is also enhanced to include the effects of shadows falling on adjacent tree crowns or mutual shadowing. This geometric optical mutual shadowing (GOMS) model has been incorporated into this research. The theoretical basis for the GOMS model can be found in Strahler and Jupp (1990) and Li and Strahler (1992, 1986). The GOMS model is designed to simulate the bi-directional reflectance function (BRF) of individual pixels. The model treats vegetation canopies as collections of individual, discrete

objects, that cast shadows onto a contrasting background (Figure 2-7). As a geometric-optical model, it relies on the three-dimensional structure of the canopy as the primary factor influencing scene reflectance. The model assumes that the satellite or airborne measurements (pixels) are larger than the size of individual tree crowns, but smaller than the size of forest stands. The signal received by the sensor is modeled as a linear combination of reflected light from tree crowns, their shadows, and the background within the field of view of the sensor. The model is calibrated with three distinct types of data: i) data describing the physical shape of the tree crown and structure of the forest canopy; ii) spectral endmember values of scene components and; iii) viewing and illumination geometry. The physical dimensions of the individual crowns and the structure of the stand are defined by λ (stand density), r (horizontal crown radius), b (vertical crown radius), h (height) and dh (height distribution). The spectral properties of each scene component are specified as P_c (canopy endmember spectra), P_b (background endmember spectra), and P_s (shadow endmember spectra). The view geometry and terrain variables are defined with slp (slope), asp (aspect), SZA (solar zenith angle) and AZM (solar azimuth angle). These input values are outlined in Table 2-3.

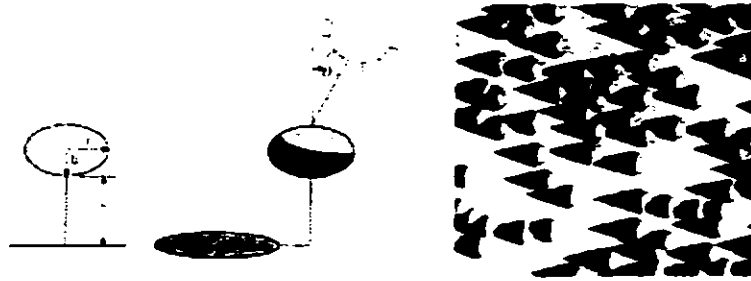


Figure 2-7 The GOMS model characterizes forest vegetation (individual tree crowns) as discrete three-dimensional spheroids, note the input parameters: h = tree height, r = crown radius and b = crown depth. The right image shows a simulated assemblage of trees, shadow and background in a pixel.

Table 2-3 Required inputs into the GOMS Optical Reflectance Model.

Symbol	Physical Description	Units
λ	Tree density within the pixel (sensor IFOV)	Trees/pixel (dimensionless)
r	Horizontal crown radius (Spheroid, Figure 2-7)	Metres
b	Vertical crown radius (Spheroid, Figure 2-7)	Metres
h	Height from ground to base of crown (Spheroid, Figure 2-7)	Metres
dh	Height distribution of trees	dimensionless
$-c$	Endmember value of sunlit canopy	% reflectance
$-b$	Endmember value of sunlit background	% reflectance
$-s$	Endmember value of shadow	% reflectance
slp	Slope of pixel	degrees
asp	Aspect of pixel	degrees
SZA	Solar Zenith Angle	degrees
AZM	Solar Azimuth Angle	degrees

These models can be used in either forward mode or in inverse mode. In forward mode the model requires as input the tree shape and canopy density together with endmember spectra and terrain values. Forward mode output consists of the pixel level reflectance value and the individual component fractions. In inverse mode, the model uses pixel reflectance values measured by airborne or satellite sensors together with endmember

reflectance values and terrain information as input, with the output consisting of tree height, shape and density within the pixel. Improvements are still needed in the ability of these models to estimate height (Woodcock et al, 1997, Franklin et al. 1988). However, these types of models provide the potential to help extract detailed biophysical parameters based on their measured spectral characteristics. Effective use of this model in simulating a real canopy requires attention to two issues. First, how to determine the appropriate endmember reflectance and the physical canopy dimension measures needed to parameterize the model, and secondly, how to relate the output to estimate stand level biophysical information.

2.7.2 Forestry Applications

Applications using forest reflectance models to extract biophysical data have often been based on model inversion (Strahler and Woodcock, 1986; Franklin et al., 1991; Wu and Strahler, 1994; Gemmell, 1998). The inversion method provides a more objective means by which to model biophysical characteristics directly from remote sensing. The inversion method works by adjusting model parameters until the model reflectance matches the radiance recorded in the image (Goel, 1998). The advantage of using reflectance models to extract biophysical data is that they do not require an empirical calibration of reflectance values in the image with measured biophysical data on the ground. Rather, reflectance models can be applied in all site and sampling conditions provided basic ecosystem characteristics are known (Gemmell, 1998). Variable results have been reported in the ability of these models to extract forest structure parameters. Woodcock et al., (1993) showed that these models can provide accurate estimates of timber volume, growth form,

species association labels and conifer cover; however, tree size labels were found to be unreliable with single date Landsat imagery.

Fewer studies have been done using forest reflectance models in high relief environments. Gemmell (1998) has incorporated the effects of terrain on the inversion of a forest reflectance model. Gemmell identifies three ways that terrain influences stand reflectance: i) sloping terrain changes the area of shadow visible to the sensor, ii) component spectral distribution are related to terrain and iii) the effect of mutual shadowing on crowns. That study focused only on stands in the principal plane of the sun so that the influence of slope, coverage and stand structure could be examined. His results showed that the influence of terrain (slope and aspect) on reflectance, if not accounted for, would preclude the extraction of forest coverage information. Accounting for the influence of terrain does not require a significant amount of additional information, as only a measure of slope and aspect are required. However, the acquisition and registration of an appropriate resolution DEM can require significant efforts.

2.8 Terrain Normalization of Spectral Data

2.8.1 Theory

One radiometric problem, which is explicitly related to high relief environments, is the influence of terrain on the data recorded by the sensor. The effects of terrain have been defined as the variation in radiance from inclined surfaces compared to the radiance from a horizontal surface as a function of the orientation of the surface to the light source and sensor position (Holben and Justice, 1980). Terrain normalization algorithms are used to reduce the

influence of terrain on remotely sensed spectral responses. However, a general problem in terrain normalization is that the effects of slope and aspect on forest reflectance are not well understood (Gemmell, 1998). Digital numbers (DNs) are used to represent the intensity of the reflected energy recorded by the sensor. Unfortunately the reflected energy recorded by the sensor is related to more than the reflective and emissive properties of the objects in the scene. There are a number of additional factors, which interact to influence the radiance recorded by the sensor, as described in section 2.3.2. If there were no atmospheric attenuation and the terrain were flat and all objects being imaged had Lambertian reflectance (reflected equally in all directions) characteristics, the radiance recorded by the sensor would simply be a function of the reflective properties of the forest and the intensity of irradiance. This section focuses on the correction of slope-aspect induced variations on irradiance values as measured by remote sensors.

2.8.1.1 Radiometric Normalization of Spectral Data

The goal of a slope-aspect terrain correction is to remove all the terrain-induced illumination variation so that two identical objects or surfaces will have the same brightness values (DNs) in the image, regardless of their different orientations toward the sun (Meyer et al., 1993, Jensen, 1996). As a visible consequence of this correction, the three-dimensional impression of terrain should be suppressed and the image should appear flat. Basic to any radiometric correction is illumination. Illumination is defined as the cosine of the angle(s) of incident solar radiation reaching a pixel. The illumination is therefore dependent on the relative orientation of the pixel towards the sun's position (Figure, 2-8) (Meyer et al, 1993).

In the following sections, four different terrain normalization methods are reviewed as identified by Teillet et al (1982). Each method is based on the amount of illumination incident on a pixel. Each of these methods requires a digital elevation model (DEM) to be geometrically registered and resampled to the same spatial resolution as the imagery (Jensen, 1996). The DEM is used to calculate measures of slope and aspect for each pixel in the image. The spatial resolution of the DEM determines to a great degree the level of illumination correction that can be achieved.

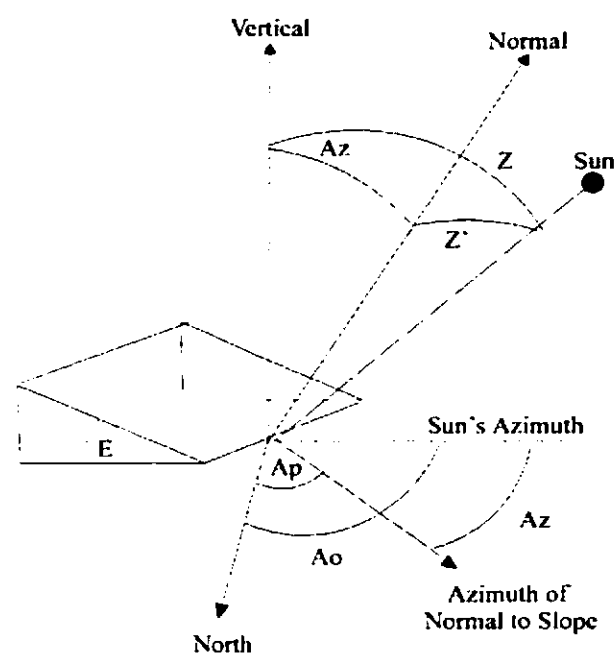


Figure 2-8 Diagram showing the zenith angle, Z , incident angle Z' , surface slope = angle of exitance, E , solar azimuth, A_o , aspect of the surface, A_p , and aspect of the surface, A_z (After Holben and Justice, 1980).

2.8.1.2 Cosine Correction

The cosine correction is a trigonometric approach which takes into account the portion of direct illumination incident on each pixel as a function of slope and aspect, (Equation 2-4). This approach makes several important assumptions: (1) the surface is Lambertian; (2) there is a constant distance between the sun and earth, and; (3) there is a constant amount of solar energy reaching the surface.

Equation 2-4 The Cosine Correction

$$L_h = L_t \frac{\cos\theta}{\cos i}$$

Where

L_h = radiance observed for a horizontal surface

L_t = radiance recorded by the sensor (the original DN in the image)

θ = solar zenith angle

i = solar incident angle in relation to the normal of the pixel

As a first approximation, this is a simple method of correction as only data on the solar zenith angle and terrain illumination are needed. However, this method does not account for diffuse illumination, which can account for a significant amount of irradiance within forest canopies and on slopes facing away from the sun.

As the $\cos i$ decreases, the magnitude of the correction increases. Consequently, for weakly illuminated areas (e.g. facing away from the sun or on steep slopes), the cosine correction applies a disproportional brightening effect (Jensen, 1996; Meyer et al., 1993).

2.8.1.3 Statistical-Empirical Method

For each location (pixel) in an image, it is possible to relate the predicted illumination ($\cos i \times 100$) from the DEM and the DN recorded by the sensor. Meyer et al., 1993 related the DNs for known forest stands with predicted illumination values by producing a scatter plot. The slope in this graph suggests that a constant forest type will appear differently (have different DNs in the image) on different terrain. By rotating the regression line to the horizontal, these effects can be reduced. The Statistical-Empirical equation is shown below.

Equation 2-5 The Statistical-Empirical Correction

$$L_h = L_t - \cos(i)m - b + \bar{L}_t$$

Where

L_h = radiance observed for a horizontal surface

L_t = radiance recorded by the sensor (the original DN in the image)

\bar{L}_t = is the average of L_t for forest pixels (constant stand type)

i = sun's incident angle interrelation to the normal of the pixel

m = slope of regression line

b = y intercept of regression line

This model assumes a linear correlation between the original DNs and illumination.

The application of this method makes a specific object independent of illumination and corrects the difference in DNs or radiance value throughout the image caused by terrain.

2.8.1.4 C-Correction

The C correction takes advantage of the statistical empirical method to help account for the effects of path illumination. Teillet et al. (1982) introduced an additive term to the Cosine correction c , as shown in equation 2-5.

Equation 2-6 The C-Correction

$$L_h = L_t \frac{\cos\theta + c}{\cos i + c}$$

Where:

- L_h = radiance observed for a horizontal surface
- L_t = radiance recorded by the sensor (the original DN in the image)
- θ = solar zenith angle
- i = solar incident angle in relation to the normal of the pixel
- c = correction parameter b/m
- m = inclination of regression line
- b = y intercept of the regression line

Teillet et al. (1982) suggest that the c parameter emulates the path irradiance not previously accounted for; however, no physical analogies were presented. Essentially, the C correction weakens the over-brightening introduced to poorly illuminated pixels or pixels on steep slopes produced by the cosine correction.

2.8.1.5 Minnaert Correction

The Minnaert correction (Equation 2-7) is the basic cosine correction (Equation 2-4) with a coefficient k introduced to account for the Lambertian properties of the surface.

Equation 2-7 The Minnaert Correction

$$L_h = \left(L_t \frac{\cos\theta}{\cos i} \right)^k$$

Where:

- L_h = radiance observed for a horizontal surface
- L_t = radiance recorded by the sensor (the original DN in the image)
- θ = solar zenith angle
- i = solar incident angle in relation to the normal of the pixel
- k = Minnaert constant

The Minnaert constant is considered to be the degree to which a surface is Lambertian. The k value varies between 0 and 1, where the smaller the k value the less Lambertian the surface. The less Lambertian the surface, the less influence the quotient has in Equation 2-6. Thus one can overcome the over correction obtained by the simple cosine correction (Meyer et al., 1993). The k parameter can be determined empirically, (Meyer et al, 1993), or alternatively values reported in the literature can be used.

The improvement provided by each method is a function of the illumination value i ($\cos(Z')$). Meyers et al., (1993) have shown that slope-aspect correction improved the

accuracy of classification between forest and non-forest in faintly illuminated areas, without having an adverse effect in sunny areas. Improvements in classification accuracy of approximately 5% were achieved in faintly illuminated areas. The differentiation of different forest classes was more pronounced in sunny areas. Meyer et al, (1993) reported that improvements of between 10 and 30% could be achieved in brightly illuminated areas with $\cos(Z') > 0.6$.

2.8.2 Sun-Canopy-Sensor Geometric Approach

Terrain correction of forested images needs to be rooted in the consideration of canopy structure (Gu and Gillespie, 1998). The above methods of terrain normalization attempt to remove variations in illumination introduced as a function of sun-surface-sensor geometry. However, these methods make no attempt to account for variations internal to the forest canopy, often leaving residual topography (under correction) or 'negative' topography (over correction) (Gu and Gillespie, 1998). These residual effects can be attributed to an oversimplification of the canopy's bi-directional reflectance function (BRDF), the neglect of diffuse illumination, and inaccurate DEMs (Gu and Gillespie, 1998). Due to the inherent internal structure of forest canopies, sun-surface-sensor geometry is not the proper approach to terrain normalization. Rather, a method that accounts for the variations internal to the stand is required. As the terrain changes so does the stand structure relative to the sun. For example, the amount of sunlit canopy, sunlit background and shadow visible to the sensor will change. There will be more sunlit canopy visible to the sensor on slopes facing the sun

compared to those facing away, which is a function of stand structure relative to the sensor and shadow length.

Gu and Gillespie (1998) introduced a method of terrain correction that accounts for the sub-pixel scale interactions within the forest canopy. This model is based on the Sun-Canopy-Sensor (SCS) geometry rather than the sun-terrain-sensor approaches (cosine, C correction etc.). The authors identify three levels of interactions between light and a natural surface. At the first scale, light interacts with individual tree elements such as branches and needles. The second level is the crown, where the interactions of light are controlled by stand density, structure, and leaf orientation. The third scale is the canopy, which is characterized by interactions of light among trees. The SCS correction does not account for the first two scales of interactions; as trees are geostropic (grow perpendicular to the gravitational field) the first two scales are independent of terrain. Terrain effects are introduced at the third scale because the stand structure relative to the sensor is controlled by terrain. The SCS model works by characterizing the amount of sunlit canopy area as a function of the geometry between the sun, sensor and terrain. The authors suggest that complications introduced by stand structure (density, age etc.) make exact characterization of the forest structure difficult, therefore approximations were made to build several simplified models of tree crown shape, tree height, and tree density. This approach is a more physically based method and shows improved results over sun-terrain-sensor correction methods. The authors acknowledged that this approach only accounts for the sunlit portion of the canopy and that shadows and canopy obscured from the sensor's view may still substantially contribute to the total pixel reflectance.

2.9 Chapter Summary

In this chapter, remote sensing of forest biophysical parameters was reviewed. The focal points included the use of spectral mixture analysis and forest reflectance models to account for the influences of terrain in predicting leaf area index. The advantage of spectral mixture analysis over traditional methods of estimating biophysical parameters is its ability to explicitly account for the influence of background vegetation and shadow in the radiance recorded by the sensor. SMA is able to quantify the abundance of each scene component that contributes to the overall pixel reflectance at the sub-pixel scale. The relationship between the sub-pixel scale fraction and forest structure has been well demonstrated in flat terrain and provides the basis for the strong predictive capability of SMA. The effect that terrain has on the scene fractions produced using SMA has not been well documented; however, it is believed that terrain changes the orientation of the forest structure relative to the sensor, limiting the ability to make an accurate estimation of LAI, if not account for. Forest reflectance models will be introduced into this analysis as they can provide the same sub-pixel scale fractions of the scene component but they also offer the ability to explicitly account for stand structure, terrain and illumination geometries. It is hypothesized that using forest reflectance to explicitly account for stand structure in images normalized for terrain will improve the estimation of LAI in mountainous terrain.

CHAPTER THREE

METHODS

3.1 Introduction

In this chapter a description of the experimental design and methodology developed to test the ability of SMA and forest reflectance models to predict LAI in mountainous terrain is presented. The chapter begins with a description of the study area and the image and field data collected. Four distinct groups of data were collected to facilitate this research, airborne CASI image data, forest structural data, spectral field data, and field positional data, each of which was necessary for this analysis. The details of collecting and processing of each data set are provided. The chapter continues with the development of an experimental design to test the use of spectral mixture analysis in high relief environments using conventional illumination based normalizations. Next, the need for a new method that accounts for the internal forest structure in terrain normalization is described and a new approach to using forest reflectance models in multiple forward mode (MFM) is introduced. The details of the development, use, and output of the MFM are discussed in detail. Finally, the analytical approach developed to evaluate these various methods for predicting LAI is provided.

3.2 Study Area and Data Set

3.2.1 Kananaskis Study Area

The study site is centered at 115°4'20"W, 51°1'13"N on the eastern slopes of the Rocky Mountains straddling Barrier Lake in Kananaskis Provincial Park, Alberta, Canada (Figure 3-3). This region covers approximately 77km² and includes a full range of terrain aspects, and slopes ranging from 3° to 30°. The site is within the montane/sub-alpine forest region M.5, and is dominated by stands of Lodgepole Pine (*Pinus contorta* LAMB.), Engelmann Spruce (*Picea engelmannii* Parry ex Engelm), White Spruce (*Picea glauca* [Moench] Voss), trembling aspen (*Populus tremuloides* Michx.), balsam poplar (*Populus balsamifera* L.) on lower, more moist slopes, and some scattered Douglas fir (*Pseudotsuga menziesii* (Mirb.) Franco) (Rowe, 1972). LAI ranged from 1 to 8 in this area. Within the greater Montane Cordilleran ecozone, this area lies near the southern border of the Eastern Continental Ranges ecoregion, as defined by Environment Canada (1997). Although these subalpine summers are cool and damp while the winters are cold with snow, there is considerable variation in temperature (e.g. Chinooks). Mean summer temperature is 12°C and the mean winter temperature is -7.5°C. Temperatures can range from -45°C to 35°C. Although only 30% of the precipitation received falls as snow, the mean annual precipitation ranges from 600-800mm, which increases with elevation from east to west. The study area ranges in elevation from approximately 1400m at Barrier Lake to 2000m at the top of Prairie View.

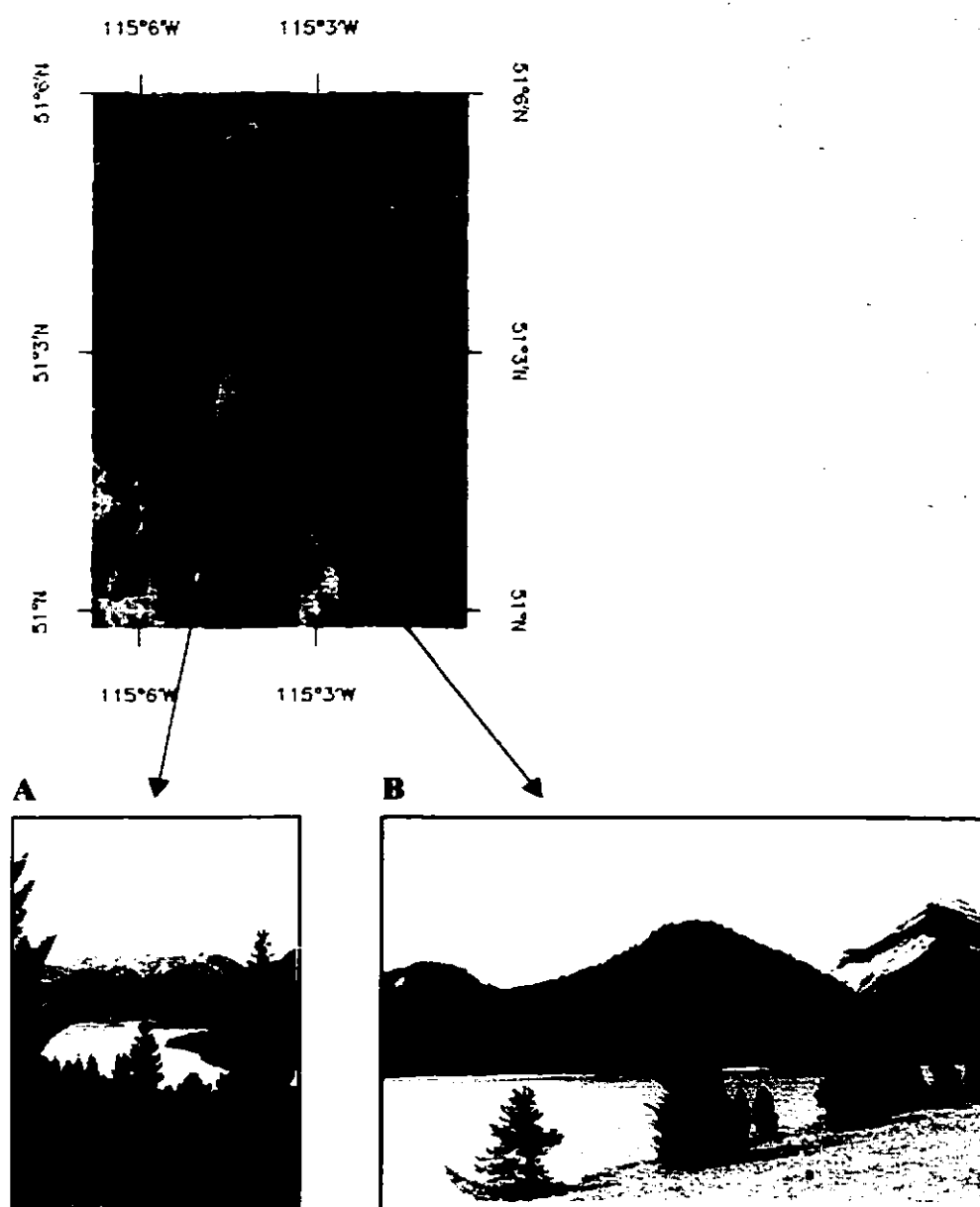


Figure 3-1 Study Area. The Barrier Lake study site is located in Kananaskis Provincial Park, Alberta, Canada, on the eastern slopes of the Canadian Rockies. Barrier Lake is centered at $115^{\circ}4'20''\text{W}$, $51^{\circ}1'13''\text{N}$. Photo A was taken looking south toward the end of Barrier Lake. Photo B was taken looking across Barrier Lake towards the southern knoll, to show the variability in terrain in the study area. The locations of the images are shown on a Landsat TM image (red arrows).

3.2.2 Field Data Collection and Processing

The collection of *in situ* ground data enabled the correction of atmospheric effects in the remote sensing imagery, serves as image and ground positional control, and provided the basis for associations between the image spectral properties and ground features (LAI in this study). Knowledge of what exists at a particular location in both the imagery and on the ground is the foundation needed to develop and test quantitative remote sensing methods.

The data collected and the routines used to make the measurements in the field were specifically designed to address the needs of this research. Four distinct sets of ground data were collected. First, field spectra data were collected to correct for atmospheric effects and to function as reference endmembers for both spectral mixture analysis and the forest reflectance model. Second, ground-based estimates of LAI were made for each plot using two optical instruments, and formed the basis for comparing different remote sensing techniques. Third, forest structural data were collected to provide the needed geometric data for the forest reflectance model. And lastly, field and image position data were acquired using a global positioning system (GPS) to ensure that field measurements could be accurately identified in the image. These sets of data are described in the following sections.

3.2.2.1 Ground Spectral Measurement

Accurate spectral measurements were key to this research since, without them the relationships between image and field data could not be established. There were two requirements for the spectral data. First, field measurements were needed of ground

radiometric calibration targets visible in the imagery to correct for atmospheric effects. A proper atmospheric correction ensures that each of the image resolutions will be calibrated not only to one another, but also to other spectral measurements taken on the ground. Second, spectral measurements were collected of individual scene components to act as reference endmembers in both spectral mixture analysis and the forest reflectance model. To facilitate these measurements a spectroradiometer manufactured by Analytical Spectral Devices was used to collect the spectral measurements (ASD, 1998). The ASD full-range (ASD-FR) spectroradiometer model used in this research measures reflected radiance in the range 350 - 2500 nm. The magnitude of energy reflected by an object is a function of the amount of incoming solar radiation (irradiance), the atmospheric conditions, the time and date (solar angle), the orientation of the material relative to the sensor, and the characteristics of the material (Milton, 1987). Variations in the intensity and nature of illumination can be accounted for by taking a ratio of radiance to irradiance over a specific wavelength range, to produce a measure of reflectance. Spectral reflectance is related only to the characteristics of the target and is independent of illumination variations (Peddle, 1999; ASD 1995). This measurement can then be related directly to other reflectance measurements taken under different conditions, and is therefore the standard unit of spectral measurement in remote sensing.

3.2.2.2 Spectroradiometer Instrumentation

The ASD spectroradiometer is designed with a fibre-optic cable which extends to a pistol grip that holds a field-of-view (FOV) barrel. The FOV barrel allows the area viewed

by the sensor to be controlled (Figure 3-2). The pistol grip was attached to a tripod so that the view angle and sensor height above the target could be accurately controlled. A measuring tape was used to establish the height of the FOV barrel above the target and an inclinometer was used to ensure that the FOV barrel was nadir. A 5° FOV barrel was used for all measurements to ensure a good spatial coverage of the target and to prevent the viewing of material other than the sample. The spectroradiometer used in this fieldwork was able to acquire rapid, multiple measurements of the target. To ensure an acceptable signal to noise ratio, each sample was the average of 10 spectral scans. To remove signal noise internal to the spectroradiometer, a dark current measure was recorded prior to each measurement. This measurement allowed any internal signal to be removed from the final spectral measurement (ASD, 1995).



Figure 3-2 ASD spectroradiometer setup for radiance measurements in the southern parking lot during image acquisition.

3.2.2.3 Reflectance Calibration

To acquire a measurement of irradiance coincident to the target radiance measurement, a reflectance panel is typically used. These panels have known spectral and angular reflective properties, that allow for an accurate measurement of irradiance to be obtained (Peddle, 1998). The panel used in this research was composed of pressed polytetrafluoroethylene (PTFE), commercially available as Spectralon (Labsphere, 1998). Spectralon offers nearly Lambertian properties and high reflectance values (nearly 98%) over a wide spectral range (350-2500nm). The manufacturer calibrated this panel, to allow for variation in the reflective properties of the panel to be characterized during post-processing.

3.2.2.4 Reflectance Data and Post-processing

The following procedures were followed for each set of spectral measurements. The measurement of each target consisted of a spectral radiance measurement of the target and irradiance spectra collected from the Spectralon panel. Spectral reflectance values for a given SZA (θ) and at nadir view angle (ϕ) were computed over the full wavelength range recorded by the spectroradiometer, using equation 3-1. Subsequently, these values were reassigned to match the spectral bands collected in the CASI imagery. A linear spectral response function was used to relate the spectroradiometer measurements with the CASI band set. The individual spectral values measured by the spectroradiometer between the beginning and end point of each CASI band were averaged to produce a single spectral value representing that band (Figures 3-5, 3-6 and 3-7).

Equation 3-1 Surface Reflectance Equation

$$\text{Reflectance } (\theta, \phi) = \frac{\text{Target Radiance}}{\text{Panel Radiance}} \quad \chi \quad \text{Panel Calibration}$$

Where: Reflectance (θ, ϕ) = is the spectral reflectance for a given SZA (θ) and view angle (ϕ)

3.2.2.5 Airborne Image Calibration

To aid in atmospheric correction, ground based radiometric calibration spectra were collected during image acquisition at the south parking lot near Barrier Lake. Radiance measurements were acquired over four 3 x 3 m calibration targets, in addition to the asphalt parking lot (Figure 3-3). The radiometric targets were constructed of coloured bristle board. The radiance measurements were corrected to reflectance using calibrated irradiance measurements from the Spectralon panel. These targets were located in the imagery and used as pseudo-invariant targets to perform a linear atmospheric correction (Jensen, 1996). Subsequent examination of the reflectance values of each target showed that the white cardboard panels had nearly specular reflectance properties. Therefore, the white target was not used in the atmospheric correction.

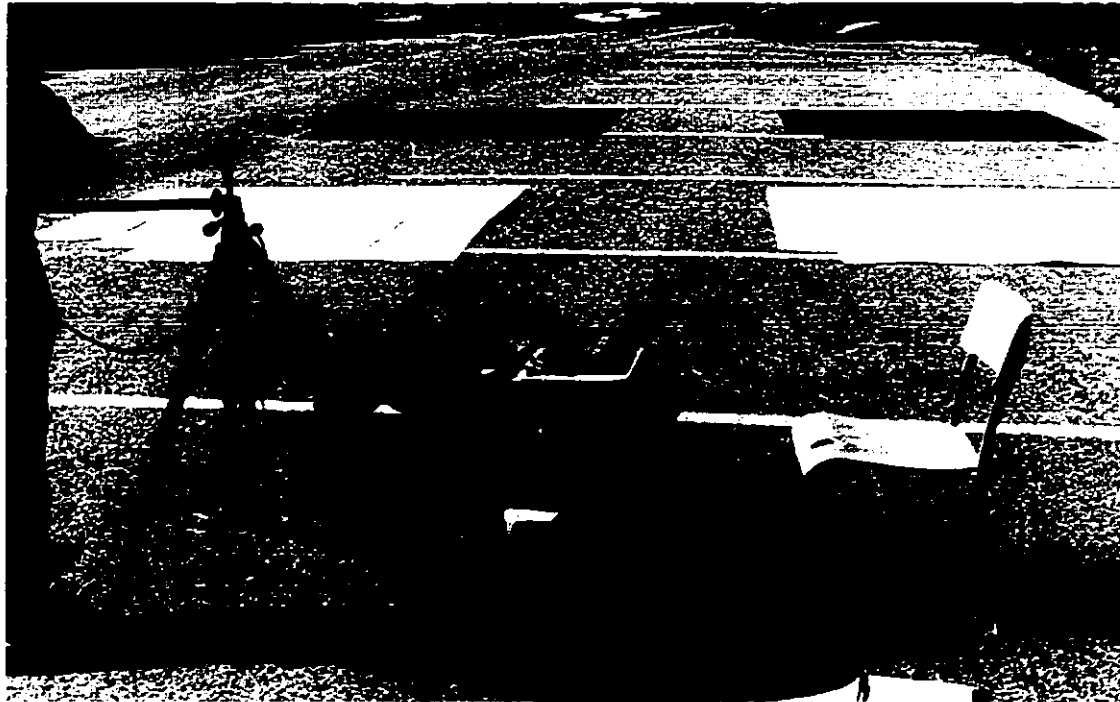


Figure 3-3 Calibration targets placed in the southern parking lot during image acquisition. Each target was 3 X 3 m to ensure that a pure pixel of each target could be located in the 60cm, 1m and 2m data sets. The collection site was established in an open area away from adjacent vegetation to avoid any illumination variations.

3.2.2.6 Endmember Spectra Collection

As a first step in endmember or scene component spectral data collection, each dominant canopy and understory species in the study area was identified. For each component, two separate spectral measurements were needed, a sunlit and shadowed spectra. The sampling strategy described by Peddle (1998) was used to acquire the needed component spectra. A stationary field measurement site was established in an open parking lot at the

southern end of the study site. This site ensured accurate measurements of spectra, avoiding the influence of adjacent, or understory vegetation, uneven terrain, and any other variations in the setup of the spectroradiometer. For this study, pure samples of each scene component were required. To facilitate these measurements, component samples were collected and removed to the measurement site. Samples were clipped from the vegetation of interest and assembled together into an optically thick stack, as described by Goward et al (1994) and Peddle (1998). Great care was taken to ensure that the natural orientation of the material was maintained while creating an opaque configuration such that the background was obscured from the sensor. The advantage of this method was that the operator could ensure that only component material of interest was visible to the sensor. The potential drawback would be an alteration in the natural orientation of the material; however, with due attention this approach can provide an efficient and accurate means of acquiring endmember spectral values.

The acquisition of sunlit component spectra was straightforward once the samples had been collected and arranged into optically thick stacks. The spectroradiometer was arranged such that the sample filled the FOV of the sensor. Two measurements were collected for each sample; the first was a target radiance measure, the second was a coincident measure of incident irradiance taken as the radiance of the Spectralon panel under the same illumination conditions. These measures were subsequently used to calculate the reflectance measure for each material, as described earlier. In contrast, the acquisition of shadowed component spectra was more involved. Radiance measurements of each target were collected under diffuse light conditions. A sheet of plywood was positioned in the principal plane of the sun in order to block all direct solar illumination (Figure 3-4). This

setup was used to acquire target radiance measurements of each of the samples of background and canopy component vegetation. Coincident with each diffuse target illumination measurement, a fully illuminated incident irradiance measurement was acquired using the Spectralon panel. Subsequently, an *apparent reflectance* measure (Peddle et al, 2000) was calculated, taking the ratio of diffuse target radiance to incident irradiance to generate the shadow component endmember. This method of computing the shadow component spectrum provides an appropriate representation of shadow for use in spectral mixture analysis and forest reflectance modeling (Peddle, 1998). Figures 3-5 and 3-6 show spectral curves of the reference endmember set for a pine stand as measured with the spectroradiometer. Note that in these figures the unusually high reflectance values at 1400nm, 1800nm and 2500nm are a result of signal errors near the ends of the spectral range of individual detectors within the ASD spectroradiometer (it has three detectors).

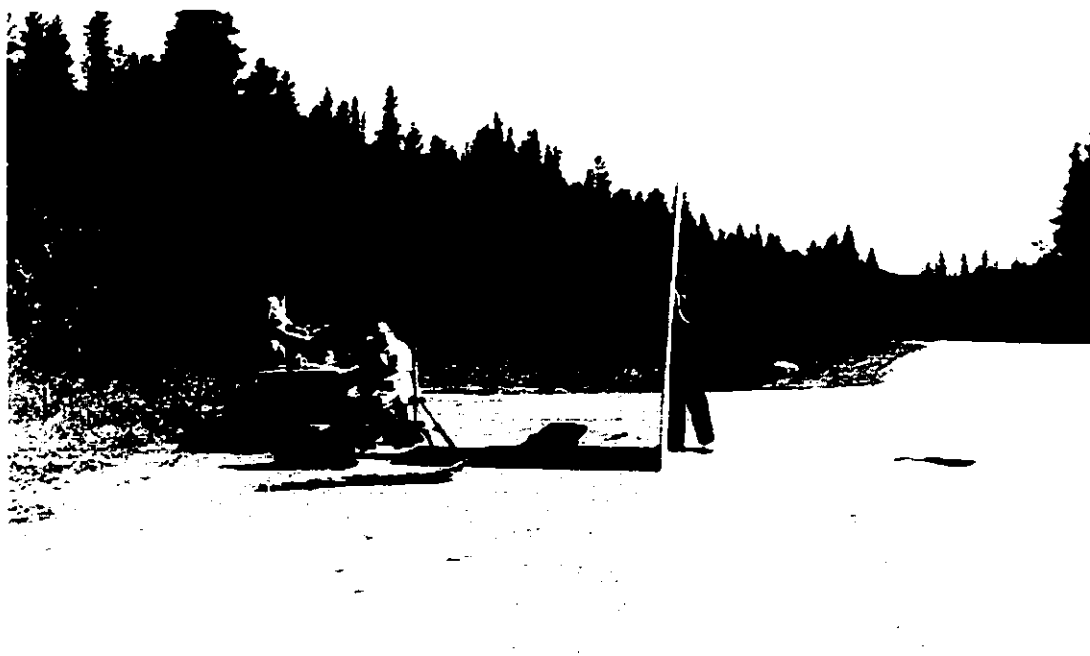


Figure 3-4 The collections of apparent reflectance spectra to represent the shadow endmember in the reference endmember set.

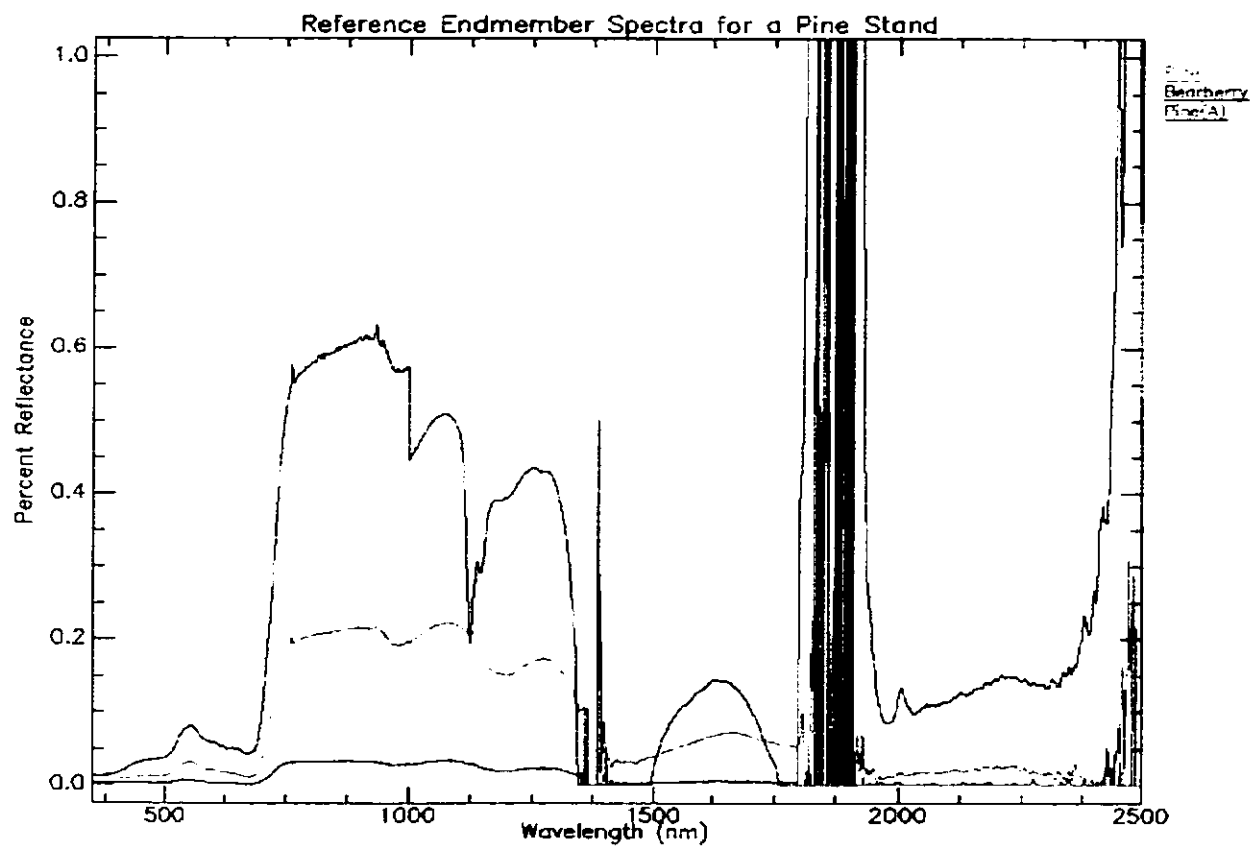


Figure 3-5 Reference endmembers reflectance spectra for a Lodgepole pine stand, measured with the spectroradiometer. The reference measurement for sunlit pine canopy is shown in green; sunlit background is shown in blue and the apparent reflectance value for the shadow pine endmember is shown in red.

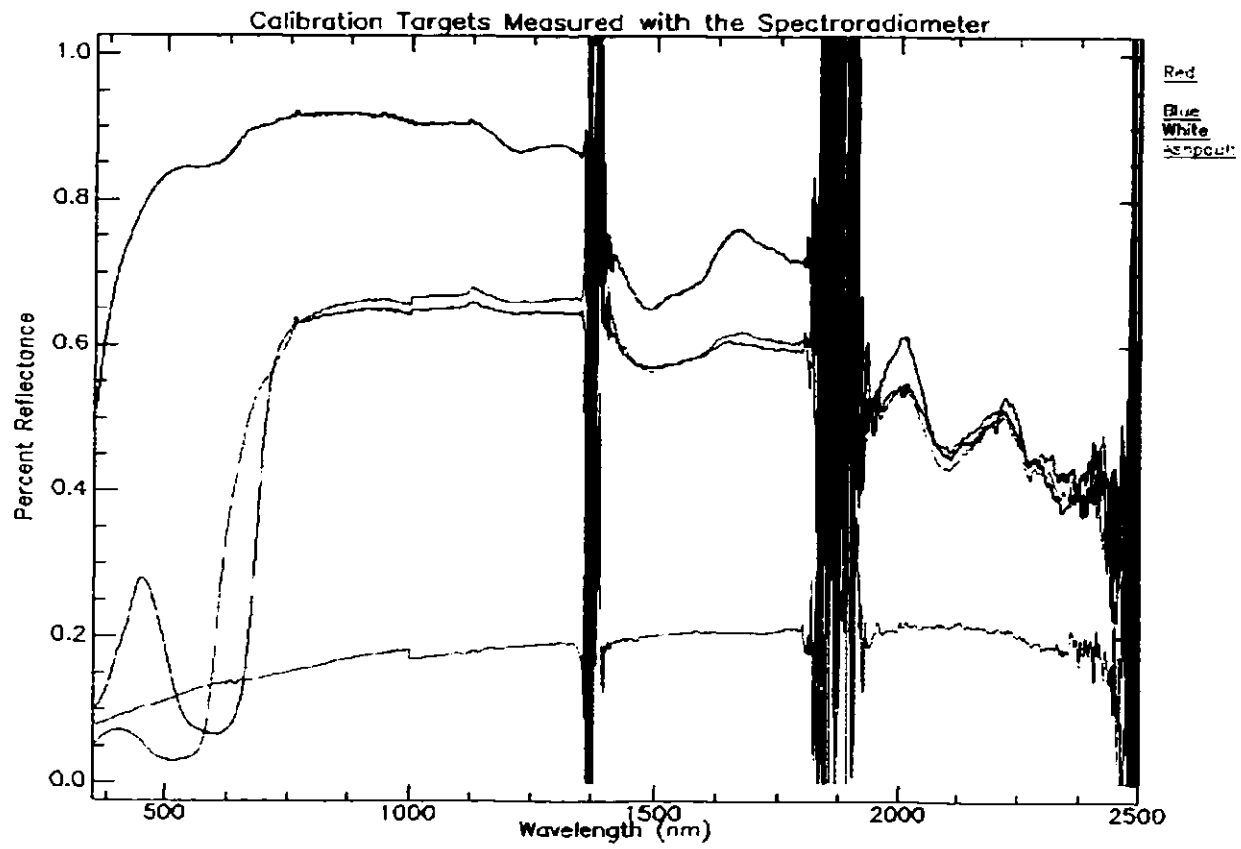


Figure 3-6 Spectroradiometer measurements of calibration targets collected during image acquisition. These measurements were subsequently resampled to the CASI band set and used in the atmospheric correction.

3.2.2.7 Forest Structural Data

The field collection was undertaken with the knowledge that optical reflectance models would be incorporated into the study. Therefore, stand structural data required for these models were collected. These variables were used to define the shape and spatial distribution of trees within a stand. Of interest, then, were tree species, stand density, crown closure, horizontal crown radius, vertical crown radius, tree height, and height distribution (derived from field measurements). Other forest structure measurements collected included ground-based estimates of slope and aspect, diameter at breast height (DBH), ground cover vegetation composition, and plot maps detailing the location of each tree.

Comprehensive sets of structural measurements were collected at each site. Data collection began by locating the centre of the plot and setting out the boundaries as described above. Next, each tree within the plot was flagged, labeled and mapped, and tree species were recorded. Tree height and the height to live crown were collected using a clinometer at an average distance of 15m from the tree. The horizontal crown radius of each tree was measured using a metric measuring tape from opposite edges of the main tree canopy projected vertically to the ground. A second measurement of crown radius was also obtained perpendicular to this measurement and the average of the two was used to represent the horizontal crown radius of the tree. Crown closure measurements were taken 2m in from each corner and at the center of the plot using a spherical densitometer. Tree diameter at breast height (DBH) measurements were collected at 1.3m above the ground using a DBH

tape for each tree. Tree cores were also collected for a representative sample of trees at each plot, based on the number of each tree species in the plot.

3.2.2.8 Plot Location

One requirement of data collection in this study was to capture variability in both forest structure and terrain. Plots were located to capture a full range of slopes and aspects as well as to provide a wide variety of forest structures. Due to the timing of the airborne data collection, much of the fieldwork had to be completed prior to image collection. This led to several constraints on plot location, as the images could not be used as a guide. To ensure that the plots would be located within the imagery, the proposed centerlines of the CASI airborne image flight lines were used as a base location in the field. From this point plots were randomly located along these lines with respect to the criteria of capturing a range of forest structure and terrain variability. A total of 31 plots were initially identified. Each plot was 10m x 10m, to ensure that a good number of pixels at each spatial resolution would be within the plot. Each plot was aligned north-south with the corners labeled clockwise beginning at the northwest corner #1, and the plot center labeled as 5, (Figure 3-7). This consistent scheme provided for easy comparison between plots. Also, since the orientation of the flight lines was either north-south or east-west, the plot and image pixel orientation was aligned. This simplified the identification of plot locations within the image. Of the total number of plots collected, 31 were used in the study and consisted of pure and mixed softwood species (Lodgepole pine, white spruce and Douglas fir). Due to the limited sample

size, separating the plots by species was not feasible, therefore the analysis was undertaken using all the conifer plots together.

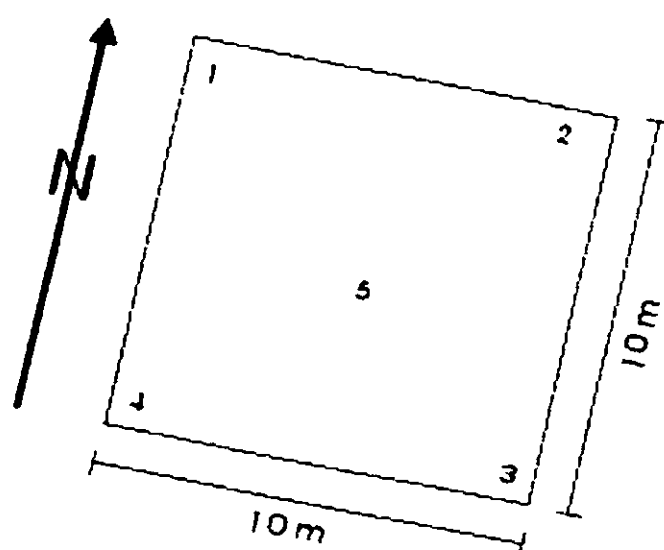


Figure 3-7 Plot Layout. Each plot was aligned with Magnetic North and a consistent labeling scheme (plot corners and center) was used to allow easy comparison between plots.

3.2.2.9 Field and Image Position

A key component of this analysis was the ability to accurately locate field measurements in the image data. To facilitate this, a differential global positioning system (DGPS) was used to obtain field positions with +/- 1m accuracy. GPS data were collected for each field plot as well as for a number of temporary and permanent ground control points (GCPs). At each field plot a GPS point was collected for each plot corner. Ground control targets were set out prior to image acquisition and the center of each was also recorded with

the DGPS (Figure 3-8). These targets were made of highly contrasting material and were easily located on the images. These were used to control and correct field and image positions. Careful examination of the geometric correction showed less than a single pixel variation between the 60 cm and 2 m resolutions (less than 2m absolute variation in alignment) which was acceptable for our analysis.

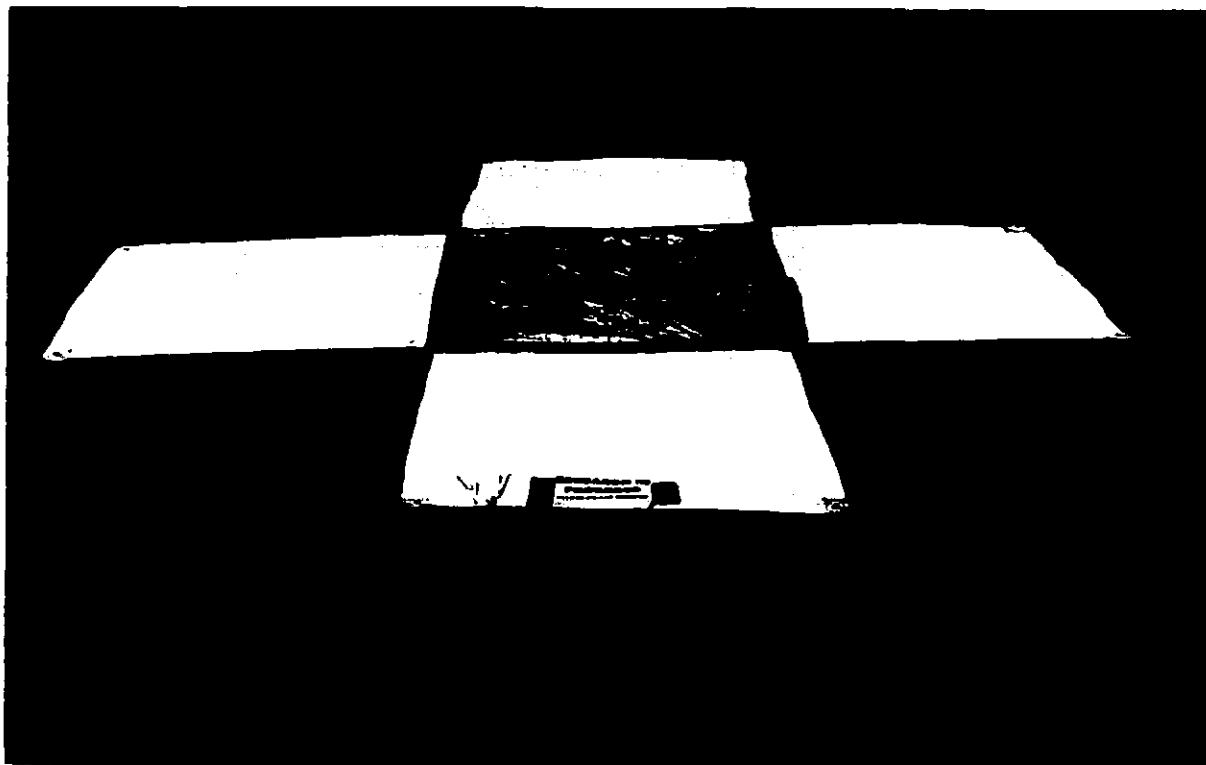


Figure 3-8 Ground Control Points (GCPs) were established throughout the study area and accurate locations were established for each using a DGPS systems, these targets were then used to test the positional accuracy of the image data set.

3.2.3 Ground Based LAI Estimation

Two optical instruments were used to estimate canopy leaf area in the test plots. The first instrument was the LAI-2000 Plant Canopy Analyzer, which provided an estimate of effective LAI (Welles and Norman 1991). The second optical instrument was the Tracing Radiation and Architecture of Canopies (TRAC) which provided an estimate of the clumping index and LAI (Chen and Kwong, 1997). Operational limitations related to the illumination requirements of each instrument precluded their use at the same time, and consequently, these limitations generally required that each plot be visited more than once. However, due to the distance between plots, time constraints, and variable sky conditions, a modified approach that allowed the two instruments to be used under clear sky conditions was adopted. In the next sections, the LAI-200 and TRAC instruments are described and their use in the field.

3.2.3.1 LAI-2000 Instrument

The LAI 2000 assumes a random leaf distribution and does not account for canopy architecture and therefore provides an estimate of effective leaf area index (eLAI) (Welles, 1990). This is not a true measure of LAI because foliage in plant communities is often not randomly distributed (Chen and Chilar, 1996). The LAI 2000 uses a fish-eye optical sensor sampled at five concentric angles (0-13, 16-28, 32-43, 47-58, 61-74 degrees) to measure the amount of foliage in the vegetation canopy as a function of the change in attenuation of radiation through the canopy. To quantify the change in radiation as it passes through the canopy, two measurements are needed: a measure of diffuse light outside the canopy, and a

second measure of diffuse light taken below the canopy. Two operational considerations with the use of the LAI-2000 included: (i) limiting data collection only to diffuse light conditions available early and late in the day, and (ii) due to the very large field of view, the LAI-2000 was difficult to use in small stands or near open areas. The LAI 2000 resolves the leaf angle orientation but assumes a random spatial leaf distribution to avoid biasing the eLAI values. The LAI-2000 is also influenced by terrain, since with the large field-of-view the outer concentric rings (i.e. angles closer to the horizon) of the sensor may not be recording incident radiation for the overstory canopy. To account for the terrain variation, the fourth and fifth rings of each measurement were evaluated and adjustments were considered for each measurement. If it was determined that the outer rings were not recording canopy attenuation, the associated measurements were removed using the LAI 2000 software.

The field logistics and the time available in the field prevented multiple visits to each plot. This presented a problem since the LAI-2000 and TRAC (described next) require different illumination conditions (diffuse and direct, respectively). However, to facilitate using the TRAC and LAI-2000 instruments together, eliminating the need for multiple trips to each plot, a modified approach was adopted which allowed the LAI-2000 to be used under clear sky direct illumination conditions. To mimic the conditions of a diffuse sky, the operator's body was used to cast a shadow onto the sensor, thus blocking all direct illumination. To prevent the sensor from including the operator in the field of view (FOV), a view cap was attached to the optics to restrict the direction of view of the sensor. The FOV cap also allowed the operator to focus the measurements beneath the canopy on the forest stand under study. Both the outside and below canopy measurements were collected in this

manner. Adopting this method of using the LAI 2000 greatly increased the efficiency of data collection since field plots could only be visited once.

3.2.3.2 TRAC Instrument

The TRAC was developed at the at the Canada Centre for Remote Sensing (CCRS) for the purpose of measuring PAR (Photosynthetically Active Radiation, 400 - 700nm), from which LAI can be calculated (REFERENCE). The instrument consists of three quantum sensors. Two of these sensor are pointed upwards to measure the down-welling total diffuse PAR, with the third sensor pointed downward to measure the reflected PAR from the ground. In addition, the TRAC measures sunfleck width, which is related to gaps in the overhead canopy. Based on the assumption that foliage is rarely distributed randomly in canopies, the resulting gap fraction and gap size distribution are used to calculate a foliage-clumping index in the TRAC software to produce the final LAI value.

The TRAC collects continuous measurements while the operator walks a transect perpendicular to the principal plane of the sun and parallel to the slope. Optimal data collection occurs within two hours of solar noon when the solar zenith angle is less than 55° . The TRAC also requires clear sky conditions with minimal or no cloud cover.

As the TRAC is dependent on sunfleck area it is also influenced by terrain. Shadow length and sunfleck area change as a function of slope and aspect. A terrain normalization method was developed based on the depth of canopy which the light had to penetrate. As the orientation of the terrain changes so does the depth of canopy relative to flat ground. As a first order normalization, the LAI value produced by the TRAC software was multiplied by a ratio of the depth of the canopy on flat ground by the depth of canopy on sloped terrain.

Although this normalization method was developed in conjunction with the designer of the TRAC system (Chen, pers. comm., 1999), it is recognized that this represents only a first order normalization. Development of a more robust normalization method would be desirable; however, this lies beyond the scope of this research.

3.2.4 Remote Sensing Imagery and Digital Elevation Data

3.2.4.1 Airborne Imagery

The multispectral Compact Airborne Spectrographic Imager (CASI) (Anger et al, 1991) from Itres Research in Calgary, Alberta is designed to provide the user with a high performance visible-near infrared (VNIR) pushbroom imaging spectrograph (Wulder et al, 1996). The CASI incorporates a charge-coupled device (CCD) into a two-dimensional sensor array. The sensor array is analogous to having an array of 512 separate spectrographs simultaneously imaging adjacent points across the field of view beneath the aircraft (Wulder et al, 1996a; Anger et al, 1994). The ground coverage and pixel size is dictated by aircraft altitude above ground level, and the aircraft speed. The across track pixel resolution (i.e. perpendicular to flying direction) is determined by aircraft altitude, whereas the along track resolution (in the direction of flight) is a function of aircraft speed over the target and the integration time of the sensor. The length of the flight line is limited only by the storage constraints of the CASI system. The CASI sensor has a spectral range of 545 nm, which may be located within 400 nm to 1000 nm. The actual spectral resolution of the CASI sensor is 2.2 nm at Full Width Half Maximum (FWHM) (Wulder et al, 1996a). The CASI has three operating modes that balance the collection of spatial and spectral information: spatial,

spectral, and full frame mode. In spatial mode, the CASI has the potential to obtain a maximum of 19 spectral bands. The bandwidths and locations are fully programmable with the only constraints being that the bands may not overlap and must fall within the 545 nm spectral range of the sensor. In spectral mode, the CASI records a continuous spectrum from 430 to 870 nm in 1.9nm increments. In this mode, the sensor is limited to 101 imaging points and results in a spatially non-contiguous data set (Wulder et al, 1996a). In full frame mode, the sensor collects 288 spectral bands for each of the 512 spatial pixels.

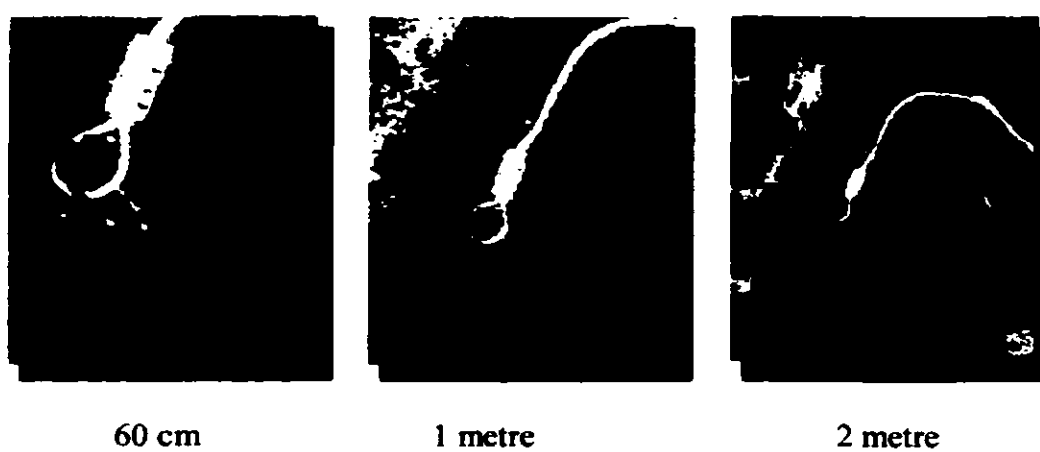


Figure 3-9 Sub-area of multi-scale CASI imagery collected over Kananaskis Provincial Park. The southern parking lot used for radiometric data collection is shown near the center of each image.

A CASI image data set was acquired over Kananaskis from 9:30 to 13:00 hrs on July 18, 1998. The image data set was acquired at three nominal spatial resolutions of 60cm, 1m, and 2m (Figure 3-9). The weather during image acquisition was judged to be ideal throughout the mission, with clear skies and only light winds. For this analysis, the CASI was used in a modified spatial mode configuration. At the 1m and 2m spatial resolutions, 18 separate spectral bands were recorded; however, at the 60cm resolution a maximum of 8 bands could be collected. The spectral bands that were acquired at the 60cm spatial

resolution are shown in Table 3-1. Eight of the 18 bands acquired at 1m and 2m spatial resolutions, were selected that correspond to those recorded at the 60cm. The spectral curves for a pine stand resampled to these 8 bands are shown in Figure 3-10. The discrepancy in the number of bands collected is a function of the finite rate at which the CASI sensor can record data. At the flying elevation required to capture 60 cm data, aircraft speed was too fast for the sensor to integrate 18 spectral bands. Therefore, a compromise between spectral and spatial information had to be made.

Table 3-1 CASI Image Band Set collected at all spatial resolutions.

Band Number	Wavelength (nm)	
	Start	End
1	450	500
2	540	560
3	610	640
4	640	680
5	690	715
6	730	755
7	790	810
8	850	875

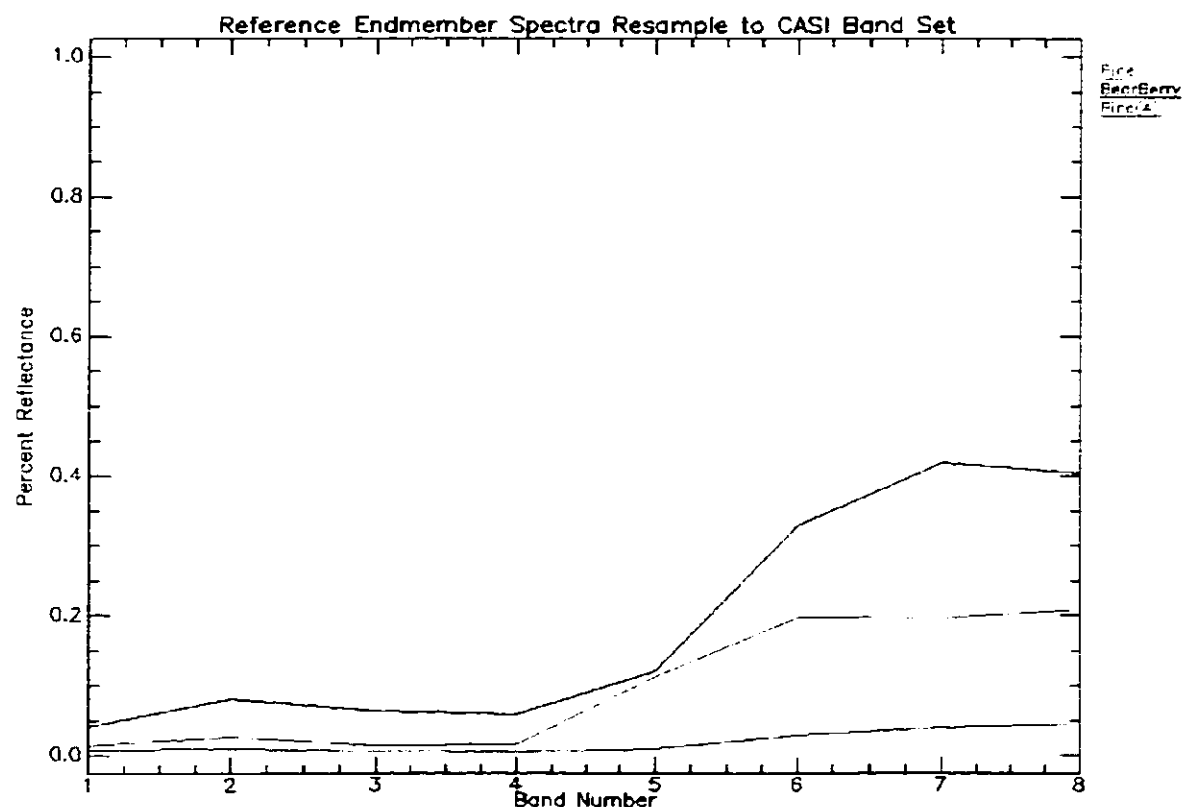


Figure 3-10 The ASD measurements collected in the field were resampled to the 8 CASI bands using a linear spectral response function. The reference measurement for sunlit pine is shown in green; sunlit background is shown in blue and the apparent reflectance value for the shadowed pine endmember is shown in red.

Several geometric and illumination issues had to be considered during mission planning because of the terrain within the study area. The terrain prevented the aircraft from maintaining a constant elevation above the ground surface during image acquisitions; therefore, the across track pixel resolution varied along all flight line. This was accounted for by identifying a nominal flying datum (1550m ASL), which distributed the amount of variation more evenly throughout the study site. Imagery were collected at three flying altitudes above this datum to produce imagery at 60cm, 1m and 2m spatial resolution. The

mountainous terrain further constrained the range of solar position and illumination conditions for acceptable data collection.

There were three important considerations taken into account when determining the best time to collect the image data. First, it has been shown that understory vegetation can limit extraction of biophysical information about the forest canopy. Therefore, a high solar zenith angle was desirable to increase canopy shadowing thus obscuring the background vegetation. Second, the orientation of terrain in the study area with respect to the morning solar azimuth was preferable for data collection to prevent large shadows cast by mountains from falling on the study site. Third, clear sky conditions suitable for image acquisition were more likely to occur in the morning, than in the afternoon. Cloud cover generated by surface warming and characteristic diurnal mountainous weather patterns typically generate early to mid afternoon cloud. All data were acquired in the same flight direction from north to south to maintain the across track illumination difference caused by the position of the sun. This was facilitated using a race-track pattern of image acquisition. The aircraft collected data only on the south bound leg of a circuit (which was into the sun) and then flew back to the beginning of the flight lines to collect the next image. Each adjacent image flight line was collected to ensure a 40% sidelap, which ensured good spatial coverage over the study area.

In addition to the preparations for image acquisition, ground control points (GCPs) were established throughout the study area to assess the geometric correction provided by Itres Research. These GCPs were discussed in more detail in section 3.2.2.9.

3.2.4.2 Image Preprocessing

Itres Research performed the initial image pre-processing and the data set was provided as a geometrically-corrected image data set. The corrections performed by Itres accounted for aircraft attitude that include roll, pitch and yaw. To correct for these effects, real-time attitude measurements were recorded during image acquisition using an Inertial Navigation System (INS). The imagery was also digitally resampled to the nominal image resolution thereby removing the across track variation in pixel resolution. This provided a good correction on most moderately sloping terrain, however, on very steep slopes it did introduce some error. These errors represented only a very small portion of the study area and did not influence our analysis as none of them fell on the study sites.

Further corrections applied once the data set was provided included an empirical radiometric normalization performed to account for the atmospheric variations between images. Four pseudo-invariant targets placed in the southern parking lot were identified in the imagery and used to normalize each image resolution to the ground based reflectance spectra measured for each target, as described earlier. The ground based reflectance values for the calibration targets and asphalt were related to the CASI data using a linear spectral response function for each image band. Careful examination of the data set showed that there was considerable variation in the radiance recorded at the different spatial resolutions; however, variations between images from adjacent flight lines at the same resolution were negligible. Given these characteristics of the data set, the parking lot and pseudo-invariant targets were identified in one image at each resolution. Three sets of normalization equations were calculated and applied to all images with respect to their spatial resolution (Jensen, 1996). This produced a radiometrically normalized image data set corrected to reflectance.

3.2.4.3 Digital Elevation Model

The Miistakis Institute for the Rockies provided a 10m resolution digital elevation model (DEM) of the study area. The DEM was acquired from the provincial data base and was compiled using data photogrammetrically compiled from 1:60 000 scale aerial photographs (Altalis, 1999), and subjected to detailed post processing to remove or minimize data errors. The DEM was resampled and co-registered to the spatial resolution of each image by Itres Research as part of the product they provided. A limited amount of post processing was required to generate a measure of slope and aspect for each plot within the study area. These values were easily generated using algorithms provided in the Environment for Visualizing images (ENVI) image analysis system (ENVI, 1997). Slope and aspect values were generated for each pixel within the DEM and then aggregated to the plot level (10m x 10m), to produce a single slope and aspect value for each plot.

3.3 Spectral Mixture Analysis

Spectral mixture analysis (SMA) is based on the fact the IFOV of a sensor is composed of a number of individual surface components which together contribute to the overall pixel level reflectance recorded (Adams et al., 1993). It is a tool to estimate the sub-pixel scale abundance of each scene component (or endmember) based on their individual spectral properties. Changes in forest structure result in different levels of scene component fractions. The relationship between component fractions and forest structure is the basis for the strong predictive capabilities of biophysical information using SMA (Hall et al, 1995;

1996; Peddle et al, 1995; 1997; 1999b). To test the ability of spectral mixture analysis to predict forest leaf area in mountainous terrain, a series of tests was designed.

As a basis for comparison, a SMA trial was first performed without any attempt to account for the variations induced by terrain. Subsequent SMA trials were performed after applying various terrain normalizations to the imagery. Four Terrain normalization equations (Cosine, Statistical-Empirical, Minnaert, and C-corrections) were evaluated in terms of their ability to improve scene fraction extraction using SMA. The scene fractions obtained from the various terrain-normalized images were compared to optical LAI measurements taken in the field with the TRAC and LAI-2000. These results were also compared to NDVI to determine how similar these measures were at the different spatial resolutions of imagery.

In this study, three main scene components were identified as sunlit canopy, sunlit background, and shadow. SMA does not require a great deal of parameterization; however, the accurate spectral characterization of these main scene components is central to the ability of SMA to derive accurate scene component fractions, and to make accurate estimates of LAI. Three different sets of spectral endmembers were collected. The component endmember values used were based on the species composition recorded in the field data for each plot. Each SMA trial was repeated for the different endmember sets, which allowed both the terrain normalization methods and endmember types to be evaluated in terms of predicting LAI. The three endmember sets: reference, image and integrated are described in 3.4.1, 3.4.2 and 3.4.3.


3.4 Component Endmember Specification

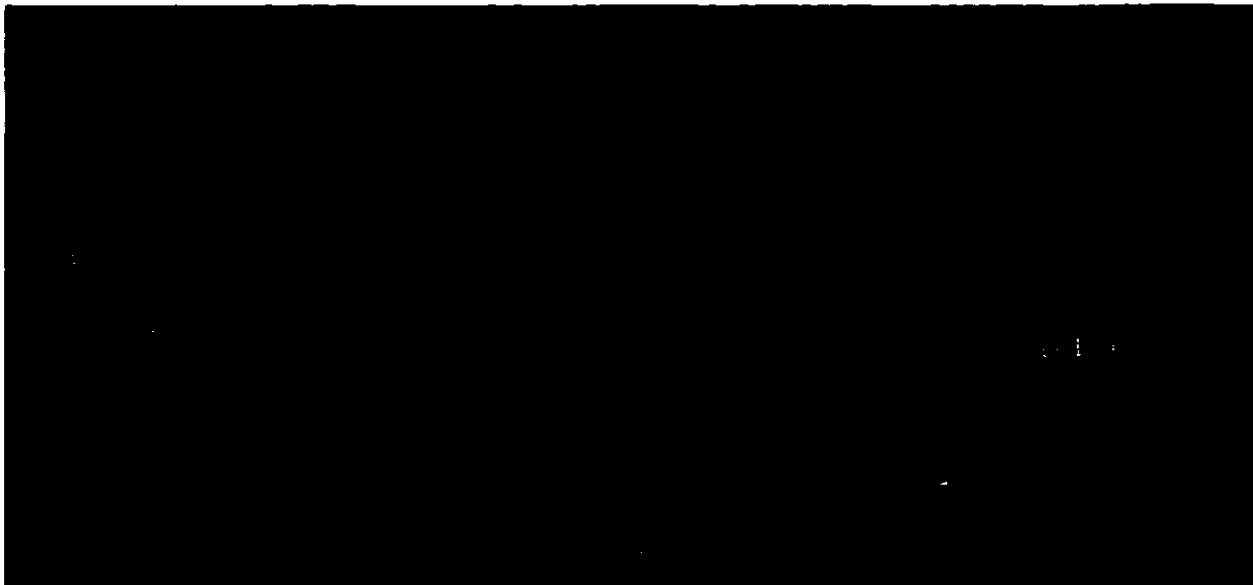
To ensure consistency throughout the study, three sets of endmember inputs were identified for the spectral mixture analyses, as well as for use with the optical reflectance model. The first set was composed of reference endmembers measured in the field with the spectroradiometer, as described earlier. The second set was composed of image endmembers selected directly from the 60cm image data. The third set was composed of both reference and image endmembers to take advantage of benefits from each approach. These endmember sets were held constant throughout the remainder of the research, allowing each to be used to predict leaf area index using either SMA or the optical reflectance model.

3.4.1 Reference Endmember Set

The reference endmember spectra used were selected from a spectral library of measurements collected in the field using the spectroradiometer. The canopy endmember was the reflectance obtained for lodgepole pine, white spruce or Douglas-fir, depending on the species composition of the plot. The reference values from the main species present on the forest floor in these plots (pine grass (*calamagrostis rubescens* buckl.), step moss (*Shepherdia canadensis* (L.) Nutt) and buffalo berry) were aggregated to produce the background endmember spectrum. This did not account for the complexity of the forest floor as other species (e.g. juniper) were not measured, nor was the spatial abundance of each background component considered. The shadow endmember was chosen as the darkest apparent reflectance measure of the canopy and background species, which was pine grass. The reference endmember set is outlined in Table 3-2.

Table 3-2 Description of reference endmembers and reflectance curves of Sunlit Background, Sunlit Canopy and Shadow


Image Endmember	Description
Sunlit Canopy	Reflectance measure of lodgepole pine, white spruce, or Douglas-fir
Sunlit Background	Average reflectance measurement of dominant background species
	<i>Apparent Reflectance</i> measurement of pine grass

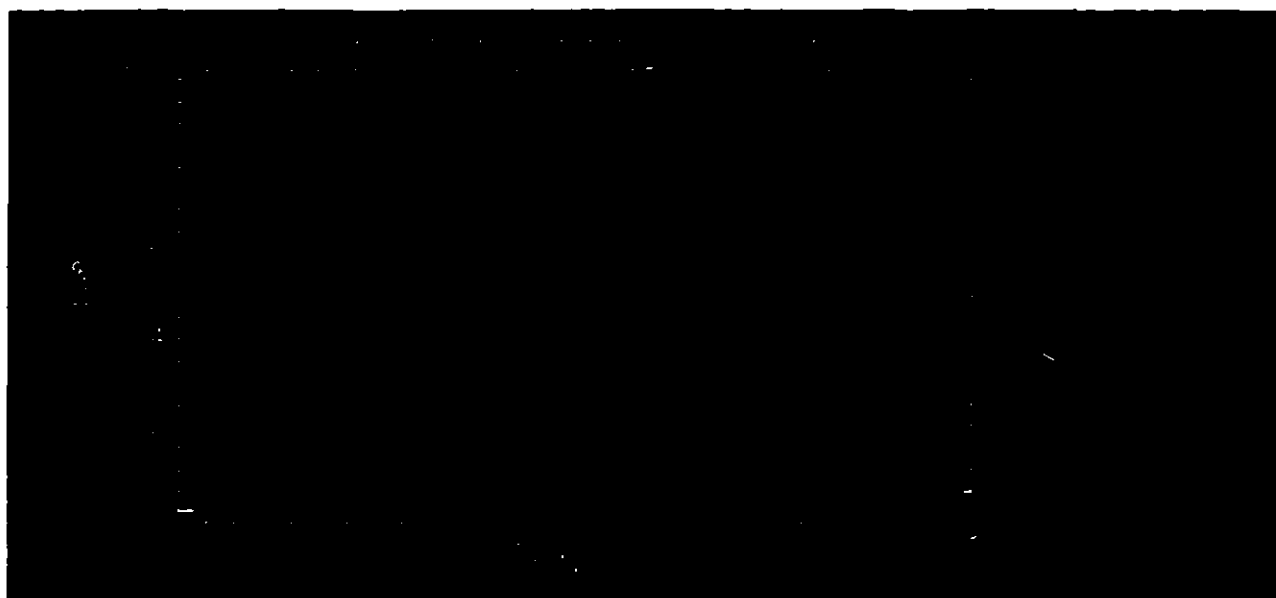


3.4.2 Image Endmember Set

Image endmembers selected from all eight bands of the 60cm image data were interpreted to represent pure samples of the scene components under investigation (Table 3-3). Image endmembers were selected based on spectral plots using the n-dimensional visualization capability available in the ENVI image analysis system (ENVI, 1998). In each band, the sunlit canopy endmember was selected based on the brightest canopy pixel value representation of lodgepole pine, white spruce, or Douglas fir trees. The sunlit background endmember was selected from an adjacent clearing that had similar vegetation composition as the forest floor and again the brightest image values were used. Three types of canopy shadowing were evident in the imagery: (1) infinitely dark, (2) transitional, and (3) diffuse shadow, as outlined in Seed et al, (1997) and Peddle and Johnson (2000). The darkest image endmember was selected as the purest case of shadow. Preliminary sets of SMA results were produced and their Root Mean Square (RMS) error evaluated against what were deemed to be pure pixels in the image prior to final endmember selection.

Table 3-3 Description of image endmembers and reflectance curves of Sunlit Background, Sunlit Canopy and Shadow.

Image Endmember	Description
Sunlit Canopy	Brightest canopy pixel from each band
Sunlit Background	Brightest background pixel selected from adjacent clearing for each band
	Darkest image value from shadow pixels



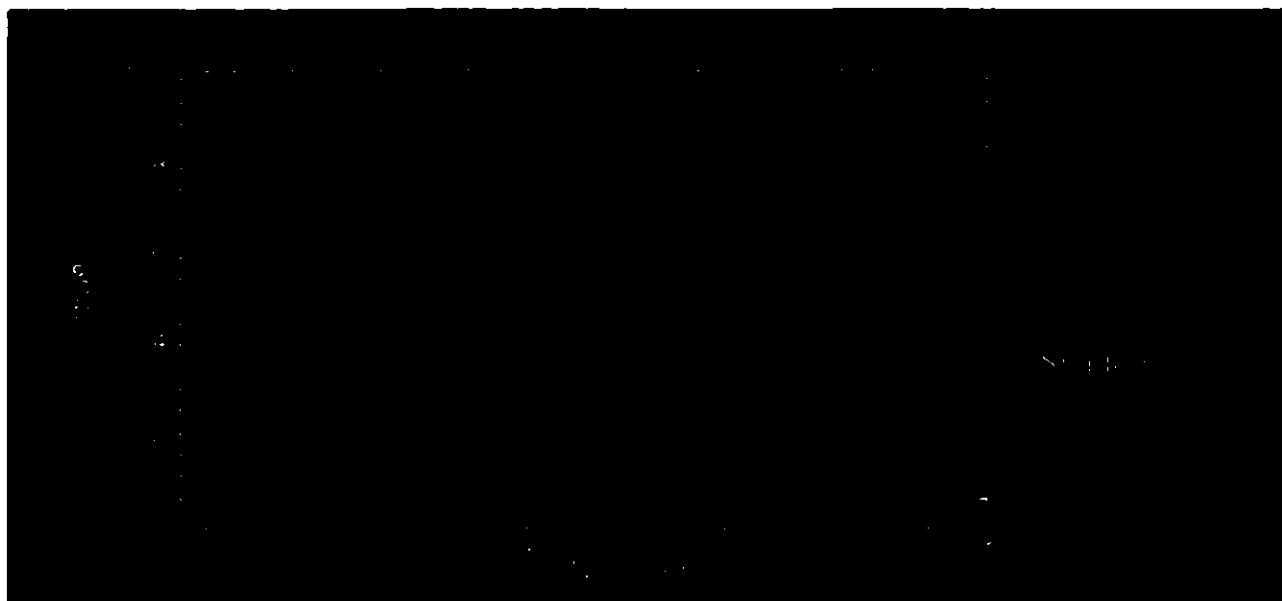
3.4.3 Integrated Endmember Set

The integrated endmember set was created to take advantage of both the image and reference endmembers (Table 3-4). The integrated endmember set used the reference measure of sunlit canopy (lodgepole pine, white spruce, or Douglas fir), to represent a purer sample than could be identified in a 60cm image pixel. Image endmembers were selected for the sunlit background and shadow endmembers. The sunlit background image endmember

more accurately represented the complex mixtures of background vegetation compared to combinations of individual reference endmember spectra. Both the image shadow and reference shadow endmember values were very similar to each other in bands 1 through 5; however, the image endmember values were chosen since they were darker in bands 6 through 8.

Table 3-4 Description of integrated endmembers and reflectance curves of Sunlit Background, Sunlit Canopy and Shadow

Integrated Endmember	Description
Sunlit Canopy	Reference measure of lodgepole pine, white spruce or Douglas-fir
Sunlit Background	Image background endmember
Shadow	Image shadow endmember



3.5 Spectral Mixture Analysis Post Processing, Evaluation and LAI Prediction

3.5.1 Spatial Aggregation of Fractions to the Plot Scale

The SMA algorithm produces a set of scene fraction values and an estimate of RMS error for each pixel. The fraction values produced by the algorithm represent the physical abundance of these materials on the ground which were visible to the sensor.

To match the scale of the LAI measurements collected on the ground, the output of the SMA needed to be aggregated to the plot scale. There were two options considered to facilitate this. First, the spectral values of each pixel could be resampled to produce a single reflectance value for the plot. This single spectral value could then be unmixed and the fractions would be at the plot scale. Alternatively, each individual pixel which composed the plot could be unmixed and the resulting scene fractions summed and averaged over the plot area. To avoid the difficulty of resampling the spectral values to the plot scale, the scene fraction values were aggregated. In a physical sense, the scene fractions represent the spatial abundance of material on the ground, which is an appropriate measurement to aggregate, whereas resampling the spectral values does not have the same simple physical analogy. This approach also allowed SMA fractions of individual pixels to be evaluated (e.g. RMS error, fraction over flow or under flow) which would not have been possible if the spectral data were aggregated prior to mixture analysis.

3.5.2 Scene Fraction Validation

Once the scene fractions have been scaled to the plot level, they need to be validated to ensure that they accurately represent the spatial abundance of materials on the ground. The validation of sub-pixel scale fractions is important when using SMA in more complex environments such as mountainous terrain. If the sub-pixel fractions of scene components are to be used to predict physical variables, it is important first to quantify their accuracy.

The results of each SMA trial were a set of three fractions corresponding to sunlit canopy, sunlit background, and shadow, as well as an estimate of RMS error for each pixel. A quantitative validation of sub-pixel scale fractions at 1m and 2m resolution was performed using a maximum likelihood (ML) supervised classification of sunlit canopy, sunlit background and shadow at the 60cm resolution. This validation was then repeated for each endmember set (i.e. reference, image and integrated). For example, a 10 x 10 m test plot contained approximately 25 pixels at 2m resolution for which a set of scene fractions were produced and aggregated. These scene fractions were compared to the ML classification of nearly 280 pixels at the 60cm resolution that comprised the same plot area. A supervised classification approach was used to classify the image into three classes (sunlit canopy, sunlit background and shadow), using training data obtained from the 60cm imagery. This provided a way of validating the fractions produced using the three sets of endmembers at the 1m and 2m image resolutions. Potential error can be introduced into this analysis due to the mixtures of materials that occur within a 60cm pixel as well as from errors in classification. However, the method of validation used in this study provided a meaningful way of evaluating the SMA fractions prior to biophysical analysis (Johnson and Peddle, 1998).

3.5.3 Leaf Area Index Prediction

After the scene fractions were validated, each set of fractions from the different endmember sets and terrain normalization methods were evaluated in terms of their ability to predict ground-based measurements of leaf area index acquired using the LAI-2000 and TRAC. Separate linear regression analyses to predict LAI values were performed using the shadow, sunlit canopy and sunlit background fractions produced from each endmember set, at different image resolutions and using different normalization methods. This resulted in a total of 180 separate regression trials, as outlined in Table 3-5. The ability to predict LAI was based on the magnitude of the regression coefficient of determination (r^2). These results were also compared to the ability of NDVI to predict the measurements of LAI.

Table 3-5 The number of regression trials is a function of different combinations of various options and data sets available in the study.

Total Number of Separate Regression Analyses	
Variable Name and Description	Number of Variables (N)
Number of scene fractions (Sunlit canopy, sunlit background and shadow)	3
Normalization method (None, Cosine, C-correction, Statistical-empirical, and Minneart)	5
Image resolution (1m and 2m)	2
Number of endmember sets (Reference, Image and Integrated)	3
Different LAI measurements (LAI 2000 and TRAC)	2
TOTAL	180

3.6 Geometric Optical Reflectance Modeling

For the modeling analysis, the Li and Strahler (1992) Geometric Optical Mutual Shadowing (GOMS) model was selected because of several advantages over other geometric optical reflectance models. Firstly, the GOMS model represents tree crowns as spheroids that have been shown to be superior to other crown geometric forms such as cylinders and cones (Peddle et al ,1999b). Secondly, the GOMS model provides capabilities to deal with complex crown mutual shadowing influenced by solar zenith angles and influenced by stand structure. Mutual shadowing is more likely at higher latitudes and in mountainous terrain where shadows are often longer. Thirdly, the GOMS model is relatively easy to parameterize from fieldwork or baseline inventory data (e.g. Alberta Vegetation Inventory). Fourthly, the GOMS model uses slope and aspect in model calculations and is therefore more appropriate for mountainous terrain compared to other models which do not have this capability.

The model can be used in either forward or inverse mode. In forward mode, the model produces as output an average pixel level reflectance value in each spectral band, as well as scene component fraction values. As input, the forward mode requires an estimate of tree dimension, illumination geometry, stand density, and the spectral component reflectances. In inverse mode, the model provides as output the physical descriptions of forest structure (tree height, stand density, and tree height distribution, and horizontal and vertical crown radius). Requirements for inverse modeling are pixel level reflectance values, spectral properties of each individual stand component, and the sun and view positions. In the next section, a new approach using the GOMS model is introduced, which is capable of accounting for changes in pixel level reflectance as a function of stand structure and terrain.

3.6.1 Multiple Forward Mode (MFM) Approach

Terrain has no influence over the sun-crown geometry because trees are considered geotropic (perpendicular to the geoid) (Gu and Gillespie, 1997). Terrain roughness and slope/aspect position, however, influences the position of trees within the canopy relative to the sensor, thus changing the contribution of sunlit canopy, sunlit background, and shadow to the overall pixel radiance recorded by the sensor (Figure 3-11). As has been described above, the signal recorded by the sensor is a collective radiance of the main scene components within the sensor's instantaneous field of view weighted by their spatial abundance. To account for differences introduced in the abundance of subpixel components as a function of terrain and forest structure, a new approach was developed to account for these differences at the sub-pixel scale. This new approach for mountainous terrain has been adapted from previous work in a flat, mixed forest environment in eastern Canada, in which the multiple forward mode idea was first developed (Peddle et al. 1999a).

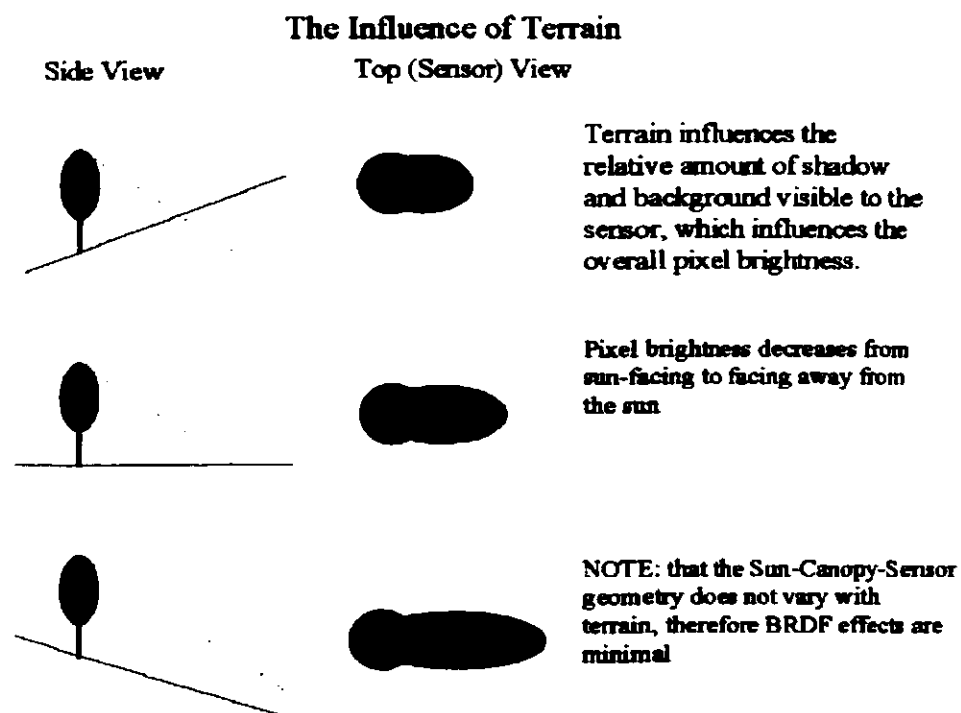


Figure 3-11 Influence of terrain on stand structure. Terrain influences the relative amount of shadow and background visible to the sensor, which influences the overall pixel brightness. Pixel brightness decreases from sun-facing to facing away from the sun. NOTE: Sun-Canopy-Sensor geometry does not vary with terrain, therefore BRDF effects are minimal

Typically, any study focused on providing quantitative forest structural information is set in the context of model inversion since that mode provides physical descriptors of stand structure based on spectral input data. However, an approach that provides the proper basis for quantifying forest reflectance as a function of varying stand structure and terrain is needed. This method should be able to characterize the variability in physical structural data as a function of pixel reflectance values. To this end, an approach that is able to quantify the change in scene component fractions was desired. Not only would such a method provide a means of characterizing forest reflectance as a function of terrain, but it would also provide an inherent ability to normalize these effects. Accordingly, a method has been developed to

provide a framework to quantify forest reflectance as a function of stand structure and terrain at the sub-pixel scale.

To account for these variations, a modified approach using the GOMS model in "multiple forward mode" (MFM) has been developed. In standard forward mode, the user must provide input data for each model trial. The model then computes a single pixel value corresponding to the set of physical inputs and spectral component measurements. The MFM permits a range of input values to be specified. For example, instead of specifying a single stand specific value for horizontal crown radius, the user may provide a range of values and a model increment. This method allows the user to explicitly address the variability in the stand. The model then runs multiple times in forward mode for each possible combination of physical canopy descriptors, view geometries, and illumination angles, over the full range specified for each parameter. For a given set of physical inputs, all values are considered throughout the range with respect to the increment steps specified by the user. As output, the model produces a large array or look-up-table of values that relates pixel level reflectance, scene component fractions, and input structure and illumination geometry values. A graphical form of these tables appears in Figure 3-12. These MFM look-up tables were computed over the full range of forest structural and terrain variability in the study area. These tables can then be searched and sorted to retrieve quantitative information relating scene reflectance or scene component fractions to any model input.

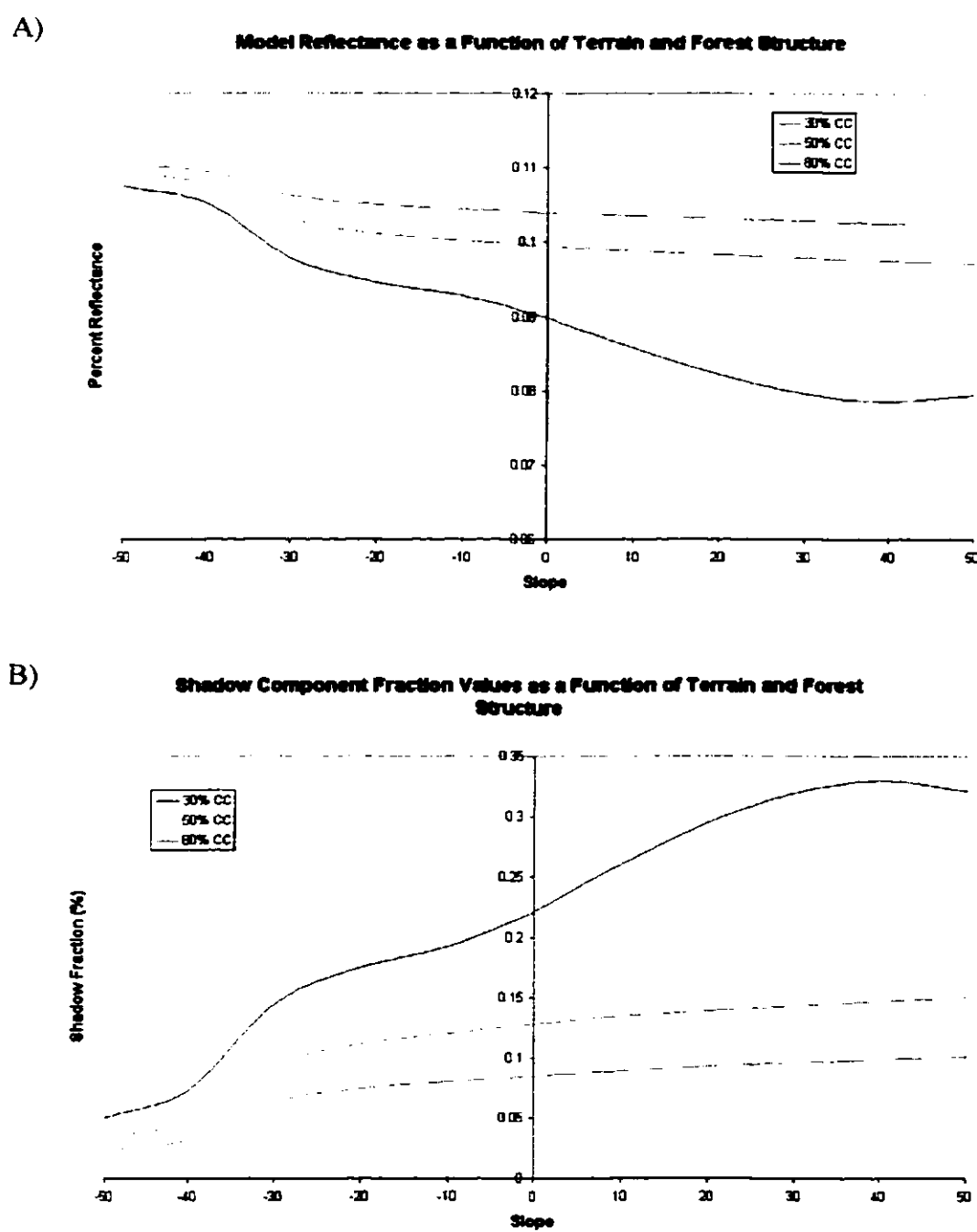


Figure 3-12 Graphical representation of the look-up tables produced using the MFM approach. A) variation in modeled reflectance; B) variation in shadow fraction. Each diagram is in the principal plane of the sun with a SZA of 45° and an azimuth of 180° . Negative slope values represent slopes facing the sun while positive slopes are facing away from the sun. Three stand densities are shown for a pine stand with 30%, 50% and 80% crown closure (CC). Note the increased effect terrain has on both reflectance and shadow fraction in lower density stands.

In terms of forest image analysis and reflectance modeling, the MFM approach provides several advantages. The first advantage is that the MFM approach allows a wide range of structural and illumination inputs to be tested in a single set of model runs. The model can also be parameterized to focus on a single input variable while several other parameters are held constant. For example, varying only the slope and aspect values (holding all other values constant) allows the model to test the effects of changing terrain on modeled spectral response. Another advantage of the MFM approach is it does not require specific or exact physical parameters. Instead, only a range is required which can more easily be discerned from baseline inventory data or field data. If this information is unknown, the MFM can still be used by specifying the full range of possible model inputs. Lastly, unlike typical modeling which produces a single set of output results (e.g. inversion models), the MFM produces a range of output values related to variations in forest structure and illumination allowing a better understanding of the influence of stand structure and terrain on scene reflectance.

3.6.2 Multiple Forward Mode User Interface

The graphical user interface developed provides a researcher with an easy method to enter tree dimensions and form parameters, scene component endmember values as well as illumination and view angles (Figure 3-13). The current software is based on software developed by Peddle (1997) that was designed to facilitate GOMS model input and execution. Once all the input parameters have been set, the program builds the input files and a batch file to control all model processing. The program first computes the geometric

form factors used by the GOMS model as a function of the user inputs. The new MFM software calculates each possible combination of input parameters and produces a set of input files for the GOMS model. The software also records the input data used for each trial so that these values can be included with the output data in the look-up tables.

In addition to creating all the input files required by the GOMS model, the MFM software writes either a UNIX command shell file or a Windows WinBatch file to direct batch (i.e. automated) mode execution of all model runs. After creating the input files, the batch program is run as either a system command shell file in UNIX or as a WinBatch file in Windows. Once the GOMS model has completed all model runs, a second program called GROUP is used to format the output into a look-up table suitable for search, analysis or query. Examples and a description of the GOMS input files and the MFM software are provided in Appendix 1.

The screenshot shows the GOMS MFM graphical user interface. The window title is "GOMS MFM" and the menu bar includes "File", "Edit", "GOMS", and "Help". The interface is divided into several sections:

- GOMS FileName:** A text input field containing "Pine_terrain".
- Number of Trials:** A text input field.
- Parameter Table:** A table with three columns: "Minimum", "Maximum", and "Interval".

	Minimum	Maximum	Interval
Tree Density (Lam)	0	1	0.1
Horizontal Crown Radius (r)	1.5	2.0	0.5
Vertical Crown Radius (b)	2.0	3.0	0.5
Tree Height (h)	7	14	2
Tree Height Distribution (dh)	9	9	1
Slope	0	30	10
Aspect	0	360	45
Solar Azimuth	120	170	10
Solar Zenith Angle	10	45	5
- Reflectance Parameters:** Three text input fields:
 - Sunlit Canopy Reflectance: 0.014076
 - Sunlit Background Reflectance: 0.08077
 - Shadow Reflectance: 0.004889
- Comment:** A text area with the label "Comment" and the prompt "Enter a comment here."

Figure 3-13 MFM graphical user interface provides the user with an easy way of parameterizing the model.

3.6.3 Multiple Forward Mode Parameterization

The GOMS model requires three fundamental types of data: 1) spectral component endmember values, 2) physical descriptors of stand structure, and 3) view and illumination geometry. The MFM approach provides the user with the ability to characterize variations in the stand using input ranges rather than single values to characterize forest structure. For accurate results, it is important to understand how the GOMS model uses the structural input data to derive forest reflectance and scene fractions prior to assigning input ranges. The GOMS model uses the five measures of forest structure to derive four model-input

parameters. Using these input parameters the model is able to reduce the sensitivity to any single input value.

Appropriate ranges of physical input data were assessed based on direct measurements collected in the field. Each range of input values was expanded beyond the variability seen in the field to ensure that the model captured all the variability in the scene. The view angle was held constant as nadir and the illumination geometry was assigned based on the solar positions during the CASI airborne image acquisition. The terrain inputs were assigned based on the variation in slope and aspect derived from the DEM. Each endmember set was used in a separate trial of the MFM software to allow the ability of each to parameterize the model to be tested. The modeling intervals for each parameter were selected based on two criteria. First, an interval was selected which allowed sufficient variation in stand structure to be characterized. Secondly, since a smaller interval size resulted in more model runs, a balance between model intervals and numbers of trials was also considered. A sample model parameterization is shown in Figure 3-13.

3.6.4 Terrain Normalization

The main hypothesis presented in this research is that a terrain normalization method that explicitly accounts for forest structure will provide improved estimates of leaf area index in mountainous terrain. The first step in the development of such a method is the validation of the scene component fractions produced by the MFM approach. To facilitate this, the MFM model was parameterized with the stand structure and terrain variables of each plot, from which scene component fractions were produced from the model runs. Both SMA and

the GOMS MFM require endmember spectral inputs, and both approaches produced sub-pixel scale fractions as output. This permits SMA and GOMS MFM fraction output to be directly compared. This was done for each set of endmembers (reference, image and integrated). Initial observation of these results showed that the SMA fractions and those produced using the MFM approach consistently indicated acceptable agreement. The next step was to quantify the influence of terrain on scene fraction values given the same stand structure. This was easily achieved using the MFM interface, as input stand structural values for a given stand were held constant and only the slope and aspect values were input as ranges. The output was a graphical look-up table that quantified the influence of terrain on forest reflectance and scene fraction values. Three-dimensional graphical representation of the influence of terrain on forest stand reflectance and the amount of shadow visible to the sensor appear in Figures 3-14 and 3-15. These figures are a graphical representation of the change in reflectance and shadow fraction as a function of terrain. For this model trial forest structure was held constant, a crown closure of 50% was used and only the terrain variables were allowed to change. Terrain was modeled at 45° aspect intervals and 10° slope intervals.

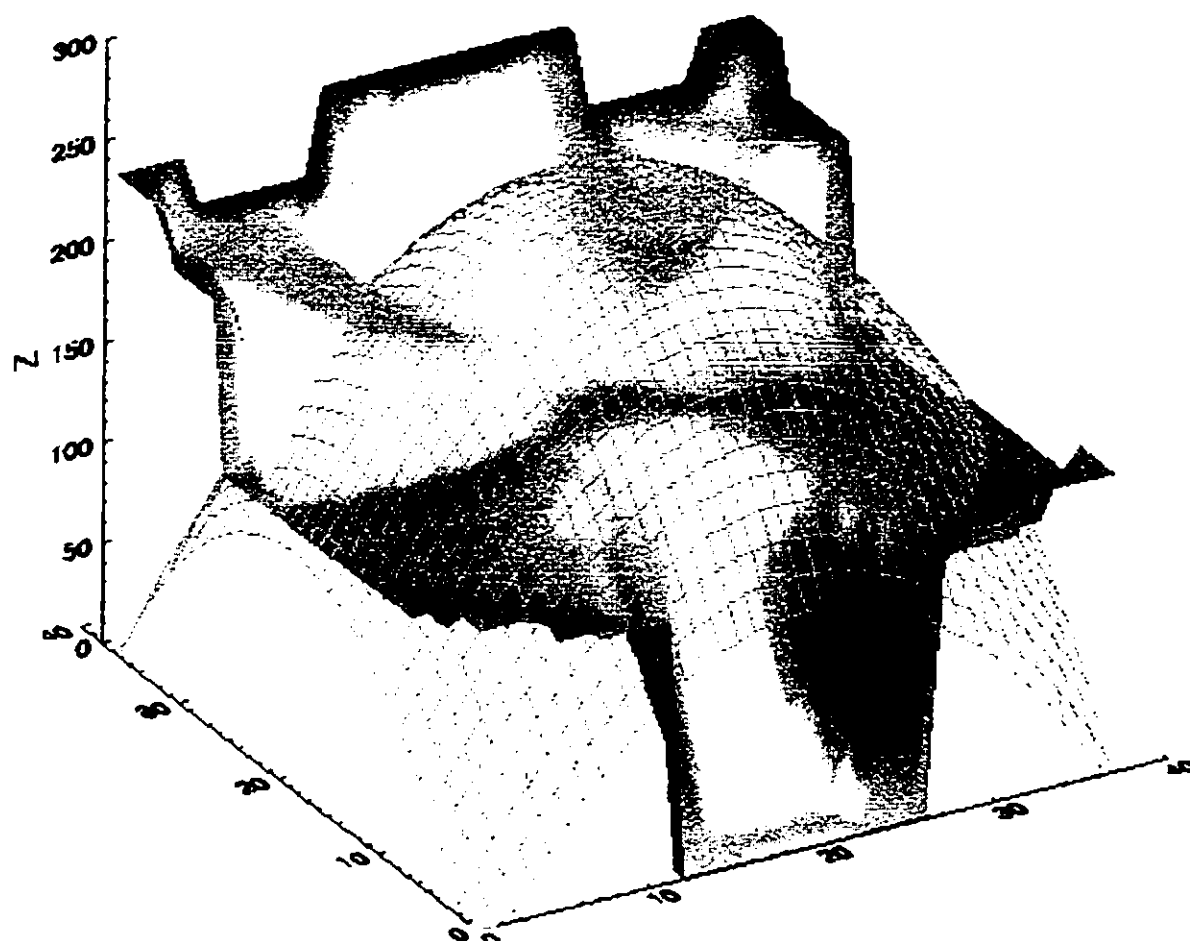


Figure 3-14 Forest reflectance as a function of terrain. Shaded surface represents the relative change in reflectance as a function of terrain variables (slope and aspect). The wire mesh surface represents a generic terrain surface. Forest structure is constant with a 50% crown closure, terrain was modeled at 45° aspect intervals and slope was modeled with 10° intervals. The sun position would be behind the shaded surface casting light towards the front.

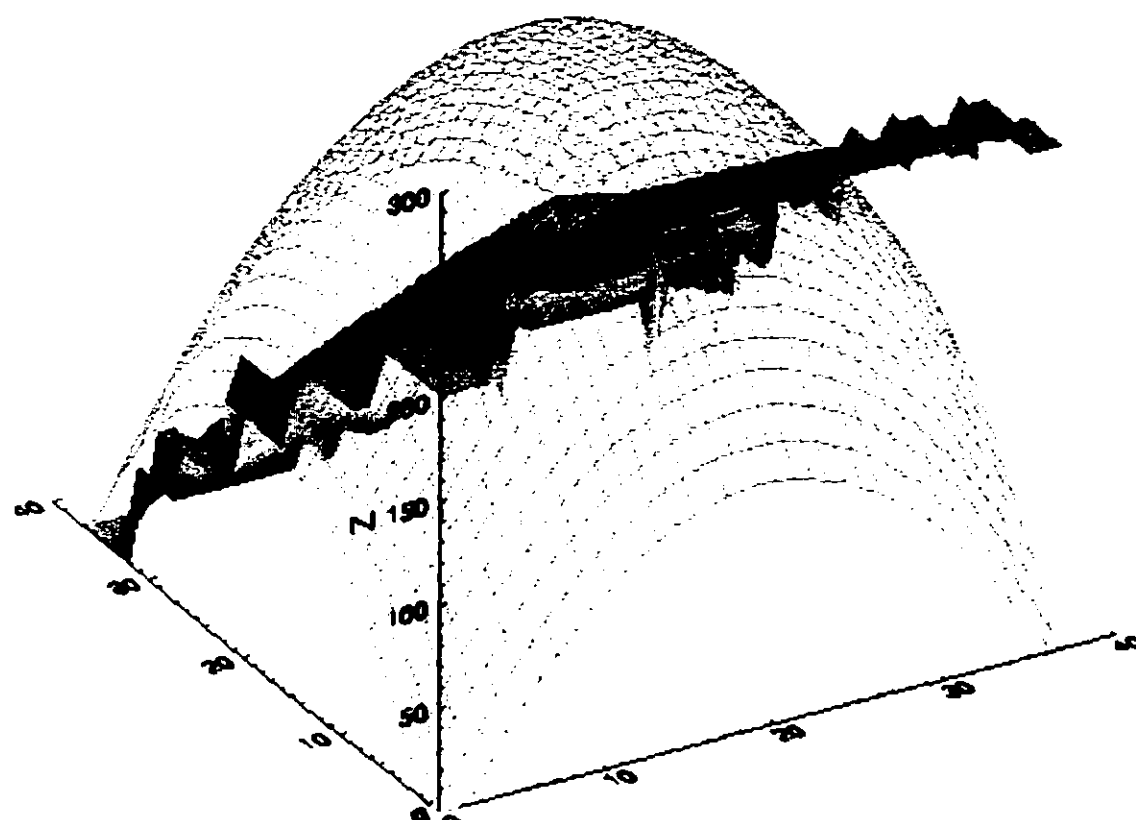


Figure 3-15 Forest shadow fraction as a function of terrain. Shaded surface represents the relative change in shadow as a function of terrain variables (slope and aspect). The wire mesh surface represents a generic terrain surface. Forest structure is constant with a 50% crown closure, terrain was modeled at 45° aspect intervals and slope was modeled with 10° intervals. The sun position would be behind the shaded surface casting light towards the front.

Using this look-up table approach, the reflectance and scene fraction values for any forest stand can be normalized to flat terrain. To accomplish this, several steps were followed. First, the MFM model was parameterized with the range of forest structure measured on the ground for a given plot. The illumination and terrain inputs were kept constant for the time of image acquisition and the position of the plots, respectively. Then for each endmember set, the scene fraction output from the GOMS MFM was compared to scene fractions produced for the plot using SMA. Once a match was found, the structural inputs, which produced them, were recorded from the look-up table. This set of forest structure variables most accurately characterizes the stand structure variability in the plot. Next the MFM model was re-parameterized using these structural values and the slope and aspect values were adjusted to flat terrain. The output from this trial was a set of terrain normalized scene fraction values that this stand structure would produce on flat terrain.

The normalized scene fraction values were then used to predict LAI using linear regression analysis. These regressions were repeated for both the 1m and 2m image resolutions and for the different endmember sets, resulting in 36 regression trials, as outlined in Table 3-6. The ability to predict LAI was again based on the magnitude of the coefficient of determination (r^2).

Table 3-6 The number of regression trials is a function of different combinations of various options and data sets available in the study.

Total Number of Separate Regression Analyses	
Variable Name and Description	Number of Variables (N)
Number of Scene fractions (sunlit canopy, sunlit background, and shadow)	3
Image Resolution	2
Number of endmember sets (reference, image and integration)	3
Different LAI measurements (LAI 2000 and TRAC)	2
TOTAL	36

3.7 Chapter Summary

In this chapter, two separate methods were presented and developed for improved prediction of ground-based measurements of leaf area index. The first method is based on spectral mixture analysis of terrain normalized images using illumination-based algorithms at the pixel scale. This method was designed to build on the continued success of spectral mixture analysis in low relief environments. The second method was developed to incorporate physically-based optical reflectance models to account for stand structure at the sub-pixel scale in terrain normalization. This method was developed to provide a means of characterizing the variability in terrain and forest structural information as a function of pixel reflectance values. When used in this context the GOMS MFM approach can provide an improved information for relating forest structure and terrain with pixel level reflectance.

CHAPTER FOUR

RESULTS AND DISCUSSION

4.1 Introduction

In this chapter, the ability of scene fraction values derived using SMA and GOMS MFM to predict leaf area index (LAI) will be assessed and compared. It will be shown that a terrain normalization method that accounts explicitly for forest structure and terrain improves the ability to predict LAI using scene fraction values. Prior to testing the relationship between scene fraction values and forest leaf area, scene fraction values produced by SMA and the forest reflectance model had to be validated. The scene fractions produced at the 1m and 2m image resolutions using the two methods were tested against a maximum likelihood (ML) classification performed at the 60cm image resolution. This provided a way of testing the scene fractions produced using the different endmember sets.

Once the fractions had been validated, separate linear regression analyses were performed to test each endmember set and terrain normalization method for predicting field based LAI measurements from the LAI-2000 and TRAC systems at the 1m and 2m image resolutions. Linear regression analysis was used to assess the statistical relationship between remote sensing derivatives and forest leaf area. The regression analysis was employed to assess the amount of variation in the dependent variable, leaf area index, which may be explained by the independent variables, scene fraction values. The ability to predict the leaf area index was based on the magnitude of the regression coefficient of determination r^2 for the bivariate case and R^2 for the multivariate case. A multivariate regression analysis was also performed using the best SMA fractions with NDVI to examine the possibility of using

these two methods together. The initial NDVI results were significantly lower than the mixture fractions, however, NDVI was incorporated into the regression analysis to determine if it provided any additional information not contained in the SMA fractions. The combined ability to predict forest leaf area was again determined by the magnitude of the coefficient of determination R^2 . All regression results are based on the use of 27 field plots composed of softwood species, lodgepole pine, white spruce and Douglas-fir.

4.2 Spectral Mixture Analysis

4.2.1 Scene Fraction Validation

Each set of scene fractions and RMS error produced using each endmember set and normalization method were evaluated separately to ensure that the fractions produced were correct in a physical scene prior to any attempt to predict LAI. During the initial testing of the algorithms, it was obvious that the cosine correction was unusable in most of the study area. The correction factors produced using the cosine correction method could not account properly for steep slopes and aspects facing away from the sun. The correction produced adjusted the digital values of the pixels to such an extent that the endmembers no longer properly characterized the scene as depicted in Figure 4-1. Only 8 plots were considered usable based on the amount of correction applied by the cosine method. The cosine correction did, however, improve the estimation of LAI in these stands compared to the same 8 stands with no terrain correction. As a result of this over correction, the cosine correction approach to terrain normalization was removed from the subsequent analysis.

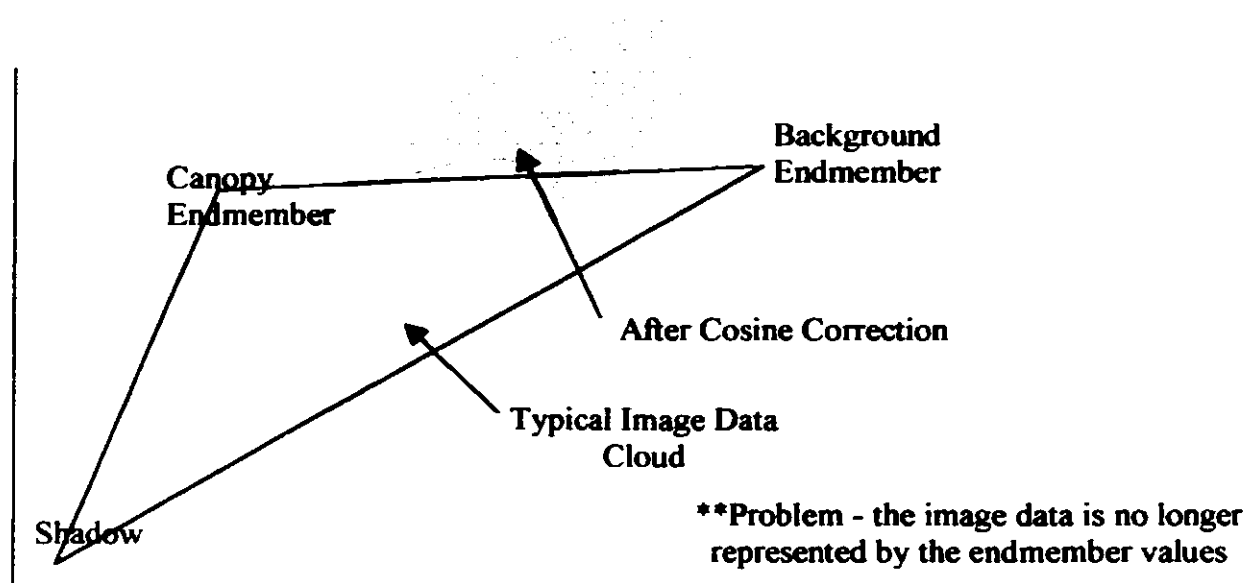


Figure 4-1 The over correction produced by the cosine correction adjusted the raw DN's to such an extent that the different endmember sets were no longer able to characterize the scene components. As a result, the cosine correction was removed from subsequent analyses.

As a first test, the RMS error produced from each endmember set and normalization method was used as an initial indicator of the endmembers ability to represent the scene. The RMS error was low in all trials, (maximum of only 0.02%), which suggested that the endmembers used in each case were representative of spectral values in the scene.

The amount of error found between the scene fractions produced at 1m and 2m scales and the ML supervised classification of scene components at the 60cm scale are shown in Figures 4-2, 4-3 and 4-4. The terrain normalized fractions were produced by first applying each terrain normalization method (c-correction, statistical-empirical, Minneart) to the original CASI imagery. Then, SMA was applied to each normalized image, and the resulting fractions compared to the ML classification of the normalized image. Prior to any attempt to

normalize terrain. There was good agreement between the fractions produced at the 1m and 2m resolutions with the ML supervised classification at 60cm resolution. The difference, expressed as a percentage, was determined for each of the three scene components sunlit canopy, sunlit background and shadow with respect to the ML classification. The reference endmember case offered the closest agreement between the SMA fractions and the ML classification results. Differences ranged between 3% and 6% for each scene component, with the maximum variation observed for the shadow component. The image and integrated endmembers cases showed a greater difference between the ML classification result and SMA fractions. Differences ranged from 3% to 11% (mean = 6%) for the shadow endmember. The image sunlit canopy and background fractions ranged between 4% and 6% difference (mean=4%). Image scale seemed to have little effect on the results obtained from the 1m and 2m CASI data. These results suggest that the SMA trials were in fact producing representative scene fractions prior to terrain normalization.

Difference between 1m Scene Fractions using Reference Endmembers and 60cm ML Classification

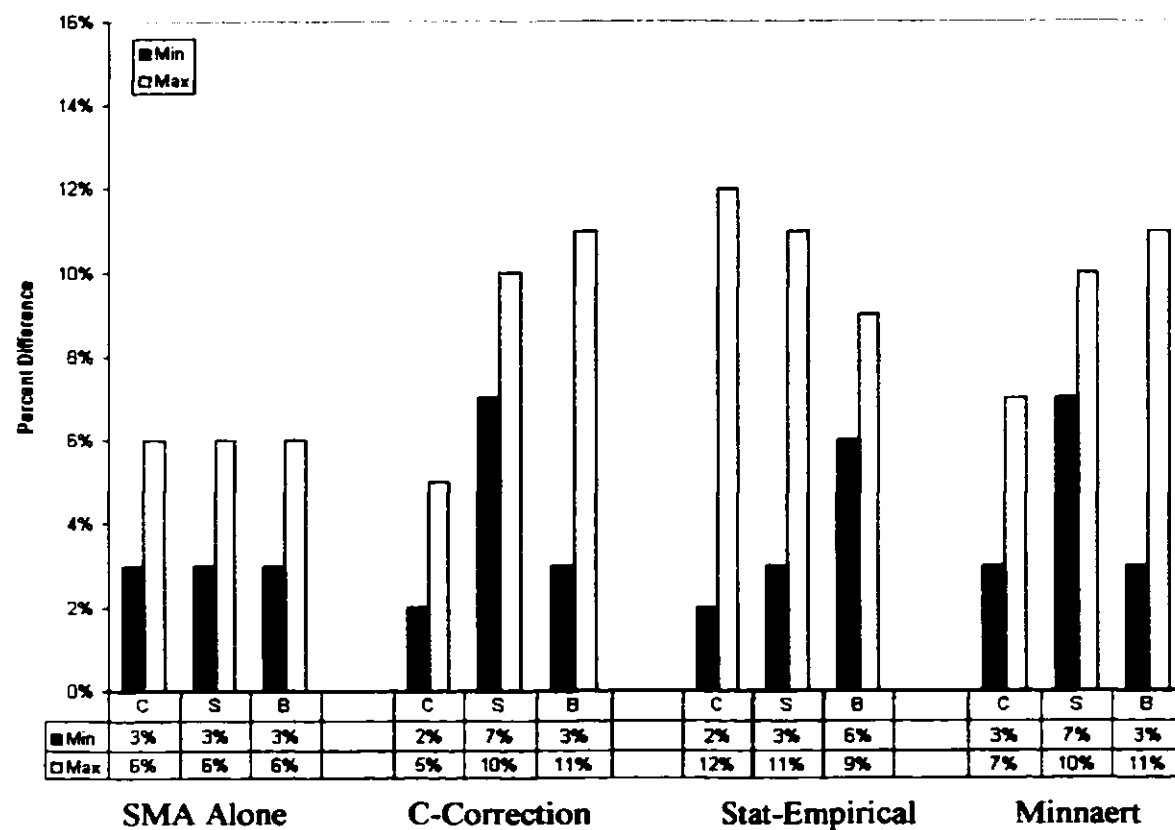


Figure 4-2 Difference between the scene fractions produced using the reference endmember set and ML supervised classification under different terrain normalization conditions. The minimum and maximum difference is shown for each scene component, C (sunlit canopy), S (shadow) and B (sunlit background). The best overall results were without terrain normalization.

Difference between 1m Scene Fractions using Image Endmembers and 60cm ML Classification

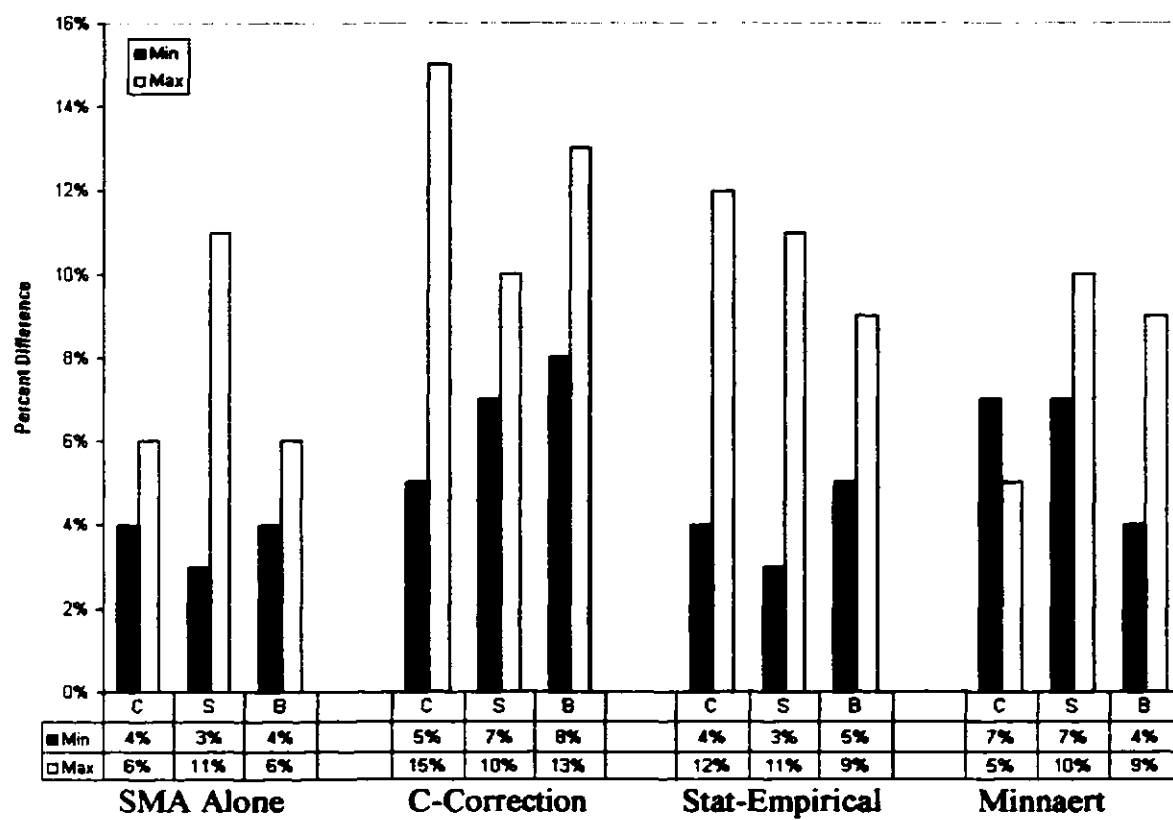


Figure 4-3 Difference between the scene fractions produced using the image endmember set and ML supervised classification using different terrain normalizations. The minimum and maximum difference is shown for each scene component, C (sunlit canopy), S (shadow) and B (sunlit background). The best overall results were found without terrain normalization.

Difference between 1m Scene Fractions using Integrated Endmembers and 60cm ML Classification

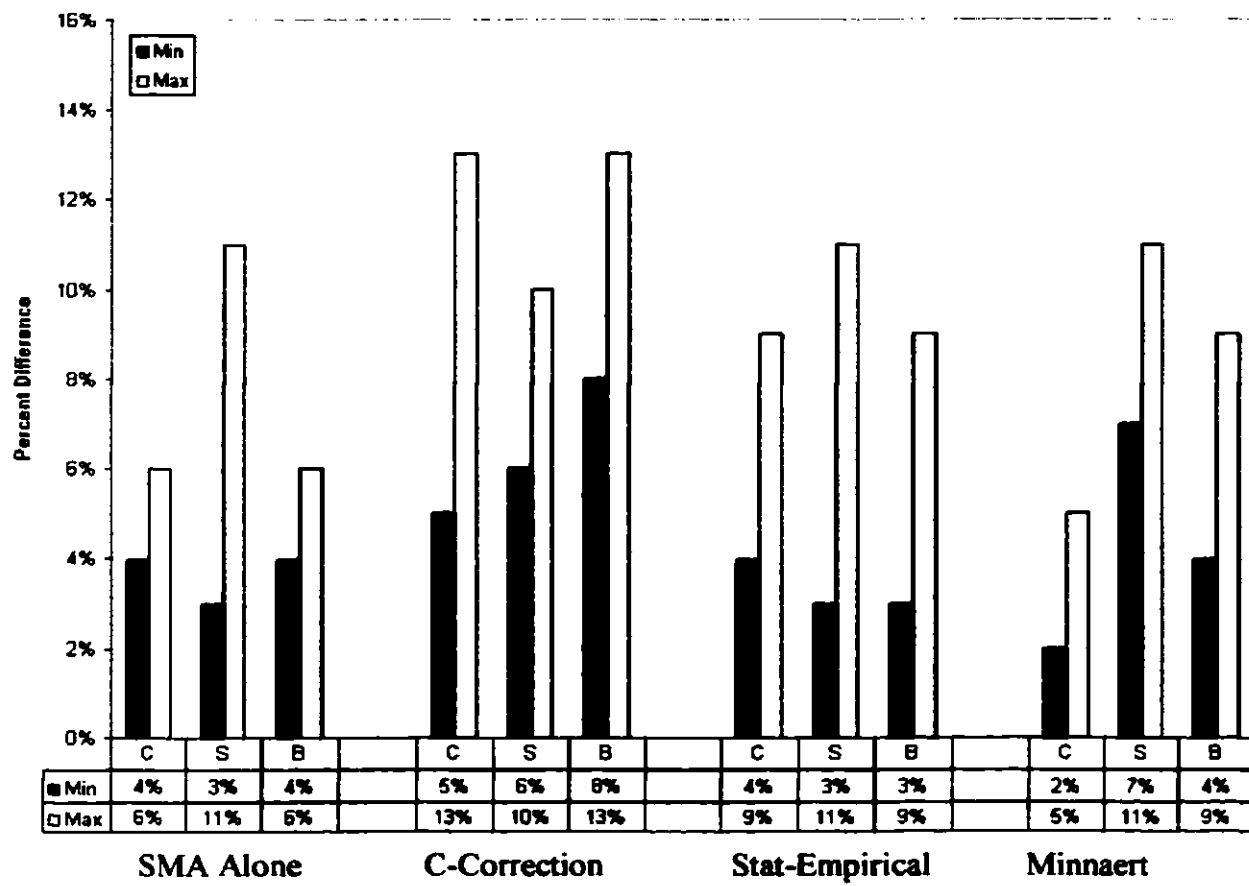


Figure 4-4 Difference between the scene fractions produced using the integrated endmember set and ML supervised classification using different terrain normalizations. The minimum and maximum difference is shown for each scene component, C (sunlit canopy), S (shadow) and B (sunlit background). The best overall results were without terrain normalization.

When the terrain normalizations were applied prior to SMA the percent difference increased using each of the C-correction, Statistical-Empirical and Minnaert approaches for each endmember set. The best overall correspondence between the scene fractions and ML classification was found using the reference endmember set and the C-correction. Differences ranged between 2% and 5% for the sunlit canopy component (Figure, 4-2), providing a small improvement over that obtained without terrain normalization. The difference increased for the sunlit background and the shadow component from 7% to 10% and 3% to 11%, respectively (Figure 4-2). There was little difference between the image and integrated endmembers sets for each normalization trial, however, the poorest overall results were found using the image endmember set with the C-correction with the difference ranging from 5% to 15% (Figures 4-3, 4-4).

These results were important as they suggest that terrain normalizations based on pixel level illumination differences did not properly account for the variations induced by changes in slope, aspect and forest structure at the sub-pixel scale. However, as will be shown later, they still provided an improved estimate of LAI over no terrain normalization.

4.2.2 LAI Prediction using Spectral Mixture Analysis

The results of the linear regression analysis to predict two sets of leaf area index measurements from the TRAC and LAI-2000 are summarized in Tables 4-2 to 4-6 for the 1m and 2m resolutions. Each scene component fraction was used as an independent variable in predicting both LAI and eLAI measured from the two optical instruments. The tables below summarize the results and show only the best predicting variable in each case, sunlit canopy

(c), sunlit background (b) or shadow (s) (Tables 4-1, 4-2). As a basis for comparison, NDVI was also computed from each terrain normalization method and used as an independent variable for the various regression trials. The results show that prior to terrain normalization, the reference endmember set provided the best overall results. The best results were r^2 of 0.69 and 0.67 for the TRAC measurements (Table 4-1, 4-2) and r^2 of 0.62 and 0.72 for the LAI-2000 (Table 4-3, 4-4) for the 1m and 2m resolutions respectively. NDVI yielded r^2 of 0.33 and 0.34 (Table 4-1, 4-2) for the TRAC, with r^2 0.45 and 0.44 obtained for the LAI-2000 (Table 4-3, 4-4) measurements at the 1m and 2m resolutions.

Table 4-1 Magnitude of the regression coefficient of determination (r^2) using SMA applied to images corrected with different terrain normalization methods to predict TRAC LAI at 1m image pixel resolutions. The best scene fraction for each SMA trial is shown in brackets for sunlit canopy (c), sunlit background (b) and shadow (s).

Image Spatial Resolution	Endmember Set & NDVI	SMA of original image	SMA after Minnaert correction	SMA after C-correction	SMA after Stat-Empirical correction
1m	Reference	0.69(b)	0.72(c)	0.76(c)	0.77(c)
1m	Image	0.61(s)	0.69(c)	0.74(s)	0.74(b)
1m	Integrated NDVI	0.68(s)	0.70(s)	0.77(s)	0.78(s)
		0.33	0.51	0.41	0.46

Table 4-2 Magnitude of the regression coefficient of determination (r^2) using SMA applied to images corrected with different terrain normalization methods to predict TRAC LAI at 2m image pixel resolutions. The best scene fraction: for each SMA trial is shown in brackets for sunlit canopy (c), sunlit background (b) and shadow (s).

Image Spatial Resolution	Endmember Set & NDVI	SMA of original image	SMA after Minnaert correction	SMA after C-correction	SMA after Stat-Empirical correction
2m	Reference	0.65(b)	0.70(s)	0.75(c)	0.75(s)
2m	Image	0.55(b)	0.69(s)	0.68(s)	0.71(s)
2m	Integrated NDVI	0.67(c)	0.72(s)	0.71(c)	0.71(s)
		0.34	0.50	0.41	0.48

Table 4-3 Magnitude of the regression coefficient of determination (r^2) using SMA applied to images corrected with different terrain normalization methods to predict LAI-2000 eLAI at 1m image pixel resolutions. The best scene fraction: for each SMA trial is shown in brackets for sunlit canopy (c), sunlit background (b) and shadow (s).

Image Spatial Resolution	Endmember Set & NDVI	SMA of original image	SMA after Minnaert correction	SMA after C-correction	SMA after Stat-Empirical correction
1m	Reference	0.62(b)	0.70(c)	0.71(c)	0.68(c)
1m	Image	0.52(b)	0.62(c)	0.66(s)	0.66(b)
1m	Integrated	0.55(c)	0.62(s)	0.69(s)	0.71(s)
	NDVI	0.45	0.54	0.48	0.50

Table 4-4 Magnitude of the regression coefficient of determination (r^2) using SMA applied to images corrected with different terrain normalization methods to predict LAI-2000 eLAI at 2m image pixel resolutions. The best scene fraction: for each SMA trial is shown in brackets for sunlit canopy (c), sunlit background (b) and shadow (s).

Image Spatial Resolution	Endmember Set & NDVI	SMA of original image	SMA after Minnaert correction	SMA after C-correction	SMA after Stat-Empirical correction
2m	Reference	0.62(b)	0.70(s)	0.69(c)	0.68(s)
2m	Image	0.53(b)	0.63(s)	0.68(s)	0.68(s)
2m	Integrated	0.72(c)	0.69(s)	0.70(c)	0.70(s)
	NDVI	0.44	0.55	0.48	0.50

In terms of overall improvement in prediction using SMA, the C-correction and statistical-empirical methods showed improvements in r^2 of 0.14 and 0.15 using the image endmember set at the 1m and 2m image resolution respectively for the LAI 2000 as compared to SMA alone (Tables 4-3, 4-4). The magnitude of the prediction for the TRAC values still remained higher; however, they showed smaller improvements in prediction compared to the improvements found using the LAI-2000. The greatest improvements in

predicting TRAC LAI were again using the C-correction and statistical-empirical approach, with improvements in r^2 of 0.13 and 0.08 using the image endmember set at the 1m and 2m resolutions, respectively. Improvements to NDVI were significant, with maximum increases in r^2 of 0.18 and 0.11 using the Minnaert to predict LAI and eLAI, respectively. However, the ability to predict LAI using NDVI remained lower than the SMA fractions in all cases.

Previous research (Peddle, 1997; Hall et al, 1995) has shown that the shadow fraction is consistently the best predictor of LAI in low relief environments, however, these results have shown no pattern in which a particular fraction provided consistently better results. This is likely to be a function of terrain, which influences which scene fraction is most visible to the sensor.

4.2.3 Multivariate Regression using NDVI and SMA Fractions

A multivariate regression analysis was performed using the best SMA fraction with NDVI to examine the possibility of using these two methods together, under each of the normalization methods. Although results from NDVI alone were significantly lower than results from SMA alone a set of tests were undertaken to see if using both SMA and NDVI together in a multiple regression would provide any additional improvements.

This would determine if NDVI provided any new or additional predictive information not included in the SMA fractions. Since NDVI is simple to compute, it would not be impractical to use both methods together. The best results of the multivariate regression are shown in Tables 4-5 and 4-6 (for the 1m and 2m images respectively), in which the far right column shows the improvement provided by incorporating NDVI.

Table 4-5 Improvements provided by incorporating NDVI into the prediction of TRAC LAI and LAI-2000 eLAI using the uncorrected SMA fractions at 1m image pixel resolution.

Image Spatial Resolution	Endmember Set	TRAC LAI R ² SMA and NDVI	Improvement over SMA Fraction Alone	LAI-2000 eLAI R ² SMA and NDVI	Improvement over SMA Fraction Alone
1m	Reference	0.74	0.05	0.62	0.02
1m	Image	0.72	0.11	0.54	0.02
1m	Integrated	0.73	0.05	0.56	0.01

Table 4-6 Improvements Provided by Incorporating NDVI into the Prediction of TRAC LAI and LAI-2000 eLAI using the Uncorrected SMA Fractions at 2m image pixel resolution.

Image Spatial Resolution	Endmember Set	TRAC LAI R ² SMA and NDVI	Improvement over SMA Fraction Alone	LAI-2000 eLAI R ² SMA and NDVI	Improvement over SMA Fraction Alone
2m	Reference	0.72	0.07	0.62	0.00
2m	Image	0.67	0.12	0.54	0.01
2m	Integrated	0.67	0.00	0.73	0.01

The incorporation of NDVI provided very limited improvements for predicting LAI and eLAI. The inclusion of NDVI showed improvements in R² values between 0 and 0.12 for the prediction of TRAC LAI. The greatest improvements were found using the image endmember set which were R² values of 0.11 and 0.12 for the 1m and 2m resolutions. In terms of improvement the inclusion of NDVI provided a maximum increase in R² of 0.2 to the prediction of eLAI measured with the LAI-2000.

Using the SMA fraction from the image endmember set in combination with NDVI improved the prediction of TRAC LAI to a level similar to the reference endmember set when used alone. For the prediction of eLAI, the inclusion of NDVI provided only minimal improvements. It is therefore concluded that use of the reference and integrated endmember sets provided the best estimates of LAI and eLAI when used alone. The inclusion of NDVI with the SMA image endmember fractions can provide estimates of LAI that are comparable with the estimates provided by the reference endmember set. This would be an option if the collection of reference spectral data were not possible, however, the inclusion of NDVI did not provide any significant improvement to the prediction of eLAI using image endmembers.

4.3 Multiple Forward Mode Results

The output from the MFM approach was evaluated in a similar manner as the SMA results. The first step was to validate the scene fractions produced from the reflectance model. The same ML supervised classifications produced at the 60cm resolution to test the SMA results were used here to test the output of the MFM approach. The first, significant difference between the SMA results and the MFM approach was that the MFM approach produced its output as a series of scene fractions based on structural input parameters, whereas, SMA produced a single set of fraction values based on spectral input values. In the GOMS model, the fractions of material visible to the sensor (scene fractions) are solely a function of geometry, whereas, in SMA the abundances produced are solely a function of the spectral endmember values for each scene component. For each plot, the MFM model was parameterized with a range of structural information measured on the ground, the solar zenith

position and azimuth during the time of image acquisition, endmember values for each set (reference, image and integrated) and the terrain variables of slope and aspect derived from the DEM. The MFM runs produced scene fractions as well as pixel level reflectance values. The variation between the ML supervised classification results and the MFM scene fractions were variable based on the structural information used to parameterize the model. However, for all plots there was a range of structural data near the mean for the plot which showed good overall correspondence between the classification and MFM scene fractions (Table 4-5).

The results shown in Figure 4-5 are the minimum and maximum for the entire range of input structural data. The reference endmember set provided the best correspondence between the classification and the MFM scene fractions. Differences ranged from 3% to 17%, with the largest difference found in the shadow fraction. Image resolution had no effect on the difference in scene fractions as the fractions produced were only a function of the model-input measurements collected on the ground. The results from the image and integrated endmember sets were more variable. The image endmember set had the largest differences of the three sets tested. Results ranged from 3% to 26% difference, with the maximum difference again found with the shadow fraction. The integrated endmember set performed better, with differences ranging from 2% to 20%. In this case, the background fraction exhibited the maximum variation. Examination of the structural input data for each trial showed that the maximum errors occurred near the extremes of the structural range provided to the model for each plot. The results suggest that, as expected, the extremes in the structural range measured on the ground did not accurately characterize the plot and that the mean structural data provided the best representation of stand structure based on the

magnitude of difference between the ML classification and scene fractions produced from the MFM.

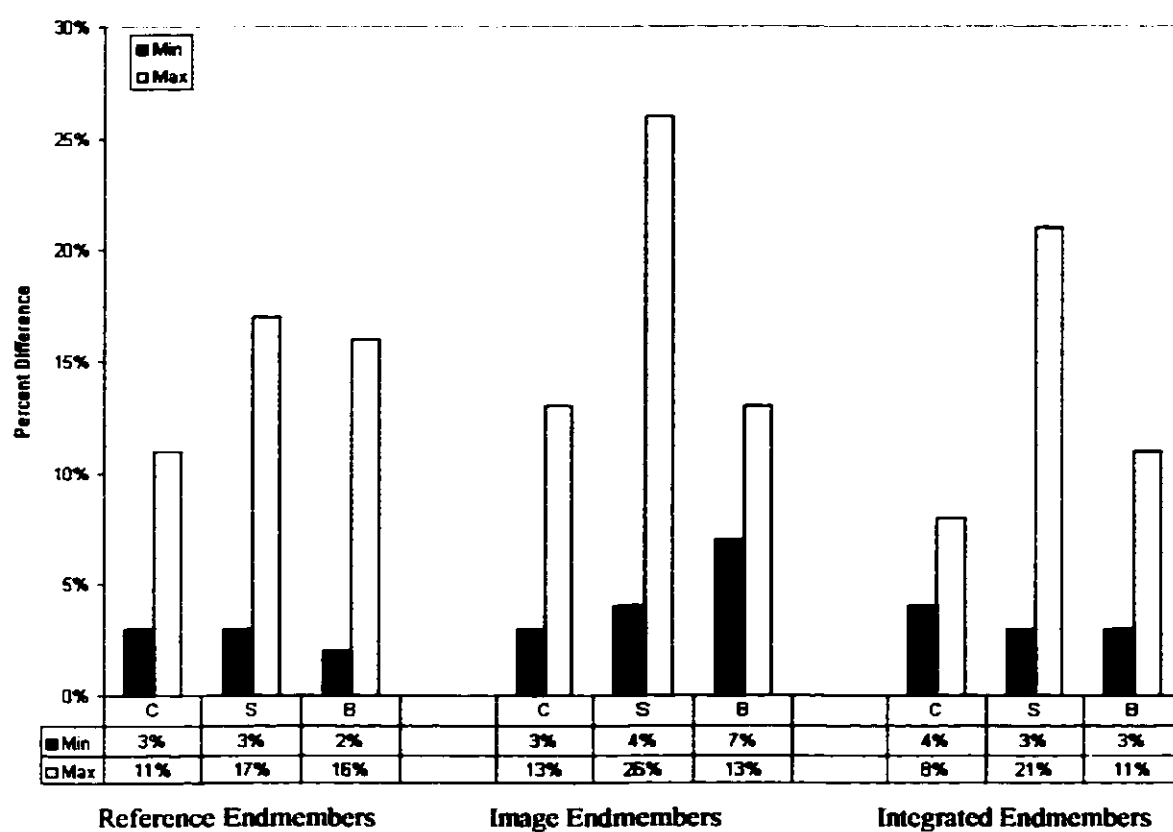


Figure 4-5 Difference between the scene fractions produced using the MFM model and ML supervised classification using each endmember set. The minimum and maximum difference is shown for each scene component, C (sunlit canopy), S (shadow) and B (sunlit background).

4.3.1 SMA and MFM Fraction Matching

For each plot, scene fraction values were computed using SMA with each of the three endmember sets. The MFM lookup table containing the full set of modeled fractions was then searched to find modeled fractions which matched those produced by SMA. Once a match had been found, the structural input data associated with that set of modeled fractions were recorded. This structural information was then used to re-parameterize the model prior to terrain normalization. This first step ensured that the forest structure inputs to the MFM model accurately characterized each stand. After the match had been established the model was re-parameterized with this structural data and the terrain variables were adjusted to flat terrain. The output from this second model trial was a set of scene fractions which had been normalized to flat terrain. These scene fractions were subsequently used in the linear regression analyses.

4.3.1.1 MFM prediction of Leaf Area Index

The results of the linear regression analyses to predict the two sets of leaf area index estimates from the TRAC and LAI-2000 are summarized in Tables 4-7 and 4-8 for the 1m and 2m resolutions. Each scene component fraction was used in a separate regression analysis to test the ability to predict leaf area index. The highest magnitudes of r^2 were found for the prediction of LAI measured with the TRAC using the shadow fraction produced from the reference and integrated endmember sets (Table 4-9). For the reference endmember set r^2 values ranged from 0.83 to 0.82 for the 1m and 2m data. The integrated set had r^2 values of 0.83 and 0.77 for the 1m and 2m data, respectively.

The results for the LAI-2000 were similar, with r^2 values of 0.82 and 0.79 for the 1m and 2m data (Table 4-10). The best result of 0.82 was based on using the background fraction as the independent variable in the regression analysis at the 1m resolution. This result was the only case where the shadow fraction did not provide the best prediction of both LAI and eLAI. This result is consistent with previous research where the shadow fraction was the best predictor of forest biophysical parameters (Hall et al, 1995 and Peddle, 1997). Therefore, the results obtained here suggest that this normalization method is accounting for forest structure at the sub-pixel scale. Overall improvements in prediction of LAI provided by the MFM approach are shown in Tables 4-9 and 4-10.

Table 4-7 Magnitude of the regression coefficient of determination (r^2) using the MFM approach to predict TRAC LAI at the 1m and 2m image resolutions. The best result is shown in bold for each image resolution.

Image Spatial Resolution	Endmember Set	Canopy Fraction	Shadow Fraction	Background Fraction
1m	Reference	0.82	0.83	0.60
1m	Image	0.64	0.82	0.79
1m	Integrated	0.55	0.83	0.80
2m	Reference	0.14	0.80	0.79
2m	Image	0.45	0.79	0.50
2m	Integrated	0.12	0.77	0.15

Table 4-8 Magnitude of the regression coefficient of determination (r^2) using the MFM approach to predict LAI-2000 eLAI at the 1m and 2m image resolutions. The best result is shown in bold for each image resolution.

Image Spatial Resolution	Endmember Set	Canopy	Shadow	Background
1m	Reference	0.69	0.79	0.47
1m	Image	0.46	0.76	0.82
1m	Integrated	0.38	0.80	0.69
2m	Reference	0.69	0.75	0.34
2m	Image	0.12	0.79	0.72
2m	Integrated	0.37	0.73	0.71

Table 4-9 Improvements provided by the Multiple Forward Mode Approach to Predict TRAC LAI

Image Spatial Resolution	Endmember Set	Magnitude of r^2 using MFM using the Shadow Fraction	Improvement over SMA Fraction without terrain correction	Improvement over best terrain normalized SMA Fraction	Improvement over terrain normalized NDVI
1m	Reference	0.83	0.14	0.06	0.32
1m	Image	0.82	0.21	0.08	0.31
1m	Integrate	0.83	0.15	0.05	0.32
2m	Reference	0.80	0.15	0.05	0.30
2m	Image	0.79	0.24	0.08	0.29
2m	Integrate	0.77	0.10	0.05	0.27

Table 4-10 Improvements provided by the Multiple Forward Mode Approach to Predict LAI-2000 eLAI

Image Spatial Resolution	Endmember Set	Magnitude of r^2 using MFM using the Shadow Fraction	Improvement over SMA Fraction without terrain correction	Improvement over best terrain normalized SMA Fraction	Improvement over terrain normalized NDVI
1m	Reference	0.79	0.17	0.08	0.25
1m	Image	0.82	0.30	0.16	0.32
1m	Integrate	0.80	0.25	0.11	0.26
2m	Reference	0.75	0.13	0.05	0.20
2m	Image	0.79	0.26	0.11	0.24
2m	Integrate	0.73	0.01	0.03	0.18

The greatest improvements in predicting LAI were provided using the MFM approach to account for the effects of terrain, and forest structure as compared to each normalization method. The highest r^2 values for predicting TRAC LAI were 0.83 and 0.80 using reference endmembers at the 1m and 2m resolutions (Table 4-9). Increases in r^2 values of 0.21 and 0.24 were obtained using the image endmembers to predict TRAC LAI values at the 1m and 2m resolutions respectively, compared to SMA without normalization (Table 4-10). The MFM also provided improvements in r^2 of 0.32 and 0.30 compared to the best normalized NDVI results. Prediction of LAI-2000 eLAI increased by a magnitude of 0.25 and 0.26 using the image and integrated endmember sets at the 1m and 2m image resolutions, compared to SMA without normalization. The best prediction of eLAI values showed r^2 values of 0.80 and 0.73 using the integrated endmember set with the MFM approach for the 1m and 2m image resolutions. The MFM approach also provided improvements in estimating eLAI over terrain normalized NDVI with increases in r^2 of 0.32 and 0.24 for the 1m and 2m data respectively. These improvements can be attributed to accounting for the internal stand structure during terrain normalization using the MFM approach.

4.3.2 Discussion

Summaries of all the results obtained are shown in Figures 4-6 and 4-7, which outline the magnitude of the coefficient of determination r^2 for each method tested (NDVI, NDVI with terrain normalization, SMA, SMA with terrain normalization and MFM). This provides a way to compare results with respect to the different types of endmember sets (reference, image and integrated), the different image resolutions (1m, 2m), and the different LAI

instruments (TRAC and LAI-2000). The most appropriate method to use would depend on the research objectives of the particular study as well the data sets available.

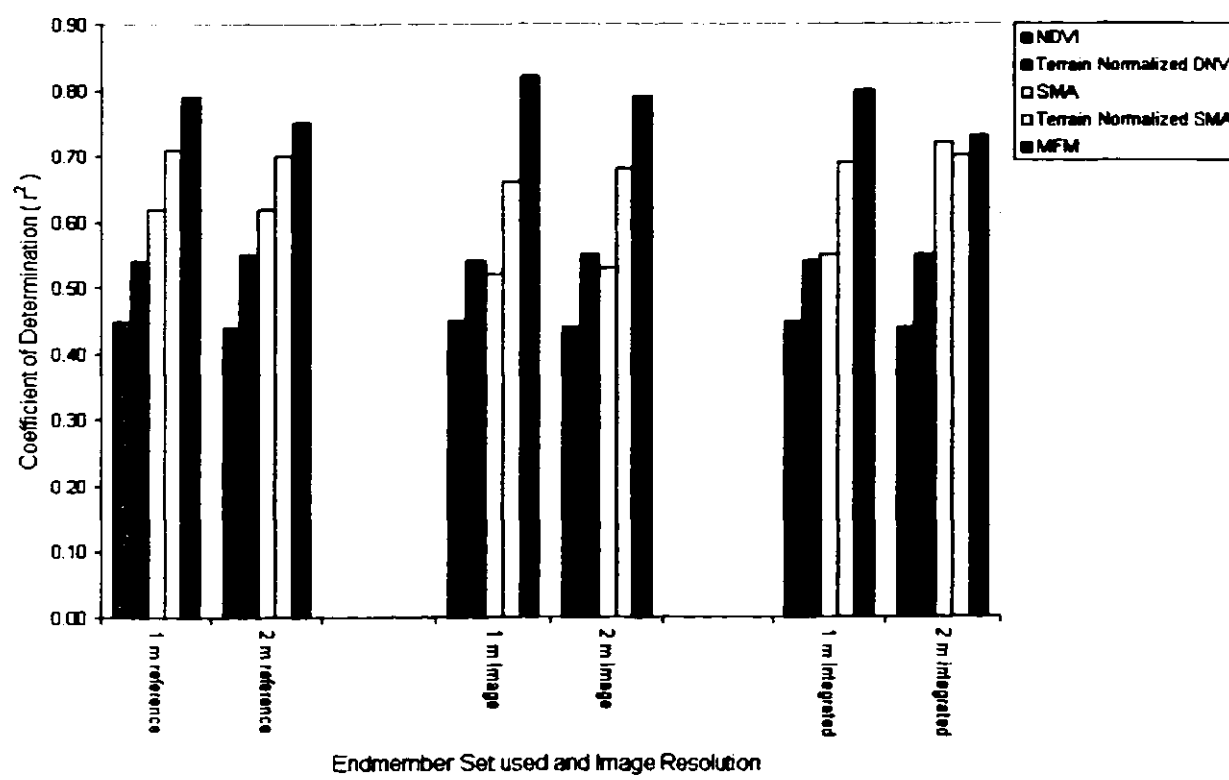


Figure 4-6 The magnitude of the coefficient of determination for each method tested is shown for predicting TRAC LAI

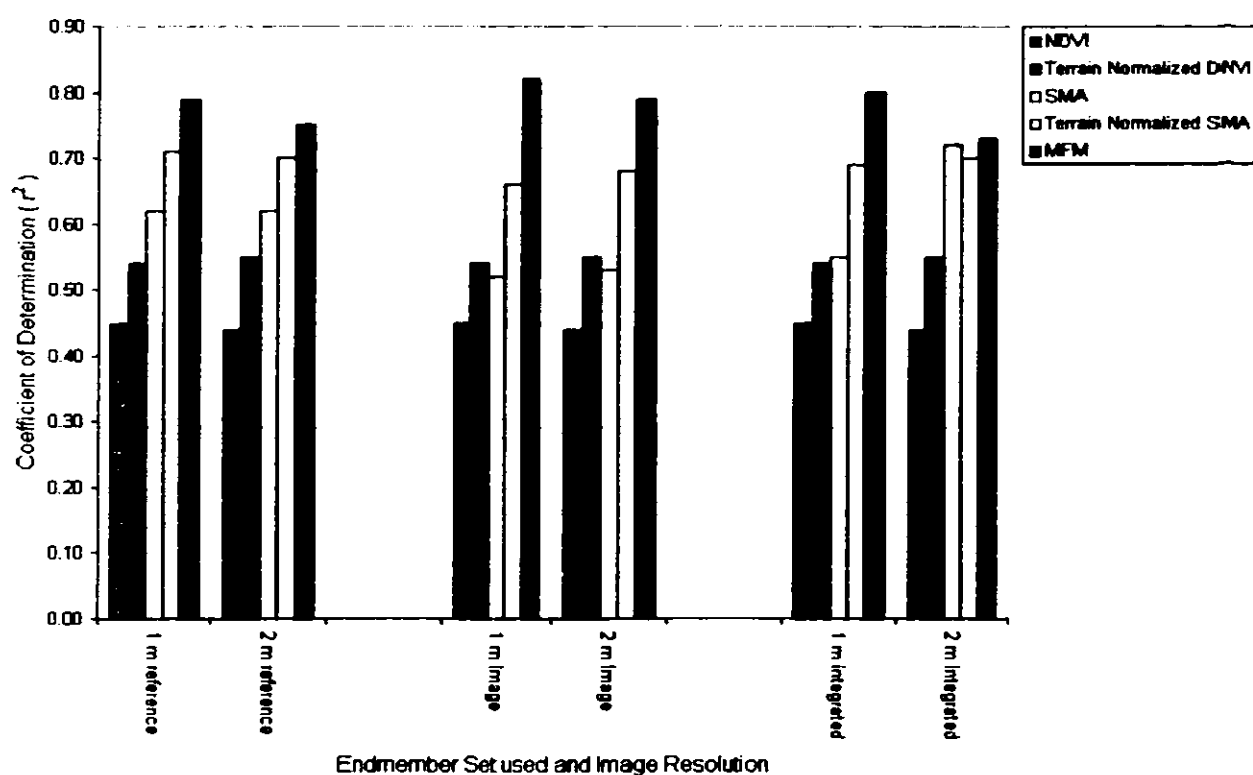


Figure 4-7 The magnitude of the coefficient of determination for each method tested is shown for predicting LAI-2000 eLAI

The reference and image endmember sets provided better results, compared to the integrated set. This result was surprising as it was thought that the integrated endmember set would be better able to characterize the canopy using the reference endmember, and the background and shadow components with the image endmembers. Overall, for most applications the use of image or reference endmember with the MFM approach provided the best overall predictions of forest LAI in mountainous terrain.

The difference between the 1m and 2m image resolutions had little influence on the ability to predict leaf area index using any of the methods tested. Generally, a decrease in the spatial resolution in the remote sensing imagery will cause a decrease in the variance among pixels, reducing the ability to extract biophysical information using traditional methods.

However, neither spectral mixture analysis nor the geometric optical reflectance model were considerably affected by this resolution change. The relative change in image resolution did not affect the analysis to a great extent, as the pixel resolution in both cases was still smaller than individual tree crowns. If the pixel size was larger than an individual tree crown (low resolution), the effects may have been more notable.

Based on the results obtained, the ability to predict LAI measured with the TRAC was greater than the ability to predict eLAI measured with the LAI-2000. There are two possible reasons for this. First, the orientation of the optics on the TRAC instrument constraint the FOV to only the canopy above the sensor, which was inside the plot boundaries, whereas, the large FOV of the LAI-2000 may have included an area of canopy outside the plot. This is significant since image analysis was performed only on pixels within the boundaries of the plot. Therefore, it is possible that the LAI-2000 captured information from outside the plot, which was not accounted for in the image analysis. Second the TRAC accounts for the non-random nature of forest canopies by measuring sunfleck width, which is related to gaps in the overhead canopies. These sunfleck values are strongly related to the canopy structure and geometry. Both SMA and the GOMS MFM account for forest structure as part of their predictive ability. SMA estimates the abundance of sunlit canopy, sunlit background and shadow visible to the sensor, which is directly related to forest structure. The GOMS MFM approach directly accounts for forest structure through the structural model inputs provided by the user.

Accurate forest information is particularly important if the results are to be used in process based ecophysiological models where LAI is one of the primary variables used to characterize the forest canopy. The MFM approach provided the best results in all cases, in

terms of the ability to predict LAI. With respect to practicality and ease of use, the MFM approach required additional inputs. However, based on the relative ease with which the input data can be acquired through base line vegetation inventories such as the Alberta Vegetation Inventory (AVI), and the relaxed requirement for detailed forest measurements using the MFM, approach it is a suitable approach in most circumstances. This approach does not require exact forest measurements; instead a range of values is required as input, which is easily obtained. Detailed field measurements are not required for this approach to be used effectively.

4.4 Chapter Summary

In this chapter, two sets of results were presented and discussed for predicting ground-based measurements of leaf area index. Each set of scene fractions were validated against a ML supervised classification of the 60 cm spatial resolution imagery prior to LAI prediction. The first set of results were based on spectral mixture analysis of terrain normalized images using illumination based algorithms. These results have shown that the cosine correction was inappropriate for the high relief environment present in the study area. The C-correction and Statistical Empirical normalization method provided the greatest improvements for predicting LAI measured with the TRAC, using the SMA approach. There was very little difference between the Minnaert, C-correction and Statistical method for the prediction of eLAI measured with the LAI-2000, using the SMA approach. The second set of results from the MFM trials has shown that a method of terrain normalization that explicitly accounts for

forest structure provided improved estimates of LAI in mountainous terrain. The MFM approach provided the best estimates of LAI and eLAI compared to all other methods tested.

CHAPTER FIVE

CONCLUSIONS

5.1 Summary of Results

The ability to provide accurate and timely estimates of forest biophysical information over mountainous terrain provides improved parameterization of regional and global scale process-based ecological models. These models form the foundation, upon which predictions about regional and global scale carbon budgets can be based, which is important in studies of global change. Forest leaf area is an important structural parameter of forest ecosystems, as it provides information on energy, gas and water exchange with the atmosphere. LAI is related to NPP, which is important in global climate change research since NPP can be related to carbon storage.

Significant improvements in the estimation of LAI have been shown using spectral mixture analysis in low relief environments (Peddle et al, 1997, 1999b). However, previous to this thesis, little research had been done to assess the ability to predict LAI in mountainous terrain using SMA. The Barrier Lake study site in Kananaskis Provincial Park, Alberta, Canada, provided an environment well suited to studying and accounting for the effects of terrain in the prediction of LAI. The Barrier Lake site provided a range in forest species, stand structure and terrain needed for this study. The influence of terrain has been shown to affect the amount of scene components visible to the sensor thereby affecting the radiance recorded by the sensor.

In this research the use of geometric optical reflectance models, and in particular the introduction of a new 'multiple forward model' (MFM) approach has provided a means to

account for the influence of terrain at the sub-pixel scale, improving the estimation of LAI. The best overall remote sensing estimates of ground-based LAI measured with the TRAC instrument were found using the MFM approach with the reference endmember set with r^2 values of 0.83 and 0.82 for the 1m and 2m image resolutions, respectively. The best estimates of eLAI measured with the LAI-2000 were found using the image endmember set with r^2 values of 0.82 and 0.79 for the 1m and 2m image resolutions, respectively. The inclusion of NDVI provided only minimal improvements in the prediction of LAI when combined with SMA, with improvements in R^2 values between 0 and 0.12 for the prediction of TRAC LAI and a maximum increase of 0.2 in the prediction eLAI. No improvements were found in the prediction of LAI when NDVI was incorporated with the MFM results, which suggests that NDVI provides no additional information to the MFM approach.

5.2 Conclusions

A number of major conclusions have been drawn from this research:

- Use of spectral mixture analysis and optical reflectance models provided substantial improvements over traditional vegetation index methods for estimating LAI in mountainous terrain.
- Terrain significantly influences the relative proportions of sunlit canopy, sunlit background and shadow visible to the sensor, thereby reducing the ability to predict LAI using traditional methods. Without some type of terrain normalization, the ability of image processing techniques to predict LAI is compromised. The best SMA

results were obtained from imagery which had been subjected to prior terrain normalization.

- Using geometric optical reflectance models in the multiple forward mode to account explicitly for forest structure in terrain normalization provided a way to characterize the change in sub-pixel scale fractions as a function of terrain and provided the most accurate LAI estimates in this mountainous environment. The predictive ability achieved using this approach was compared to other forested areas (e.g. flat boreal forest) and provided an acceptable level of accuracy for a mountainous environment.
- The multiple forward mode approach to geometric optical reflectance modeling eliminated the need for exact model inputs, by allowing the user to provide ranges of terrain and structural inputs. This has made these powerful physical models more accessible and easy to use, as well as providing a valuable source of forest information which provides explicit linkages between forest structure, terrain and image reflectance.

A number of additional conclusions may be drawn with reference to the observations made during this research:

- The reference endmember set consistently provided the best estimates of LAI measured using the TRAC using both the SMA and MFM approaches.
- The measurements of eLAI from the LAI-2000 were best predicted using image endmembers and integrated endmembers, regardless of the method used.

- The integrated endmember set did not perform as well as expected - it was assumed that this endmember set would provide the best combination of the advantages which the reference and image endmember sets provide. This suggests it may not be desirable to use different sources for endmembers in this type of mountainous environment.
- The C-correction and Statistical Empirical approaches to terrain normalization provided the best improvements in the prediction of LAI measured using the TRAC. There was very little difference among the Minnaert, C-correction and Statistical Empirical methods for the prediction of eLAI as measured using the LAI-2000.
- The inclusion of NDVI in a multiple regression analysis provided only limited improvements to the prediction of LAI using the SMA approach, and provided no improvements when combined with the MFM approach.
- Based on the regression results obtained, the TRAC system appeared to be more related to the scene fraction values compared to those obtained from the LAI-2000 (eLAI). This is probably because both the TRAC estimates of LAI and the scene fraction values are related to a great extent to the canopy gap distribution and architecture.
- The relationship between the scene fractions and the TRAC measurements were greater than for the LAI-2000, since both the TRAC and scene fractions are related to gap size distribution and canopy architecture.
- In terms of image spatial resolution, the results obtained from 1m and 2m CASI data were similar. This is likely due to the similarities in spatial scale, and that both were smaller than the main objects being sensed on the ground (tree canopies).

5.3 Contribution to Research

Contributions of this thesis to the research community include:

- A new approach to using geometric optical reflectance models in forest remote sensing studies. The new MFM approach provides researchers with easy-to-use tools to investigate the influence of forest structure, illumination and terrain on scene reflectance through new software which provides an interface with the GOMS optical reflectance model.
- Using the MFM approach, the influence of terrain on forest reflectance can be quantified and reduced, providing improved estimates of LAI in mountainous terrain.
- A comparison of the different endmember sets in the prediction of forest leaf area.

5.4 Future Research

Based on the work accomplished to date there are a number of areas for future research:

- Testing the ability of this method to predict other forest biophysical parameters such as biomass and NPP.
- Continued work using the MFM approach could provide a basis for greater understanding of the influence of terrain and stand structure on forest reflectance.

- Integration with other methods, such as tree delineation algorithms (Gougeon, 1995; Fournier et al, 1995), to possibly provide further improvements over that obtained using MFM alone.
- The expansion of this method to regional scales using satellite remote sensing imagery. This would also facilitate further development of a physically based approach to integrate land classification and biophysical parameter estimation (after Hall et al, 1997; Peddle et al, 1997), as well as the investigation of scale issues.
- There is also the potential of using the MFM approach in change detection studies.
- Application of this approach to other mountainous forests, and possibly to other types of forested ecosystems.

References Cited

- Adams J.B, Smith, M.O. and Gillespie, A.R., 1989. Simple models for complex natural surfaces: a strategy for the hyperspectral era of remote sensing. In, Proceedings of IGARSS'89/12th Canadian Symposium on Remote Sensing, Vancouver, B.C. vol.1: 16-21.
- Adams J.B. Smith, M.O. and Gillespie, A.R., 1993. Imaging spectroscopy: interpretation based on spectral mixture analysis. In, Remote Geochemical Analysis: Elements and Mineralogical Composition (C.M. Pieters and P. Englert, editors. LPI and Cambridge University Press, Cambridge ch. 7
- Altalis, 1999. Description of Elevation Data. <http://www.altalis.com/1to20000dem.htm>.
- Anger, C.D. S. Mah and S. Babey, 1994. Technological enhancements to the compact airborne spectrographic imager (CASI). In: Proceedings of the First International Conference on Airborne Remote Sensing, Strasbourg, France. Vol II, p. 205-213.
- ASD, 1998. Analytical Spectral Devices Inc. FieldSpec FR User's Guide. Boulder, Colorado. Variously paged.
- Blackburn, G.A, and Milton, E.J, 1995. Seasonal variation in the spectral reflectance of deciduous tree canopies. International Journal of Remote Sensing, vol. 16 no.4: 709-720.
- Bonan. G.B., 1990. Carbon and nitrogen cycling in North America boreal forests. II Biogeographical patterns. Can. J. For. Res. Vol. 20: 1077-1088.
- Bonan, G.B. 1991. Seasonal and annual carbon fluxes in a boreal forest landscape. Journal of Geophysical Research vol. 96. No. D9: 17,329-17,338.
- Bonan, G.B, 1993. Importance of leaf area index and forest type when estimating photosynthesis in boreal forests. Remote Sensing of Environment vol. 43: 303-314.
- Botkin, D.B. Estes, J.E. MacDonald R.M. and Wilson, M. V. 1984. Studying the Earth's vegetation from space. BioScience vol. 34 no. 8: 508-514
- Bruniquel-Pinel, V. and Gastellu-Etchegorry, J.P, 1998. Sensitivity of texture of high resolution images of forest to biophysical and acquisition parameters. Remote Sensing of Environment vol.65: 61-85.
- Baret, F. and Guyot, G. 1991. Potentials and limits of vegetation indices for LAI and APAR assessment. Remote Sensing of Environment vol. 35: 161-173

- CDIAC, 1999. G. Marland, T. A. Boden, R. J. Andres, A. L. Brenkert, and C. A. Johnston
http://cdiac.esd.ornl.gov/trends/emis/em_cont.htm
- Chen, J.M. 1996a. Evaluation of vegetation indices and a modified simple ratio for boreal applications. *Canadian Journal of Remote Sensing*. Vol. 22:229-249.
- Chen, J.M. 1996b. Optically based methods for measuring seasonal variation of leaf area index in boreal conifer stands. *Agriculture and Forest Meteorology* vol.80 135-163
- Chen, J. and J. Cihlar, 1996. Retrieving leaf area index of boreal conifer forests using Landsat TM images. *Remote Sensing of Environment*, Vol. 55, pp.153-162.
- Chen, J. and M. Kwong, 1997. *Manual for TRAC: a new optical instrument for ground measurements of LAI and FPAR*. Variously paged.
- Chen, J., P.D. Blanken, T.A. Black, M. Guilbeault, and S. Chen, 1996. Radiation regime and canopy architecture in boreal aspen forest. *Agricultural and Forest Meteorology* vol. 86, 107-125.
- Chen, J., and M. Guilbeault, 1996. Examination of vegetation indices for retrieving biophysical parameters of boreal forests, *Proceedings 26th Canadian Remote Sensing Symposium, Vancouver*, pp. 168-171.
- Curran, P. 1988. The Semivariogram in remote sensing: an introduction. *Remote Sensing of Environment* vol. 24: 493-507.
- Curran, P. 1989. Remote sensing of foliar chemistry. *Remote Sensing of Environment* vol. 30: 271-278.
- Curran, P., Dungan, J.L., and Gholz, H.L. 1992. Seasonal LAI of slash pine estimated with Landsat TM. *Remote Sensing of Environment* vol. 39: 3-13.
- Curran, P., and H Williamson, 1987. GLAI estimation using measurements of red, near infrared and middle infrared radiance, *Photogrammetric Engineering & Remote Sensing*, vol. 53, pp. 493-507.
- D'Arrigo, R, G.C. Jacoby and I.Y. Fung, 1987. Boreal forest and atmosphere exchange of carbon dioxide. *Nature* vol. 329 321-323.
- DeMoraes, J.F.L , Seyler, F., Cerri, C.C., and Volkoff, B. 1998. Land cover mapping and carbon pools estimates in Rondonia, Brazil. *International Journal of Remote Sensing* vol.19 no. 5: 921-934.
- Duguay, C.R. and D.R. Peddle, 1996. Comparison of Evidential Reasoning and Neural Network Approaches in a Multisource Classification of Alpine Tundra Vegetation.

- Canadian Journal of Remote Sensing. 22(4), p. 433-440.
- ENVI, 1998. The Environment for Visualizing Images: ENVI 3.1 and IDL 5.1 User's manuals. Research Systems Inc. Boulder Colorado USA. Variously paged.
- Fournier, R.A., G. Edwards and N.R. Eldridge, 1995. A catalogue of potential spatial discriminators for high spatial resolution digital images of individual crowns. Canadian Journal of Remote Sensing. 21(3):285-298.
- Franklin, J., 1986. Thematic mapper analysis of coniferous forest structure and composition. Int. J. Remote Sensing. Vol. 7 no. 10: 1287-1301.
- Franklin, J., Logan, T., Woodcock, C. and Strahler, A. 1986. Coniferous forest classification and inventory using Landsat and digital terrain data. IEEE transactions on Geoscience and Remote Sensing vol. 24: 1233-1241.
- Franklin, J and Strahler, A.H., 1988. Invertible canopy reflectance modeling of vegetation structure in semiarid woodland. IEEE Transactions on Geoscience and Remote Sensing, Vol. 26, No. 6: 809-825.
- Franklin, J., S.D. Prince, A.H. Strahler, N. P. Hanan and D.S. Simonett, 1991. Reflectance and transmittance properties of West Africa savana trees from ground radiometer measurements. International Journal of Remote Sensing. Vol. 12 no. 6: 1369-1385
- Franklin, S.E., 1999. Modeling Forest Net Primary Productivity with Reduced Uncertainty by Remote Sensing of Covertype and Leaf Area Index. In Perspectives on Uncertainty in Ecological Data. Editors Hunsaker, Goldchild, Friedl, Case.
- Franklin, S.E. and Peddle, D.R., 1987. Texture analysis of digital image data using spatial coourence. Computers and Geoscience vol. 13 no. 3:293-311.
- Franklin, S.E. and Peddle, D.R., 1989. Spectral texture for improved class discrimination in complex terrain. International Journal of Remote Sensing. Vol. 11 no. 3: 551-556.
- Franklin, S.E. and Peddle, D.R., 1990. Classification of SPOT HRV imagery and texture features. International Journal of Remote Sensing vol.14: 2331-2348.
- Gates, D.M., 1990a. Climate change and forests. Tree Physiology vol. 7: 1-5.
- Gates, D.M., 1990b. Climate change and the response of forests. Int J. Remote Sensing. Vol. 11 no. 7: 1095-1107.
- Gemmell, F., 1998. An Investigation of Terrain Effects on the Inversion of a Forest Reflectance Model . Remote Sensing of Environment, Vol: 65, no. 2:155-169.

- Gholz, H. 1982. Environmental limits on above ground primary production, leaf area index, and biomass in vegetation zones of the Pacific Northwest. *Ecology* vol. 54: 152-158.
- Gregor, D.H(jr), 1986. Ecology from Space. *BioScience* vol. 36 no.1: 429-431
- Goel, N.S., Grier, T. 1986. Estimation of canopy parameters for inhomogeneous vegetation canopies from reflectance data. I. Two dimensional row canopy. *International Journal of Remote Sensing* vol.7: 665-681.
- Goel, N.S., 1989. Inversion of canopy reflectance models for estimation of biophysical parameters from reflectance data. In: *Theory and Applications of Optical Remote Sensing*, G. Asrar (ed). John Wiley and Sons, New York. p. 205-251.
- Goetz, A.F.H., and Herring, M. 1989. The high resolution imaging spectrometer (HIRIS) for EOS. *IEEE Transactions on Geoscience and Remote Sensing* vol. 27 no. 2: 136-143.
- Gougeon, F.A, 1995. A crown-following approach to the automatic delineation of individual tree crowns in high spatial resolution aerial images. *Canadian Journal of Remote Sensing*. 21(3):274-284.
- Goward, S.N., and K.F. Huemmrich , and R.H. Waring, 1994. Visible-near infrared spectral reflectance of landscape component in western Oregon. *Remote Sensing of Environment*, Vol. 47: 190-203.
- Graham, R.L., Turner, M.G., and Dale, V.H. 1990. How increasing CO₂ and climate change affect forests. *BioScience* vol. 40 no. 8: 575-587
- Gu, D and Gillespie, A. 1998. Topographic normalization of Landsat TM images of forest based on subpixel sun-canopy-sensor geometry. *Remote Sensing of Environment* vol. 64: 166-175.
- Guyot, G., Guyon, D. and Riou, J. 1989. Factors affecting the spectral response of forest canopies: a review. *Geocarto International* vol. 3: 3-18.
- Hall, F.G., Shimabukuro, Y.E., and Huemmrich, K.F., 1995. Remote sensing of forest biophysical structure using mixture decomposition and geometric reflectance models. *Ecological Applications* vol.5 no. 4: 993-1013.
- Hall, F.G., D.R. Peddle, and E.F. LeDrew, 1996. Remote Sensing of Biophysical Variables in Boreal Forest Stands of *Picea Mariana*. *International Journal of Remote Sensing* 17(15), p. 3077-3081.
- Hall, F.G., D.E. Knapp and K.F. Huemmrich, 1997. Physically based classification and satellite mapping of biophysical characteristics in the southern boreal forest. *Journal of Geophysical Research, BOREAS Special Issue*, 12-26-97. 102(D24): 29567-29580.

- Hall, J.P., 1996. Remote sensing & criteria and indicators of sustainable forest management. Canadian Forestry Service – Ottawa
- Hall, R.J and Crown, P.H. 1987. Spectral classes and forest land classification: a philosophical discussion paper. (unpublished) File Report NOR 0204/1 Canadian Forest Service.
- Holben, B. and Justice, C.O., 1981. An examination of spectral band ratioing to reduce the topographic effect on remotely sensed data. *International Journal of Remote Sensing* vol. 2 no. 2, p. 115-133.
- Horowitz, H.M., Nalepka, R.F., Hyde, P.D. and Morgenstern, J.P. 1971. Estimating the proportions of unresolved objects within a single resolution element of a multispectral scanner. In *Proceedings of the 7th International Symposium on Remote Sensing of Environment*. Michigan, USA. Pages 1307-1320.
- Janinski, M.F., 1990. Functional relation among sub-pixel canopy cover, ground shadow, and illumination ground at large sampling scales. In: *Society of Photo Optical Instrumentation Engineers, Orlando, FL. SPIE 1300, Remote Sensing of the Biosphere*. P 48-58.
- Jarvis, J., and Dewar, R. 1993. Forests in the global carbon balance: from stand to region. In Ehleringer, J. and Field, C., (Editors), *Scaling physiological processes: leaf to globe*. Toronto: Academic Press, 191-221.
- Javris, P.G., 1989. Atmospheric carbon dioxide and forests. *Phil. Trans. R. Soc. Lond. B* 324: 369-392.
- Jensen, J. 1996. *Introductory digital image processing: a remote sensing perspective*. Englewood Cliffs, NJ, Prentice-Hall.
- Johnson, P.J., 1969. *Remote Sensing in Ecology*. University of Georgia Press.
- Johnson, R. L. and D.R. Peddle, 1998. Spectral Mixture Analysis of Airborne Multispectral Video Images in Mountainous Terrain, Kananaskis Alberta: Multi-scale Scene Fraction Validation. In: *Proceedings, 20th Canadian Symp. on Remote Sensing*, Calgary, AB., Canada. p. 203-206.
- Kimmins, J.P. 1997a. Biodiversity and its relationship to ecosystem health and integrity. *The Forest Chronicle* vol. 73. No.2: 229-232
- Kimmins, J.P., 1997b. *Forest Ecology: a foundation for sustainable management*. 2nd Edition. Prentice Hall, Upper Saddle River, New Jersey.
- LabSphere, 1998. *Labsphere Diffuse Reflectance Materials* www.labsphere.com

- Li, X. and Strahler, A.H., 1985. Geometric-optical modeling of a conifer forest canopy. *IEEE Transactions on Geoscience and Remote Sensing*, Vol. GE-23 no. 5:705-720.
- Li, X. and Strahler, A.H., 1986. Geometric-optical bidirectional reflectance modeling of a conifer forest canopy. *IEEE Transactions on Geoscience and Remote Sensing*, Vol. GE-24 no. 6: 906-919.
- Li, X and Strahler, A.H., 1992. Geometric-optical bidirectional reflectance modeling of the discrete crown vegetation canopy: effect of crown shape and mutual shadowing. *IEEE transactions on Geoscience and Remote Sensing* vol.30: 276-296.
- Lillesand, T.M. and Kiefer, R.W. 1994. *Remote Sensing and Image Interpretation*. John Wiley and Sons, New York, NY.
- Linder, P., B. Elfving, and O. Zackrisson, 1997. Stand structure and successional trends in virgin boreal forest reserves in Sweden. *Forest Ecology and Management*, vol. 98, 17-33.
- Marceau, D.J. , Howarth, P.J., Gratton, D.J. 1994. Remote sensing and the measurement of geographic entities in a forested environment. 1. The scale and spatial arrangement problem. *Remote Sensing of Environment* vol. 49; 93-104.
- McCrary R.L. and E.J. Jokela, 1998. Canopy dynamics, light interception, and radiation use efficiency of selected Loblolly Pine families. *Forest Science*, vol 44. 64-72.
- Milton. E. 1987. Principles of field spectroscopy. *International Journal of Remote Sensing* vol. 8: 1807-1827.
- Mustard, J. F., and C. M. Pieters, 1989. Photometric phase functions of common geologic minerals and applications to quantitative analysis of mineral mixture reflectance spectra, *J. Geophys. Res.* 94, 13,619-13,634.
- NRC 1995, *The State of Canada's Forest*. Ottawa: National Research Council.
- NRC 1998, *The State of Canada's Forest*. Ottawa: National Research Council.
- Peddle, D.R. 1995. Knowledge formulation for supervised evidential classification. *Photogrammetric Engineering and Remote Sensing* vol. 61: 409-417.
- Peddle, D.R. 1997. Remote sensing of boreal forest terrain: sub-pixel scale mixture analysis of land cover and biophysical parameters at forest stand and regional scales. Unpublished Ph.D. Thesis, Department of Geography, University of Waterloo, Waterloo, Ontario.
- Peddle, D.R., 1998. Field spectroradiometer data acquisition and processing for spectral mixture analysis in forestry and agriculture". In, *Proceedings, First International*

Conference on Geospatial Information in Agriculture and Forestry. ERIM International. Vol. II. Lake Buena Vista, Florida, USA, pp. 645 - 652. June 1-3.

- Peddle, D.R., 1999. Integration of a Geometric Optical Reflectance Model with an Evidential Reasoning Image Classifier for Improved Forest Information Extraction. *Canadian Journal of Remote Sensing*. Special Issue on Remote Sensing Models and Image Processing. 25(2), p. 189-196.
- Peddle, D.R. and Franklin, S.E. 1991. Image texture processing and data integration for surface pattern discrimination. *Photogrammetric Engineering and Remote Sensing* vol. 57 no. 4:413-420.
- Peddle, D.R. and S.E. Franklin 1993. Classification of permafrost active layer depth from remotely sensed and topographic evidence. *Remote Sensing of Environment*, Vol. 44 no. 1:67-80.
- Peddle, D.R., F.G. Hall, W. Wanner and E.F. LeDrew, 1995. Remote Sensing of Photosynthetic Activity in Boreal Forest Stands using Spectral Mixture Analysis and Geometric-Optical Reflectance Models. In: *Proceedings, 10th International Congress on Photosynthesis and Remote Sensing*, Montpellier, France, 28-31 August 1995. p. 159-170.
- Peddle, D.R., S.E. Franklin, R.L. Johnson, M. Lavigne and M. Wulder, 1999a. Multiple-Forward-Mode Reflectance Modeling of Partial Harvest Change in a Mixed Forest. Unpublished manuscript in preparation for *International Journal of Remote Sensing*.
- Peddle, D.R., F.G. Hall and E.F. LeDrew, 1999b. Spectral mixture analysis and geometric optical reflectance modeling of boreal forest biophysical structure. *Remote Sensing of Environment*, Vol. 67, No. 3, pp. 288-297.
- Peddle D.R. and R. L. Johnson, 2000. Spectral mixture analysis of airborne remote sensing imagery for improved prediction of leaf area index in mountainous terrain. Kananaskis Alberta. *Canadian Journal of Remote Sensing*; (in press).
- Peddle, D.R., F.G. Hall, E.F. LeDrew and D.E. Knapp, 1997. Classification of forest land cover in BOREAS. II: Comparison of results from a sub-pixel scale physical modeling approach and a training based method, *Canadian Journal of Remote Sensing*. Special Issue: BOREAS, Vol. 23, no. 2, pp. 131-142.
- Peddle, D.R., H.P. White, R.J. Soffer, J.R. Miller and E.F. LeDrew, 2000. Reflectance Processing of Remote Sensing Spectroradiometer Data. *Computers & Geosciences* (accepted for publication).

- Peterson, D., M. Spanner and K. Teuder, 1987. Relationship of Thematic Mapper data to leaf area index of temperate coniferous forests. *Remote Sensing of Environment*, Vol. 22: 323-341.
- Pierce, L.L. and S.W. Running, 1988. Rapid estimation of coniferous forest leaf area index using a portable integrating radiometer. *Ecology* 69(6), 1762-1767.
- Pitt, D.G, Wagner, R.G, Hall, R.J, King, D.J, Leckie, D.G and Runesson, U. 1997. Use of remote sensing for forest vegetation management: a problem analysis. *The Forestry Chronicle*, vol. 73 no. 4: 459-477
- Roughgarden, G, S.W. Running, and P.A, Matson, 1991. What does remote sensing do for ecology. *Ecology* vol. 72 no. 6, 1923-1933.
- Rouse, J.W., R.Haas, J.Schell and D.Deering, 1974. Monitoring vegetation systems in the Great Plains with ERTS. *Third ERTS Symposium, NASA SP-351*, vol. 1, p.309-317.
- Rowe, J.S., 1972. *Forest regions of Canada*. Environ. Can., Can. For. Serv., Ottawa, ON. Publication No. 1300, 172 pp.
- Running, S.W. and Hunt E.R. (jr), 1994. Generalization of a forest ecosystem process model for other biomes, BIOME-BGC, and an application for global scale models. In Ehlermiger, J. and Field, C., (Editors), *Scaling Physiological Processes : leaf to globe*, Toronto: Academic Press, 141-157.
- Running, S.W. and S.T. Gower, 1991. Forest-BGC, A general model of forest ecosystem processes for regional applications. II. Dynamic carbon allocation and nitrogen budgets. *Tree Physiology*, Vol. 9:147-160.
- Running, S.W. and J.C. Coughlan, 1988. A general model of forest ecosystem processes for regional applications: 1 hydrologic balance, canopy gas exchange and primary production processes. *Ecological sensing of Environment*, Vol. 42:125-154.
- Running, S.W., S.D. Peterson, M Spanner and K. Teuber, 1986. Remote sensing of coniferous forest leaf area, *Ecology*, vol. 67, no 1, pp. 273-276.
- Seed, E.D. and D.J. King, 1997. Determination of mixed boreal forest stand biophysical structure using large scale airborne digital camera imagery, *In, Proceedings GER'97: 9th International Conference on Geomatics / 19th Canadian Symposium on Remote Sensing*, Ottawa, Canada. Published on CD-ROM.
- Sellers, P.J., 1987. Canopy reflectance, photosynthesis, and transpiration. II. The role of biophysics in the linearity of their interdependence. *Remote Sensing of Environment* vol.21:143-183.
- Smith, R.L, 1996. *Ecology and Field Biology* (5th Edition). Harper Collins, New York, N.Y.

- Spurr, S.H. and B.V. Barnes, 1973. *Forest Ecology*, (Second Edition). The Ronald Press Company, New York.
- Spurr, S. and Barnes, B. 1980. *Forest Ecology*. Toronto, Wiley.
- Strahler, A.H. and Jupp, D.L.B. 1990. Geometric optical modeling of forests as remotely sensed scenes composed of three-dimensional, discrete objects, in *Photon-Vegetation Interactions: Applications in Optical Remote Sensing and Plant Ecology* (R. Myneni and J. Ross, Eds.), Speinger-Verlag, Heidelberg, 162-190.
- Stahler, A.H. and Woodcock, C.E. 1986. On the nature of models in remote sensing. *Remote Sensing of Environment*, Vol. 20:121-139.
- Teillet, P.M., Guindon, B. and Goodenough, D.G. 1982. On the slope-aspect correction of multispectral scanner data. *Canadian Journal of Remote Sensing* vol. 8 no.2: 84-106.
- Townshed, J. and Justice, C. 1981. Information extraction from remotely sensed data. *International Journal of Remote Sensing* vol. 2: 313-329.
- Treitz, P. and P. Howarth, 1996. Remote sensing for forest ecology characterization: a review. NODA/NFP Technical report TR-12 available from Waterloo Laboratory from Earth Observations, Department of Geography, University of Waterloo, Waterloo, On.
- Tucker, C. 1979. Red and photographic infrared linear combinations for monitoring vegetation. *Remote Sensing of Environment*, Vol. 8:127-150.
- Ustin, S.L., C.A Wessman, B. Curtis, E. Kasischke, J. Way and V.C. Vanderbuilt, 1991. Opportunities for using the EOS imagery spectrometers and synthetic aperture radar in ecological models. *Ecology*, vol. 72, no. 6 1934-1945.
- Webster, H.H., 1993. Some thoughts on sustainable development as a concept, and as applied to forests. *The Forestry Chronicle*, vol. 69, no. 5, 531-534.
- Welles, J.M. 1990. Some indirect methods of estimating canopy structure. Instrumentation for studying vegetation canopies for remote sensing in optical and thermal infrared regions. *Remote Sensing Reviews*. 5:1-12
- Welles, J.M. and J.M. Norman, 1991. Instrument for indirect measurement of canopy architecture. *Agronomy Journal* Vol. 83, No. 5, pp. 818-825.
- Wickland, D.E, 1991. Mission to plant Earth: the ecological perspective. *Ecology* vol. 72 no. 6, 1923-1933.
- Woodcock, C.E, Collins, J.B., Jackbhazy, V.D, Li, X, Macomber, S.A and Wu, Y, 1997. Inversion of the Li-Strahler canopy reflectance model for mapping forest structure. *IEEE Transactions on Geoscience and Remote Sensing*, Vol. 35 no. 2: 405-414.

- Wulder, M.A, LeDrew, E.F, Franklin, S.E, and Lavigne, M.B. 1998. Aerial image texture information in the estimation of northern deciduous and mixed wood forest leaf area index (LAI). *Remote Sensing of Environment* vol. 64:64-67
- Wulder, M.A., 1998. Optical remote-sensing techniques for the assessment of forest inventory and biophysical parameters. *Progress in Physical Geography* vol. 4 no. 2: 449-476.
- Wulder, M., Lavigne, M. and Franklin, S., 1996. High spatial resolution optical image texture for improved estimation of forest stand leaf area index. *Canadian Journal of Remote Sensing* vol. 22: 441-449.
- Wulder, M., Mah, S. and Trudeau, D. 1996. Mission planning for operational data acquisition campaigns with the CASI. 2nd International Airborne Remote Sensing Conference and Exhibition San Francisco, CA. June.
- Wu, Y. and A. Strahler, 1994. Remote estimation of crown size, stand density and biomass on the Oregon transect. *Ecological Applications*, Vol. 4 no. 2:199-312.

Appendix 1: Model Inputs and Multiple Forward Mode Software

The input files required by the GOMS model include an angle file (angles*.dat) and a structural parameter file (goms*.par) and are produced using the MFM.c program. As output the GOMS model creates a file which provides the component fractions for canopy, background and shadow as well as the pixel level reflectance value (fr*.out) and the MFM program produces a file which contains the input structural data. These outputs are then arranged into the lookup table using the Group.c program.

Angles*.dat

```
1 1
(band 1 of 1 (this version of the software can only compute a single band
for each trial))
30.00000    175.8888    52.383999    138.11234
(slope)      (Aspect)      (SZA)        (Azimuth)
```

The MFM program produces a new angle file for each combination of slope, aspect, SZA and Azimuth specified by the user.

GOMS.PAR File

goms*.par

```
#ComponentSignaturesCrown: 0.040000
#ComponentSignaturesGround: 0.040000
#ComponentSignaturesShade: 0.000000
#Slope+SlopeAspect: 0.0 0.0
#
#Parameters: lambda*r^2, b/r, h/b, dh/b
MutShadwTopo {
    0.705600    3.011905    3.051383    7.272727
}
```

The MFM calculates the ratios for the structural input file based on the user specified data and intervals, the model also varies the endmember reflectance values in this file.

fr*.out

```
1 1
30.00000    175.8888    52.383999    138.11234
(slope)      (Aspect)      (SZA)        (Azimuth)
0.43234213  0.234286    0.33371      0.0321
(canopy)     (background) (shadow)     (pixel reflectance)
```

A new fr*.out is created for each model trial, the MFM program subsequently combines these files into a single output file.

MFM.C

/*

Program Name: MFM.c

Author: Ryan Johnson
 University of Lethbridge
 Ryan.johnson@uleth.ca

This C language program is a console version of the multiple forward GOMS application. The program accepts the range and modeling interval of input data for the GOMS geometric optical reflectance model. The model computes every possible combination of structural, endmember and geometric input data for the GOMS model and then produces all the needed input files for the GOMS model as well as creating a UNIX command shell file to execute all model trials in batch mode. The UNIX shell command is %sh GOMS.MFM. (A GUI version of this software is also available and run using WinBatch on any PC. - but is not shown, as the code is more complex. Email ryan.johnson@uleth.ca for a copy of the PC version.) As output then are a series of input files and the shell file. Once the batch file has run the program concatenates the GOMS output and input parameters into two separate files and removes all the input files. Subsequent use of the Group.c program will combine these files into the lookup tables.

This program is based on the bat_goms.c program (Peddle, 1997) but adds the ability to provide the model with ranges and model intervals of input parameters to run the entire scope of data in a single trial. This ability allows for the influence of terrain and structure to be explicitly examined.

*/

```
#include <stdio.h>
#include <iostream.h>
```

```
/* variable declaration
r, r2: horizontal radius of tree crown
b: half crown height
h: height from ground to center of crown
dh: height distribution of trees
```

```
*/
float r, r2, b, h, dh, Pc, Pb, Ps, hb, dhb, lam, br, td;
float slope, aspect, sza, azimuth;
float minslope, maxslope, intervalslope, holdslope, holdslope2, tempslope;
float minaspect, maxaspect, intervalaspect, holdaspect, holdaspect2, tempaspect;
float minsza, maxsza, holdsza, intervalsza, holdsza2, tempsza;
float minazimuth, maxazimuth, intervalazimuth, holdazimuth, holdazimuth2, tempazimuth;
float minr, maxr, intervalr, holdr, holdr2, tempr;
float minb, maxb, intervalb, holdb, holdb2, tempb;
float minh, maxh, intervalh, holdh, holdh2, tempb;
float mindh, maxdh, intervaldh, holddh, holddh2, tempdh;
float minlam, maxlam, intervallam, holdlam, holdlam2, templam;
float mincanopy, maxcanopy, intercanopy, holdcanopy, holdcanopy2, tempcanopy;
float minbg, maxbg, interbg, holdbg, holdbg2, tempbg;
float minS, maxS, interS, holdS, holdS2, tempS;
```

```

int filec=0, test, count, tempcount, n, count1, band_number;
float i, j, k, l, m, o, p,q;
int s,t;
float x, y, z, w;
char angle_filename[80];
int countangle, total;
char output_filename[80], tempgoms_outfilename[80], goms_outfilename[80], par_filename[80],
input_filename[80];

FILE *par_file, *sh_file, *ang_file, *var_file, *fopen();

main()
{
    //obtain user input of tree dimension and form parameters for site

    printf("\n\t Please enter the band to test (eg 1, 2, 3, ...) ?");
    scanf ("%d", &band_number);
    printf("\n\t Please enter the input parameters for the GOMS model.\n Enter the minimum and maximum value
for each.");
    printf("\n This program will then calculate the range and set up the input files.");
    printf("\n If you want to hold a variable constant set max and max equal and enter 1 for the interval.");
    printf("\n\n");
    printf("\n Minimum pixel slope (slope) ?");
    scanf ("%f",&minslope);
    printf("\n Maximum pixel slope (slope) ?");
    scanf ("%f",&maxslope);
    printf("\n Enter the interval for this range ?");
    scanf ("%f",&intervalslope);
    holdslope = maxslope - minslope ;
    printf (" The Range of r is : %f ", holdslope);
    tempslope = minslope;
    for (i=minslope; i<maxslope + intervalslope; i= i +intervalslope)
        {
            printf (" \n The values of slope will be: %f ", tempslope);
            tempslope = tempslope + intervalslope;
        }
    tempslope = minslope;
    printf("\n");
    printf("\n Minimum pixel aspect (aspect) ?");
    scanf ("%f",&minaspect);
    printf("\n Maximum pixel aspect (aspect) ?");
    scanf ("%f",&maxaspect);
    printf("\n Enter the interval for this range ?");
    scanf ("%f",&intervalaspect);
    holdaspect = maxaspect - minaspect ;
    printf (" The Range of r is : %f ", holdaspect);
    tempaspect = minaspect;
    for (i=minaspect; i<maxaspect + intervalaspect; i= i +intervalaspect)
        {
            printf (" \n The values of aspect will be: %f ", tempaspect);
            tempaspect = tempaspect + intervalaspect;
        }
    tempaspect = minaspect;
    printf("\n");

```

```

printf ("\n Minimum solar zenith angle (sza) ?");
scanf ("%f",&minsza);
printf ("\n Maximum solar zenith angle (sza) ?");
scanf ("%f",&maxsza);
printf ("\n Enter the interval for this range ?");
scanf ("%f",&intervalsza);
holdsza = maxsza - minsza ;
printf (" The Range of r is : %f ", holdsza);
tempsza = minsza;
for (i=minsza; i<maxsza + intervalsza; i= i +intervalsza)
{
    printf (" \n The values of sza will be: %f ", tempsza);
    tempsza = tempsza + intervalsza;
}
tempsza = minsza;
printf("\n");
printf ("\n Minimum solar azimuth angle (azimuth) ?");
scanf ("%f",&minazimuth);
printf ("\n Maximum solar azimuth angle (azimuth) ?");
scanf ("%f",&maxazimuth);
printf ("\n Enter the interval for this range ?");
scanf ("%f",&intervalazimuth);
holdazimuth = maxazimuth - minazimuth ;
printf (" The Range of azimuth is : %f ", holdazimuth);
tempazimuth = minazimuth;
for (i=minazimuth; i<maxazimuth + intervalazimuth; i= i +intervalazimuth)
{
    printf (" \n The values of azimuth will be: %f ", tempazimuth);
    tempazimuth = tempazimuth + intervalazimuth;
}
tempazimuth = minazimuth;
printf("\n");
printf ("\n Minimum tree density LAMBDA (lam) ?");
scanf ("%f",&minlam);
printf ("\n Maximum tree density LAMBDA (lam) ?");
scanf ("%f",&maxlam);
printf ("\n Enter the interval for this range ?");
scanf ("%f",&intervallam);
holdlam = maxlam - minlam ;
printf (" The Range of r is : %f ", holdlam);
templam = minlam;
for (i=minlam; i<maxlam + intervallam; i= i +intervallam)
{
    printf (" \n The values of r will be: %f ", templam);
    templam = templam + intervallam;
}
templam = minlam;
printf("\n");
printf ("\n Minimum Horizontal Crown Radius (r) ?");
scanf ("%f",&minr);
printf ("\n Maximum Horizontal Crown Radius (r) ?");
scanf ("%f",&maxr);
printf ("\n Enter the interval for this range ?");
scanf ("%f",&intervalr);
holdr = maxr - minr ;
printf (" The Range of r is : %f ", holdr);

```

```

tempr = minr;
for (j=minr; j<maxr + intervalr; j= j +intervalr)
{
    printf (" \n The values of r will be: %f ", tempr);
    tempr = tempr + intervalr;
}
tempr = minr;
printf("\n");
printf ("\n Minimum vertical radius (b) ?");
scanf ("%f",&minb);
printf ("\n Maximum vertical radius (b) ?");
scanf ("%f",&maxb);
printf ("\n Enter the interval for this range ?");
scanf ("%f",&intervalb);
holdb = maxb - minb ;
printf (" The Range of b is : %f ", holdb);
tempb = minb;
for (k=minb; k<maxb + intervalb; k = k +intervalb)
{
    printf (" \n The values of b will be: %f ", tempb);
    tempb = tempb + intervalb;
}
tempb = minb;
printf("\n");
printf ("\n Minimum Height to center of crown (h) ?");
scanf ("%f",&minh);
printf ("\n Maximum Height to center of crown (h) ?");
scanf ("%f",&maxh);
printf ("\n Enter the interval for this range ?");
scanf ("%f",&intervalh);
holdh = maxh - minh ;
printf (" The Range of h is : %f ", holdh);
temph = minh;
for (l=minh; l<maxh + intervalh; l= l +intervalh)
{
    printf (" \n The values of h will be: %f ", temph);
    temph = temph + intervalh;
}
temph = minh;
printf("\n");
printf ("\n Minimum Height Distribution (dh) ?");
scanf ("%f",&mindh);
printf ("\n Maximum Height distribution (dh) ?");
scanf ("%f",&maxdh);
printf ("\n Enter the interval for this range ?");
scanf ("%f",&intervaldh);
holddh = maxdh - mindh ;
printf (" The Range of r is : %f ", holddh);
tempdh = mindh;
for (m=mindh; m<maxdh + intervaldh; m= m +intervaldh)
{
    printf (" \n The values of r will be: %f ", tempdh);
    tempdh = tempdh + intervaldh;
}
tempdh = mindh;
printf("\n");

```



```

/* Obtain end-member reflectance values for each component */
printf("\n This section will require the input of the spectral signatures.");
printf("\n These values can also be input ranges:");
printf("\n Minimum End-member reflectance for \n\t Sunlit Canopy (Component signature crown, Pc) ? : ");
scanf ("%f",&mincanopy);
printf("\n Maximum End-member reflectance for \n\t Sunlit Canopy (Component signature crown, Pc) ? : ");
scanf ("%f",&maxcanopy);
printf("\n Interval for End-member reflectance of \n\t Sunlit Canopy (Component signature crown, Pc) ? : ");
scanf ("%f",&intercanopy);
holdcanopy = maxcanopy - mincanopy ;
printf(" The Range of r is : %f ", holdcanopy);
tempcanopy = mincanopy;
for (q=mincanopy; q<maxcanopy + intercanopy; q= q +intercanopy)
{
    printf(" \n The values of r will be: %f ", tempcanopy);
    tempcanopy = tempcanopy + intercanopy;
}
tempcanopy = mincanopy;
printf("\n");
printf("\n Minimum End-member reflectance for \n\t Shadow (Component signature shadow, Ps) ? : ");
scanf ("%f",&minS);
printf("\n Maximum End-member reflectance for \n\t Shadow (Component signature shadow, Ps) ? : ");
scanf ("%f",&maxS);
printf("\n Interval for End-member reflectance of \n\t Shadow (Component signature shadow, Ps) ? : ");
scanf ("%f",&interS);
holdS = maxS - minS ;
printf(" The Range of r is : %f ", holdS);
tempS = minS;
for (o=minS; o<maxS + interS; o= o +interS)
{
    printf(" \n The values of r will be: %f ", tempS);
    tempS = tempS + interS;
}
tempS = minS;
printf("\n");
printf("\n Minimum End-member reflectance for \n\t Sunlit Background (Component signature ground Pb) ? : ");
scanf ("%f",&minbg);
printf("\n Maximum End-member reflectance for \n\t Sunlit Background (Component signature ground Pb) ? : ");
scanf ("%f",&maxbg);
printf("\n Interval for End-member reflectance of \n\t Sunlit Background (Component signature ground Pb) ? : ");
scanf ("%f",&interbg);
holdbg = maxbg - minbg ;
printf(" The Range of r is : %f ", holdbg);
tempbg = minbg;
for (p=minbg; p<(maxbg + interbg); p= p +interbg)
{
    printf(" \n The values of r will be: %f ", tempbg);
    tempbg = tempbg + interbg;
}
tempbg = minbg;
printf("\n");

```

```

printf ("\n *****Please Wait this program is now writing GOMS input files to disk*****");
printf ("\n *****To run the GOMS model type sh MFM.bat - at the command
prompt*****\n");

//printf("\n Enter the OUTPUT filename for GOMS ouput: ");

//scanf ("%s", &tempgoms_outfilename);
sprintf(goms_outfilename,"modelout%d.cmb",band_number);

// start creating the input values for the GOMS model

//create the nested for loops for the angles.dat file here
countangle = 1;
tempslope = minslope;
for (x=minslope; x<maxslope + intervalslope; x = x +intervalslope)
{
    tempaspect = minaspect;
    for (y=minaspect; y<maxaspect + intervalaspect; y = y +intervalaspect)
    {
        tempsza = minsza;
        for (z=minsza; z<maxsza + intervalsza; z = z +intervalsza)
        {
            tempazimuth = minazimuth;
            for (w=minazimuth; w<maxazimuth + intervalazimuth; w = w +intervalazimuth)
            {
                sprintf (angle_filename,"angles%d.dat",countangle);
                ang_file = fopen (angle_filename, "w");
                fprintf (ang_file,"1 1\n");
                fprintf (ang_file,"%f %f %f %f", tempslope, tempaspect, tempsza,
tempazimuth);

                fclose (ang_file);
                countangle ++;
                tempazimuth = tempazimuth + intervalazimuth;
            }
            tempsza = tempsza + intervalsza;
        }
        tempaspect = tempaspect + intervalaspect;
    }
    tempslope = tempslope + intervalslope;
}

/* compute input factors from physical tree parameters */
count = 1;
templam = minlam;
for (i=minlam; i<maxlam + intervallam; i= i +intervallam)
{
    tempr = minr;
    for (j=minr; j<maxr + intervalr; j= j +intervalr)
    {
        tempb = minb;
        for (k=minb; k<maxb + intervalb; k = k +intervalb)
        {
            tempb = minb;

```

```

for (l=minh; l<maxh + intervalh; l= l +intervalh)
{
  tempdh = mindh;
  for (m=mindh; m<maxdh + intervaldh; m= m +intervaldh)
  {
    tempcanopy = mincanopy;
    for (q=mincanopy; q<maxcanopy + intercanopy; q= q
+intercanopy)
    {
      tempbg = minbg;
      for (p=minbg; p<maxbg + interbg; p= p +interbg)
      {
        tempS = minS;
        for (o=minS; o<maxS + interS; o= o +interS)
        {
          sprintf (output_filename,"fr%d.out",count);
          sprintf (par_filename,"goms%d.par",count);
          sprintf (input_filename,"parameter_MFM%d.stf",count);

          r2 = tempr*tempr;
          br = tempb/tempr;
          hb = tempb/tempb;
          dhb = tempdh/tempb;
          td = templam;

          par_file = fopen (par_filename, "w");

          fprintf (par_file, "#ComponentSignaturesCrown:
%f\n",tempcanopy);

          fprintf (par_file, "#ComponentSignaturesGround: %f\n",tempbg);
          fprintf (par_file, "#ComponentSignaturesShade: %f\n",tempS);
          fprintf (par_file, "#Slope+SlopeAspect: 0.0 0.0\n");
          fprintf (par_file, "#\n");
          fprintf (par_file, "#Parameters: lambda*r^2, b/r, h/b, dh/b\n");
          fprintf (par_file, "MutShadwTopo {\n");
          fprintf (par_file, " %8.6f %8.6f %8.6f
%8.6f\n",td*r2,br,hb,dhb);

          fprintf (par_file, " }\n");

          fclose (par_file);

          //write to the parameter file
          var_file = fopen (input_filename,"w"); // opens the
parameter file to hold inputs
          fprintf (var_file, "%f %f %f %f %f %f %f %f %f %f %f\n",
templam, tempr, tempb, tempb, tempdh,td*r2,br,hb,dhb, tempcanopy, tempbg, tempS);
          fclose (var_file);

          count ++;
          countl++;

          tempS = tempS + interS;}

          tempbg = tempbg + interbg;}

          tempcanopy = tempcanopy + intercanopy;}
tempdh = tempdh + intervaldh;}

```

```

        tempb = tempb + intervalb;}
        tempr = tempr + intervalr;}
    templam = templam + intervallam;}

total = 1;
sh_file = fopen("MFM.bat","w");          // opens the batch file
for (s=1; s<countangle; s= s +1)
    {
        for (t=1; t<count; t= t +1)
            {
                /* add next line to UNIX command shell file. BRDF2.exe is the GOMS
                executable file; angles.dat contains the view and illumination data,
                and the model is run in forward mode */
                fprintf (sh_file, "BRDF2.exe < angles%d.dat > fr%d%d.out -forward -model
goms%d.par\n",s,s,t,t);
                total++;
            }
    }
//Add the cat stament to the GOMS.MFM file
tempcount = total;
fprintf(sh_file,"cat ");

for (s=1; s<countangle; s= s +1)
    {
        for (t=1; t<count; t= t +1)
            {
                fprintf (sh_file, "fr%d%d.out ",s,t);
            }
    }

fprintf (sh_file," > %s\n",goms_outfilename);
fprintf(sh_file,"cat ");
for (s=1; s<countangle; s= s +1)
    {
        for (t=1; t<count; t= t +1)
            {
                fprintf(sh_file,"parameter_MFM%d.stf ",t);
            }
    }
fprintf (sh_file," > parameters.mfm\n");
// remove the intermediate files
fprintf (sh_file,"rm *.out\n");
fprintf (sh_file,"rm *.par\n");
fprintf (sh_file,"rm *.dat\n");
fprintf (sh_file,"rm *.stf\n");
fclose (sh_file);
printf ("%d",total);
}

```

